Phenotypic and genomic diversification in complex carbohydrate degrading human gut bacteria

Nicholas A. Pudlo[1*], Karthik Urs[1*], Ryan Crawford[2], Ali Pirani[1], Todd Atherly[3,4], Roberto Jimenez[5], Nicolas Terrapon[6,7], Bernard Henrissat[6,7,8], Daniel Peterson[5,9], Cherie Ziemer[3,4], Evan Snitkin[1] and Eric C. Martens[1]

[1]Department of Microbiology and Immunology, University of Michigan Medical School, Ann Arbor, MI 48109

[2]Department of Computational Medicine and Bioinformatics, University of Michigan Medical School, Ann Arbor, MI 48109

[3]Iowa State University, Dept. of Animal Science, Ames, IA

[4]United States Department of Agriculture Agricultural Research Station, Ames, IA

[5]University of Nebraska, Department of Food Sciences, Lincoln, NE

[6]Aix Marseille Univ, CNRS, UMR7257 AFMB, Marseille, France

[7]INRAE, USC1408 AFMB, Marseille, France

[8]Department of Biological Sciences, King Abdulaziz University, Jeddah, Saudi Arabia

[9]Johns Hopkins University, Department of Pathology, Baltimore, MD

*Authors contributed equally to this work

Correspondence to: emartens@umich.edu

Running Title: *Bacteroidetes* carbohydrate utilization

Abstract

Symbiotic bacteria are responsible for the majority of complex carbohydrate digestion in the human colon. Since the identities and amounts of dietary polysaccharides directly impact the gut microbiota, determining which microorganisms consume specific nutrients is central to defining the relationship between diet and gut microbial ecology. Using a custom phenotyping array, we determined carbohydrate utilization profiles for 354 members of the Bacteroidetes, a dominant saccharolytic phylum. There was wide variation in the numbers and types of substrates degraded by individual bacteria, but phenotype-based clustering grouped members of the same species indicating that each species performs characteristic roles. The ability to utilize dietary polysaccharides and endogenous mucin glycans was negatively correlated, suggesting exclusion between these niches. By analyzing related *Bacteroides ovatus/xylanisolvens* strains that vary in their ability to utilize mucin glycans, we addressed whether gene clusters that confer this complex, multi-locus trait are being gained or lost in individual strains. Pangenome reconstruction of these strains revealed a remarkably mosaic architecture in which genes involved in polysaccharide metabolism are highly variable and bioinformatics data provide evidence of interspecies gene transfer that might explain this genomic heterogeneity. Global transcriptomic analyses suggest that the ability to utilize mucin has been lost in some lineages of *B. ovatus* and *B. xylanisolvens*, which still harbor residual gene clusters that are involved in mucin utilization by strains that still actively express this phenotype. Our data provide insight into the breadth and complexity of carbohydrate metabolism in the microbiome and the underlying genomic events that shape these behaviors.

Introduction

Microbial communities in the distal intestines of humans and other mammals play critical roles in the digestion of dietary polysaccharides (1-3). Unlike proteins, lipids and simple sugars, which can be assimilated in the small intestine, the vast majority of non-starch polysaccharides (fibers) transit undegraded to the distal gut due to a lack of requisite enzymes encoded in the human genome (4). Microbial transformation of dietary fiber polysaccharides into host-absorbable organic and short chain fatty acids is a beneficial process that unlocks otherwise unusable calories from our diet (5), shapes the composition and behavior of the gut microbial community (6-8), provides preferred nutrients directly to the colonic epithelium (9-11) and shapes the development of immune cell populations (12, 13).

The abundance of dietary fiber in the mammalian diet, and the substantial chemical diversity within this class of molecules, provides a prominent selective pressure that drives genome evolution and diversification within symbiotic bacterial populations. The genomes of individual human gut bacteria frequently encode dozens-hundreds more polysaccharide-degrading enzymes than human secrete into the gastrointestinal tract, reflecting gut microbial adaptations to degrade dietary fibers (3, 4). As examples, the genomes of a few well-studied Gram-negative *Bacteroides* (*B. thetaiotaomicron*, *B. ovatus* and *B. cellulosyliticus*) encode between 250 and over 400 CAZymes that collectively equip them to target nearly all commonly available dietary polysaccharides (14-16). However, none of these three species is by itself capable of degrading all available polysaccharides, a conclusion that was supported by early phenotypic surveys of cultured human gut bacteria that encompassed species from other phyla (17, 18). These findings suggest that individual microbes fill multiple, specific carbohydrate degradation niches and that a diverse community is required to ensure degradation of the entire repertoire of dietary fibers. Given that hundreds of different microbial species typically coexist in an individual over long time periods (19), it is important to understand how many different polysaccharide metabolism pathways are present within the individual microbial species that compose a community and how these traits are represented across strains and species. If some species possess very similar phenotypic abilities, they may be functional surrogates or compete for similar niches and therefore seldom co-occur.

Members of the Bacteroidetes are often among the most numerous bacteria in the colonic microbiota of people from industrialized countries (19-21). These bacteria are well appreciated for their abilities to degrade a broad range of polysaccharides (16-18, 22, 23) and modify disease states in a bacterial species-specific fashion (24-26). In this study, we empirically measured the abilities of members of 29 different Bacteroidetes species to grow on a custom panel of carbohydrates that span the diversity of plant, animal and microbial polysaccharides. Our results reveal a wide range of metabolic breadth between different species, indicating that some have evolved to be carbohydrate generalists while others have become metabolically specialized to target just one or a few nutrients. Pangenome analysis of several related strains provides insight into the evolutionary events that shape carbohydrate utilization among these important symbionts and reveals a dizzying mosaic of heterogeneity at the level of discrete gene clusters mediating polysaccharide metabolism. Based on analysis of several variable loci, we provide evidence to support a mechanism of lateral gene transfer that may account for this mosaic architecture. Our results provide a glimpse into the metabolic breadth and diversity of an important group of human gut bacteria towards polysaccharide metabolism. Given the large amount of genomic and metagenomic sequence information that has been generated from the human microbiome, phenotypic studies such as the one presented here represent important next steps in deciphering the functionality of these organisms in their native gut habitat.

Results

Phenotypes are the ultimate measures of biological function. However, large-scale phenotypic analyses are still uncommon in surveys of the human gut microbiome, which have instead relied on sequence-based approaches to infer function, often with substantial uncertainty. This lack of phenotypic information is partly due to a lack of high-density (*e.g*., strain level) culture representation for the dominant taxa combined with a lack of defined growth conditions to measure behavior of these organisms. With the resurgence of gut microbial culturing, both of these gaps have begun to close (27-30), revealing an urgent need for scalable platforms to define the actual behavior of these organisms. To address this gap, we assembled a collection of human and animal gut Bacteroidetes and constructed a custom anaerobic phenotyping platform centered around carbohydrate metabolism, a key function that symbiotic gut microorganisms contribute to mammalian digestion (4). This array consists of 45 different carbohydrates (30 polysaccharides and 15 monosaccharides) that span the repertoire of common sugars and linkages present in dietary plants and meat, as well as host mucosal secretions and some rare nutrients consumed in regional populations or as food additives (see **Fig. S1** for a summary of polysaccharide structures).

The carbohydrate utilization abilities of 354 different human and animal Bacteroidetes strains were measured by individually inoculating each into this custom growth array and automatically monitoring anaerobic growth every 10-20 min for four days (see *Materials and*

Methods). Based on 16S rRNA gene sequence for each strain, this collection encompasses 29 different species based on the requirement that each strain possesses ≥98% 16S rRNA gene identity to a named type strain in a given species (**Table S1,** note that all but three strains, which were all related to each other and to *Bacteroides uniformis*, met this criterion). The resulting 31,860 individual growth curves were first inspected manually and then subjected to automated analysis to quantify total growth and growth rate parameters for each substrate (see *Materials and Methods*). A normalization scheme was employed to compensate for general growth differences in the two different defined medium formulations employed (see **Table S1** for a full list of strains assayed and all raw and normalized growth measurements, **Fig. S2** for analysis of replicates).

Members of the same species possess similar carbohydrate utilization profiles

Growth results are summarized in **Figs. 1**, **2** and **S3**. Whether considered from the perspective of how many species degrade a particular polysaccharide (**Fig. 1A**), or how many individual polysaccharides are targeted by members of a particular species (**Fig. 1B**), there was substantial variability in carbohydrate utilization among the organisms surveyed (range, 1-28 polysaccharides degraded per strain; mean, 15.6). Some polysaccharides like soluble starch/glycogen were degraded by a majority of the species tested, yet others like the edible seaweed polysaccharides carrageenan and porphyran were used by just one or two strains.

Given the diversity in observed carbohydrate utilization phenotypes, we wished to address if closely related strains display similar abilities or instead if strains of the same species have diverged from one another. To assist in visualizing the overall trends in carbohydrate utilization across this phylum, we performed unsupervised clustering of the strains based on their carbohydrate utilization profiles. While many species are not deeply represented by multiple strains, clustering based on a combination of normalized growth and rate measurements largely grouped strains of the same species together (**Fig. 2**) and, as expected, this was driven mostly by polysaccharide utilization abilities (**Fig. S4**).

Our data reveal that strains belonging to several individual species possess more similar polysaccharide degrading abilities to each other compared to their more distant relatives, a finding that has importance for interpreting or predicting function based on community sequencing data. As examples, all 56 strains of *B. fragilis* clustered together, reflecting their generally restricted abilities to utilize forms of soluble starch/glycogen, inulin and mucus *O*-glycans. Likewise, all 36 strains of *B. uniformis*, a species with broader metabolic capacity that includes digestion of plant cell wall hemicelluloses, were also grouped together into a single branch. The inclusivity of these groupings was generally independent of the time period when strains were isolated or whether they were isolated from humans or other mammals (**Fig. 2**).

Another important feature of the observed species clustering is that the grouping does not mirror the overall phylogeny of the gut Bacteroidetes. Rather, phylogenetically separated species often group adjacent to one another based on similarities in carbohydrate metabolism (*e.g.*, *B. ovatus/xylanisolvens* and *B. cellulosilyticus;* and *B. vulgatus/dorei* and *B. fragilis*; see **Fig. 3A** for a phylogenetic tree based on conserved housekeeping genes) (31, 32). In the latter case, it is interesting to directly compare *B. fragilis* and *B. vulgatus/dorei*, two groups with deep strain representation (**Fig. 2**). Despite being phylogenetically more distant, these species possess very similar phenotypic patterns that reflect degradation of soluble starch and similar molecules (glycogen, pullulan), inulin and mucin *O*-glycans. The major distinguishing feature between these groups is the presence of some, often-weak, pectin utilization among strains of *B. vulgatus/dorei*.

Some polysaccharides, especially those present in the cell walls of dietary plants, occur in the same physical context and presumably traverse the gut together, potentially exerting selective pressure for bacteria to use them simultaneously. To test for co-occurrence of traits, we performed a pairwise correlation analysis to determine the extent to which any two polysaccharides were co-utilized by the same strain (**Fig. S5**). The presence of two different soluble starches (potato and maize amylopectin) and two starch-like glycans (glycogen and pullulan) provide an internal control since they are essentially identical in their sugar and linkage chemistry but vary in the proportion and placement of branches as well as polymer length, crystallinity and solubility (**Fig. S1**). These four molecules are utilized through a single degradation/transport system in the type strain of *B. thetaiotaomicron*, which was included in our study (33). As expected, the abilities to use these four polysaccharides were among the strongest positive correlations (between 44-75%); although, there was not a perfect correlation suggesting that some finer adaptation may exist even for different structural forms of a chemically similar molecule.

We also observed positive correlations in the ability to use components of two different groups of plant cell wall polysaccharides (pectins and hemicelluloses), as well as animal tissue glycosaminoglycans, despite the fact that the polysaccharides within each of these groups often possess different chemical structures (**Fig. S1**). In the case of the hemicelluloses, there was even some apparent separation based on dicotyledonous vs. monocotyledonous sources. The predominantly dicot hemicelluloses (**Fig. 2**, blue labels) and monocot hemicelluloses (**Fig. 2**, green labels) show some exclusivity with respect to the bacteria that utilize them. Many *B. ovatus/B. xylanisolvens* strains lack the ability to utilize the three dicot hemicelluloses (GalM, GlcM, XyG); whereas the ability to degrade those from monocots (OSX, WAX, BBG) is more evenly distributed. *B. uniformis* has a partially opposite pattern, preferring substrates from dicots, while only degrading one of the two major monocot structures (BBG) and poorly degrading the two xylans tested (OSX, WAX). Similar observations were also made for pectins and GAGs and could reflect adaptations to simultaneously harvest different nutrients from digesta particles derived from dicot plant cell walls or animal tissue ingested in a carnivorous diet.

Specialization for mucus *O*-linked glycans

The most noteworthy correlation between polysaccharide utilization traits was observed between utilization of host-produced mucin *O*-glycans and many of the other polysaccharides tested. Growth on a total of 19/30 polysaccharides showed negative correlations with the ability to utilize *O*-glycans, with the strongest negative correlations being between *O*-glycans and the seven different hemicelluloses (**Fig. S5**). This negative correlation is easily observed by comparing the rightmost column in **Fig. 2** (*O*-glycan utilization) with the respective columns for hemicellulose degradation. Because this trend was observed across several species, it suggests that there could be a more general exclusive relationship between the two niches associated with foraging on mucus and hemicellulose. This idea is further supported by experiments described below, which suggest that isolates of *B. ovatus* and *B. xylanisolvens*, both adept hemicellulose consumers, are in the process of losing the ability to degrade *O*-glycans, relative to an ancestor that contained multiple gene clusters involved in the metabolism of these structures.

Interestingly, the mucin *O*-glycan mixture was the only substrate for which we observed absolute metabolic specialization among the substrates tested. A single, and only available strain of *Barnesiella intestinihominis* exhibited the ability to exclusively utilize mucin *O*-glycans, along with a subset of the sugars that are contained in these structures (**Table S1**). Three strains of

Bacteroides massiliensis exhibited similar behavior with very strong growth on mucin *O*-glycans and only weak growth on soluble starches and a few other polysaccharides (**Table S1**). These three *B. massiliensis* strains were also restricted in the repertoire of simple sugars they could metabolize with this list being limited to those found in mucin and other host glycans (galactose, *N*-acetylgalactosamine, *N*-acetylglucosamine, *N*-acetylneuraminic acid and L-fucose; weak fructose utilization by one strain was the only exception). Members of these two species are poorly represented in culture collections and remain lightly studied. However, their specific adaptations for host mucin glycans may render them important members of the microbiota, potentially thriving at the interface between the gut lumen and host tissue and relying exclusively on the host to be sustained. The continuous supply of mucin *in vivo* could explain why some species have become specialized for it as a nutrient, whereas dietary fiber degraders may need to be more generalist since the substrates available to them change with the host's meals.

Pangenome reconstruction reveals extensive genetic diversification among related *Bacteroides*

With a view of the carbohydrate utilization traits present in our gut Bacteroidetes collection, we next sought to determine if certain variable traits were being gained or lost within strains of certain species and if available genomes provide insight into the mechanisms driving genomic adaptations to particular nutrients. Connections between polysaccharide utilization phenotypes and the underlying genes involved have been systematically explored for a few *Bacteroides* species (*B. thetaiotaomicron, B. ovatus* and *B. cellulosilyticus*) with partial analyses in others (6, 16, 22, 23, 34-37). These studies have revealed that, in essentially all cases, the ability to degrade a particular polysaccharide is conferred by one or more clusters of co-expressed genes termed polysaccharide utilization loci (PULs) (38). PULs share defining features such as genes encoding homologs of outer membrane TonB-dependent transporters (SusC-like), surface glycan-binding proteins (SGBPs; or SusD- and SusE/F-like), usually an associated sensor/transcriptional regulator and one or more degradative CAZymes (glycoside hydrolase, GH; polysaccharide lyase, PL; carbohydrate esterase, CE), as well as other enzymes like sulfatases or proteases. Since the presence of one or more cognate PULs is required to utilize a given polysaccharide and these genes typically exhibit large increases in gene expression in response to their growth substrate, we rationalized that we could focus on traits that were variable in closely related strains and locate the associated PULs by transcriptomic analysis to gain insight into the basis of their acquisition or loss.

To test this, we focused on members of two closely related species, *B. ovatus* (*Bo*) and *B. xylanisolvens* (*Bx*), for which there is noticeable inter-strain variation in the ability to use mucin *O*-glycans (**Figs. 2, 3**). Investigation of these two species also benefits from substantial culture depth and many strains with available sequences. The *O*-glycans attached to mucins represent a diverse family of over one hundred different structures (39), albeit with common linkage patterns (**Fig. S1**). Correspondingly, the ability to utilize these glycans is a complex trait, involving simultaneous expression of at least 6-13 different *O*-glycan inducible PULs in *B. thetaiotaomicron, B. massiliensis*, *B. fragilis* and *B. caccae* (6, 22, 35). Quantification of *O*-glycan growth for individual *Bo* and *Bx* strains was widely variable (**Fig. 3B**). One hypothesis to explain this variability is that some *Bo* and *Bx* strains have gained the ability to utilize *O*-glycans relative to an ancestor that lacked this phenotype. If so, the PULs they express during *O*-glycan degradation might be unique to their genomes and may indicate lateral gene transfer (LGT) as has been the case for acquisition of phenotypes such as porphyran, agarose and λ-carrageenan utilization in gut *Bacteroides*, which are all components of integrative conjugative elements or mobilizable plasmids (31, 40). An alternative hypothesis is that some *Bo* and *Bx* strains are in the process of losing this ability from a common ancestor. If so, the genomes of non-degraders may still contain some PULs that are homologous to those present in more proficient *O*-glycan-degrading strains, but these strains may have lost a key step(s) that has eroded their ability to express this phenotype.

To distinguish these hypotheses, we selected seven strains (black arrows in **Fig. 3B**) that vary in their ability to degrade *O*-glycans and for which genome sequences exist. Note that three strains that degrade *O*-glycans were initially chosen because they were among the strongest degraders in our dataset with sequenced genomes when we initiated these experiments. We later identified strains with better *O*-glycan growth abilities and address one of these (strain H59) separately below. Four of the selected strains were *Bo* (two positive and two negative for *O*-glycan degradation); three strains were *Bx* (one weakly positive and two negative for *O*-glycan degradation). One of these strains (*B. xylanisolvens* XB1A) has a finished circular genome and was used as a scaffold to align the remaining six draft genome sequences, with manual curation (see *Material and Methods*), resulting in a nearly contiguous pangenome sequence that captures the spatial arrangement of homologous and variable genes that are present in these seven strains (**Table S2**, **Fig. S6**).

Analysis of the *Bo/Bx* pangenome revealed remarkable variability in gene content among just the seven strains used. A total of 12,960 different genes were delineated based on ≥90% identity in their translated amino acid sequence (**Table S2**). Remarkably, only 2,264 (17.5%) of these genes were shared among all seven strains. The largest proportion of genes (7,244; 55.9%) was only present in one of the seven strains. Separating two major classes of core PUL functions, SusC/D homologs and degradative CAZymes (GH, PL and CE), revealed that these key components of Bacteroidetes polysaccharide metabolism were also heavily represented in the "accessory gene" pool that is not common to all strains (**Fig. 4A**).

Through informatics-based and manual annotation of gene clusters containing typical PUL functions, we delineated between 180-236 different PULs in the reconstructed pangenome (ambiguity is caused by many PULs occurring adjacent to each other; although in many cases separation of adjacent PULs according to individual genomes allowed us to make more precise delineations, **Table S3**). Direct comparison of the *O*-glycan-degrading and non-degrading strains revealed that there was a substantial number of genes (3,351) that were unique to the three *O*-glycan degrading strains, including genes belonging to 51 PULs (**Fig. 4B**). However, such a distribution in gene content might be expected given the overall large proportion of non-core genes in these seven strains and there was correspondingly no indication that all three *O*-glycan-degrading strains shared overlapping PULs with each other: no PULs were common to all three *O*-glycan degraders and only five PULs were shared by any two strains (**Fig. 4C**). Considering that there are 51 total PULs that are unique to the mucin-degrading strains, if these strains have gained the ability to degrade *O*-glycans from an ancestral lineage that lacked this ability it likely occurred by acquisition of separate gene clusters. To more directly distinguish between the two hypotheses given above, we performed transcriptional profiling on all three *O*-glycan degrading strains to determine if the PUL genes that they express during *O*-glycan degradation are indeed unique to these strains.

Compared to reference growth in minimal medium containing glucose (MM-glucose), the *Bx* D22, *Bo* 3-1-23 and *Bo* D2 strains activated expression of 196, 227 and 359 total genes more than 10-fold and these gene lists included components of 14, 19, and 42 different PULs, respectively (**Tables S4-6**). As expected from studies in other *Bacteroides*, these PULs were scattered throughout the genome (**Fig. S7**), suggesting that they are autonomously regulated in response to glycan cues present in the *O*-glycan mixture. Strikingly, the majority of PULs that contained *O*-glycan-activated genes (63/75, 84%) were *not* unique to the *O*-glycan degrading strains (**Tables S4-S6, Fig. S7**). Moreover, in each of the three strains analyzed, the most highly upregulated PULs were also often shared with non-mucin degrading strains. These observations lend support to the hypothesis that strains of *Bo* and *Bx* are in the process of losing the ability to utilize *O*-glycans relative to a common ancestor that possessed a more expansive gene repertoire to successfully access these nutrients. However, we cannot rule out that individual non-degrading strains are separately acquiring PULs that are associated with mucin degradation and retaining them without the full benefit that presumably occurs with the ability to fully execute this growth phenotype. This latter idea is consistent with inter-species PUL exchange observations elaborated on below.

Finally, because we subsequently identified a *B. ovatus* strain (NLAE-zl-H59, red arrow in **Fig. 3B.**) with a substantially higher ability to use *O*-glycans relative to the strains used for pangenome construction, we performed additional RNA-seq analysis on this strain. Compared to a glucose reference, this strain activated 373 total genes in response to *O*-glycans, including genes from 30 different PULs (**Table S7**). Among these, 26 activated PULs were also present in one of the seven strains in our pangenome and 24 were homologous to PULs in strains that did not degrade *O*-glycans. However, this strain did activate expression of genes within four PULs that were completely unique to its genome compared to the seven strains used for pangenome reconstruction, suggesting that it could possess additional genes that augment its ability to grow on mucin *O*-glycans. This increased PUL expression could be responsible for the enhanced growth of the H59 strain on *O*-glycans, especially if genes included within these unique PULs are responsible for key metabolic steps required for efficient *O*-glycan utilization.

Evidence that intergenomic recombination has driven *Bacteroides* pangenome evolution

Similar to other bacteria, we observed that many accessory genes in the *Bo* and *Bx* pangenome are located in contiguous clusters or "islands" often involving PULs or capsular polysaccharide synthesis gene cluster (**Fig. S6**, **Table S2**). In contrast to previously identified *Bacteroides* PULs that have more obviously been subjects of lateral transfer (31, 40, 41) and are associated with integrative and conjugative elements (ICEs), most of the variable genomic regions that we identified were not associated with functions indicative of mobile DNA. Instead, these regions are often precisely located in between one or more core genes (*i.e.*, those common to all seven strains; herein referred to as "genomic nodes") that flank each side of the variable gene segment (**Fig. 5A,B**).

Several intergenomic transfer mechanisms might cause the observed mosaic structure of the *Bo-Bx* pangenome. The first possibility is movement of variable genes into a recipient genome by direct conjugation of individual, mobile ICEs. While such events would be expected to leave behind residual genes involved in mobilization and transfer, which were not observed, these DNA vehicles are known to target a subset of core genes, such as tRNAs (41), and may have undergone subsequent genomic deletion events that eliminated the mobile DNA. Two other known mechanisms of bacterial LGT are natural competence and phage transduction, neither of which has been observed in members of the Bacteroidetes.

A final potential mechanism is direct conjugation of the chromosome from a donor bacterium into a related recipient, followed by subsequent homologous recombination between flanking nodes to add or delete intervening DNA in the recipient genome (**Fig. 5C**). A mechanism that is conceptually similar to high-frequency recombination (Hfr) transfer in *E. coli* has been described for *B. thetaiotaomicron* and *B. fragilis* and involves chromosomal ICEs, which may have lost their ability to transfer autonomously by circularizing from the genome and instead act as transfer initiation points to conjugate a donor genome into a recipient (42-44). If such a mechanism was more broadly active in LGT between *Bacteroides*, we would expect that some of the core/node genes involved would reflect sequence identities that were more similar to the donor and this difference would be more easily detectable if the transfer was between members of different species like *Bo* and *Bx*. Moreover, such transfer events could either result in introduction of new genes into the recipient or elimination of genes depending on the genetic content in between recombination nodes from the donor chromosome.

To test this hypothesis, we took a bioinformatics approach aimed at first identifying high-confidence examples of inter-species recombination involving core genes and then assessed whether those genes were associated with co-transfer of adjacent accessory genes (**Fig. 6A**). We collected a dataset of 33 *Bo* and *Bx* genomes, which represent a subsample of the isolates for which we generated phenotypic data. We identified a set of 1,384 core genes—expectedly smaller than the core genome of the seven strains used above due to additional strains being added—that are present as a single copy in all members of both species. To identify cases of putative inter-species LGT via homologous recombination at core genes, we searched for instances in which a core gene sequence was more similar to the corresponding sequence from the other species than to sequences of the species to which a strain belonged. To this end, for each allele of each core gene, we calculated the median distance to all other alleles of both species (**Fig. 6B**). We identified instances where the median distance to the same species was high and median distance to the opposite species was low and used these genes as markers for putative LGT core loci. To identify additional accessory genes that may have been simultaneously transferred, we searched for instances in which genes were perfectly syntenic and collinear between each genome with a putative LGT core gene and genomes of the opposite species. Among these candidate LGT loci, we then investigated if any of these transfer events have resulted in pan-genome diversification, which we defined as the presence of any accessory gene(s) that was only observed adjacent to a core gene with evidence of LGT based on the above criteria.

In total, we identified 29 different loci at which exchange of core genes appeared to have occurred and LGT accessory genes were identified, including seven that appeared to involve transfer of PULs (**Fig. 6C**, **Fig. S8**). Similar numbers of potentially transferred loci were identified for each species, with 16 loci in *Bx* and 13 loci in *Bo*. Within the identified HGT events, variable numbers of HGT accessory genes were found within the loci ranging from one to thirteen genes (**Fig. 6C**, **Fig. S8**). More genes (57 total) appeared to be transferred into *Bo* than into *Bx* (36 total).

Finally, we determined if any of the identified LGT events could explain differential phenotypes measured by our high throughput growth assay by modifying the complement of PULs in individual genomes. As a specific example, we focused on a PUL that was previously associated with β-mannan degradation (23, 45) that was among our candidate loci with evidence of transfer from a *Bx* ancestor into two *Bo* strains. The presence of this PUL (PUL-A in **Fig. 6C, Fig. S9A**) was observed in all strains with the ability to grow on the β-mannan galactomannan (GalM), including two strains of *Bo* (ATCC8483 and CL02T12C04) for which the flanking node regions were more similar to *Bx*. We previously showed that deletion of this PUL from *B. ovatus*

ATCC8483 eliminated growth on GalM and glucomannan (GluM) (45), suggesting that it was both acquired from a *Bx* strain and conferred growth on these two β-mannans. However, the presence of this PUL was not perfectly correlated with growth on GalM and several strains that lacked PUL-A still exhibited robust growth. Thus, we searched for other PULs that harbor GH26 family enzymes and determined that all of the other strains that grow on GalM, but lack PUL-A, harbor another candidate GalM PUL (PUL-B, **Fig. S9A**) at a different genomic location and some strains possess both (**Fig. 6C**). Gene expression analysis by qPCR revealed that PUL-B was highly expressed in strains that lacked PUL-A during growth in GalM (**Fig. S9B**) and every strain that grew robustly on GalM had at least one of these two PULs. While we had previously shown that PUL-A was required for GluM growth in *B. ovatus* ATCC8483, there were a number of other strains (red "+" symbols in **Fig. 6C**) that displayed some ability to grow only on GlcM, while lacking both of the GalM-associated PULs, suggesting the presence of additional, partially orthogonal PULs that confer the ability to grow on variant β-mannans. Such a presence of multiple orthologous PULs that confer the same or similar functions, and some which may be moving between genomes of related species by the putative LGT mechanisms noted above, complicates the process of understanding the genotype-phenotype relationships in human gut Bacteroidetes, but will need to be resolved to make better functional predictions from sequence-based data.

Discussion

In this study we leveraged a scalable, high-throughput quantitative growth platform to characterize the phenotypic abilities that are present in a sample of hundreds of Bacteroidetes strains from the human and animal gut. Our anaerobic screening technique is directly applicable to other bacterial phyla from the human gut and other environments. Moreover, it can be adapted to include new polysaccharides or to focus on different nutrient utilization or chemical resistance phenotypes. The current study, in concert with future applications of phenotypic screening, will help close the gap between our largely sequence-based view of the human gut microbiota and the functions that its members provide. However, instances like the ones investigated here for mucin glycan and β-mannan utilization by *Bacteroides* serve as a warning that the presence or absence of genes that are experimentally associated with a particular function do not always indicate that the phenotype is expressed or not.

Pangenome reconstruction for *Bo* and *Bx* revealed extensive variability between strains of these closely related species, which is not unexpected for bacteria that engage in LGT. However, the lack of mobile DNA signatures for the majority of accessory genes and evidence of inter-genomic recombination between species at core genes provides new insight into what may be a prominent mechanism of genome diversification in members of this phylum. The previously described intergenomic transfer mechanisms in *B. thetaiotaomicron* and *B. fragilis* required the presence of active or inactive ICEs, highlighting the potential roles for these mobile elements in not just shaping genomes directly but also indirectly through their ability to catalyze exchange of broader genomic segments. In *B. thetaiotaomicron,* genome transfer was determined to initiate at genomically-integrated ICEs of which there are four in the type strain of *B. thetaiotaomicron* (VPI-5482). These have not been shown to be fully functional for circularization and mobilization. However, introduction and activation of an additional, excision-proficient conjugative transposon (either cTnDOT or cTnERL) (42), which share common features with the genomic ICEs, catalyzed expression of genes in the genomic ICEs and transfer of parts of the genome in a manner that requires *recA* and homologous DNA to be present in the recipient (42).

An additional study in *B. fragilis* showed that conjugation from a strain with multiple genomic ICEs, with one or more presumably retaining transfer activity, results in transfer of up to 435Kb of chromosome into a recipient that initiates near genomic ICEs, with individual transfer events being of variable size. The latter observation suggests that intergenomic recombination could then occurs at different homologous regions (*i.e.*, the core gene nodes observed in the pangenome), which could depend on the amount of genomic DNA transferred and the length/homology of available recombination sites. Given that the number of ICEs in individual genomes is variable, and their ability to be activated by functional conjugative transposons that are circulating in the ecosystem may also vary, it will be interesting to determine in future work if there are hotspots for genome transfer or if certain strains/species are dominant genome donors that could play a disproportionate role.

The phenotypic similarity between members of the same species (*e.g.*, *Bo* and *Bx*) and the large amount of gene diversity, including genes involved in carbohydrate metabolism, presents a paradox and raises the question of why the genome diversification observed in strains of *Bo* and *Bx* has not pushed members of these species to behave more differently and cluster based on phenotype with members of other species. One answer may be the apparent exclusion of some traits, such as mucin *O*-glycan/hemicellulose metabolism, which may limit the fitness advantage associated with acquiring new phenotypes. A second emerges from the proposed genome-exchange mechanism for which we offer new experimental support. Since this intergenomic exchange relies on homologous recombination, its frequency should decrease between genomes that are more divergent. Thus, this strategy may be one mechanism through which only closely related bacteria can share traits that are advantageous with other close relatives. The presence of orthologous PULs that confer the same function (*e.g.*, GluM and GalM utilization), some of which appear to be subjected to LGT, further complicates interpretations of genotype-to-phenotype relationships in these bacteria. Notably, the genome transfer mechanism proposed here does not account for how new genes can be incorporated between conserved nodes. Rather, this variability must pre-exist among different strains and therefore be created by different inter- and intragenomic diversification mechanisms. Nevertheless, the data that we report here underscore the notion that individual gut symbiont genomes are not just highly variable, but also dynamically so.

Materials and methods

Bacterial strains and growth conditions

A total of 354 human and animal gut Bacteroidetes were included in this study. A complete list is provided in **Table S1**, along with species designation based on 16S rRNA gene sequencing and associated meta-data. Dr. Abigail Salyers (University of Illinois, Urbana-Champagne) kindly provided many of the strains and two large portions of this collection were isolated over several decades: 99 strains with “WH” designations were collected from fecal samples of healthy human volunteers as part of the Woods Hole Summer Course on Microbial Diversity in the late 1990s; 95 additional strains with “VPI” designations were collected from human samples at the Virginia Polytechnic Institute in the 1960s-1970s. Species classifications were made based on alignment of a minimum of 734 bp of 16S rRNA gene sequence to a database containing the type strains of >29 named human gut Bacteroidetes species using the classify.seqs command with Bayesian settings in the program mothur (46); assignment for each strain was also manually checked by Blast (47). Isolates with ≥98% 16 rDNA gene sequence identity to the type strain of a named species were labeled with that species designation. This classification strategy included all except for three of the 354 strains examined, which ranged between 96.6 to 96.7% sequence identity to the *B. uniformis* ATCC type strains and based on sequential isolate numbers might be clones from the same individual (see WH15, WH16, WH17 entries in **Table S1**). Because of the small number of strains that did not satisfy our 98% cutoff, we grouped these unclassified strains with their nearest relative and label them as more divergent in **Table S1**; although, in most cases the carbohydrate phenotypes of these strains were very similar to other members of the *B. uniformis* group.

All strains were routinely grown in an anaerobic chamber (Coy Lab Products, Grass Lake, MI) at 37°C under an atmosphere of 5% H_2, 5% CO_2, and 90% N_2 on brain-heart infusion (BHI, Beckton Dickinson) agar that included 10% defibrinated horse blood (Colorado Serum Co.) and gentamicin (200 µg/ml). A single colony was picked into either tryptone-yeast extract-glucose (TYG) media (48) or modified chopped-meat carbohydrate broth (**Table S8**) and then sub-cultured into a minimal medium (MM) formulation that contained a mixture of monosaccharides, vitamins, nucleotides, amino acids and trace minerals (**Table S2** provides components and a complete recipe).

Carbohydrate growth array setup and data collection

Two different minimal medium formulations were used in the carbohydrate growth arrays (**Table S1** lists the formulation used for each isolate). The simpler of the two formulations (medium 1) was identical to the above MM, except that no carbohydrates were included and the medium was prepared at 2X concentration. The second minimal medium formulation (medium 2) was identical to medium 1, but included beef extract (0.5% w/v final concentration) as an additional supplement. We initially attempted to cultivate all of the species tested using only medium 1, but determined that beef extract was specifically required to allow growth of some species, especially *Parabacteroides* spp., *Barnesiella intestinihominis*, *Odoribacter splanchnicus* and the branch of *Bacteroides* that includes *B. plebeius* and *B. massiliensis*. Growth in the absence of an added carbohydrate source was generally not observed ot very low, except with *Parabacteroides* that may be able to grow to a low level on the added 0.5% beef extract. The corresponding negative control wells for each strain assayed were averaged and this value subtracted from the total growth calculation of the corresponding to strain on other carbohydrates tested. Despite several attempts to supplement minimal media with different components or employ more stringent anaerobic methods, we were unable to cultivate several common Bacteroidetes genera/species (*Prevotella* spp., *Paraprevotella* spp., *Alistipes* spp., and *Bacteroides coprocola* and *Bacteroides coprophilus*) in these two MM formulations and therefore did not include them in this study. All of these isolates readily grew in rich medium, suggesting that they have specific nutritional requirements that were not met in the MM formulations used.

Carbohydrate growth arrays were run as described previously (23) using a list of 45 carbohydrates (**Table S9**) that were present in duplicate, non-adjacent wells of a 96-well plate; two additional wells contained no carbohydrate and served as negative controls. Each MM was prepared as a 2X concentrated stock without carbohydrates (MM-no carb). An aliquot of each strain was taken from a MM-monosaccharides culture (grown for 16-20 h) and was centrifuged to pellet cells. Bacteria were resuspended in the same volume of 2X MM-no carb and then centrifuged again prior to suspension in a volume of 2X MM-no carb that was equal to the original volume. These washed bacterial cells were then inoculated at a 1:50 ratio into 2X MM-no carb and the suspension was added in equal volume (100µl/well) to the 96 wells of the carbohydrate growth array. Each well of the carbohydrate growth array contained 100µl of 2X carbohydrate stock (10-20mg/ml); thus, when diluted 2-fold resulted in 1X MM containing a unique carbohydrate and a bacterial inoculum that was identical to other wells. Growth arrays were monitored at kinetic intervals of 10-20 minutes using a microplate stacking device and coupled absorbance reader (Biotek Instruments; Winooski, VT) and data recorded for 4 d (variable kinetic interval times reflect variations in the number of microtiter plates present in a given batch).

Carbohydrate growth array data processing

Growth data were processed according to the following workflow: 1. data for each strain were exported from Gen5 software (Biotek Instruments; Winooski, VT) into Microsoft Excel and a previously described automated script was employed to call the points at which growth began (min) and ended (max) (23); 2. Each file was manually checked to validate that appropriate calls were made and the min and max values edited if needed (generally, only due to obvious baselining artifacts or erroneously high calls caused by temporary bubbles or precipitation); 3. "total growth" (A_{600} max – A_{600} min) and "growth rate" [(A_{600}max – A_{600} min) / (t max – t min) were calculated for each strain on each substrate (A_{600} is the absorbance value at 600 nm that corresponds to each min and max point; t is the corresponding time values in minutes); 4. Individual cultures in which total growth was ≤ 0.1 were scored as "no growth" and their A_{600} values converted to 0. Only assays in which both replicates showed an increase in A_{600} ≥ 0.1 were considered as growth; if the two replicate assays were discordant (one positive, one negative), then both values were converted to zero.

To normalize the results for each strain, the substrate(s) that provided maximum total growth and growth rate values were determined and these were set to 1.0. All other growth values for a given strain were normalized to this maximum value, providing a range of values between 0 and 1.0. We next normalized growth ability across individual substrates using the previously normalized values for each individual strain: the strain with the maximum total growth and growth rate values were identified (many of these were already set to 1.0). Then, the corresponding values for each other species on that particular substrate were calculated as a fraction of the maximum value for that substrate, yielding a range of values between 0 and 1.0 for each substrate. These values were used to create the heat map shown in **Figs. 2** and **S3** and all raw and normalized values are provided in **Table S1**.

Data clustering and statistics

Heatmaps and corresponding dendrograms were generated using the "heatmap" function in the "stats" package of R (version 3.4.0) which employs unsupervised hierarchical clustering (complete linkage method) to group similar carbohydrate growth profiles. Pearson Correlation was used to calculate co-occurrence of the ability to grow on each pair of different substrates. The normalized growth value for each substrate was compared to the corresponding growth values on all other substrates using the Pearson correlation test in R and these values are displayed in the Pearson correlation plot in **Figure S5**.

Pangenome reconstruction for *B. ovatus* and *B. xylanisolvens* strains

Since one of the seven strains used for pangenome reconstruction (*B. xylanisolvens* XB1A) was assembled into a single circular chromosome, we used this genome as a scaffold for the contigs representing the remaining six strains. Contigs from the six unfinished strains were aligned against the XB1A genome using a combination of Mauve (50), to align and orient larger contigs, and reciprocal best Blast-hit analysis using ≥90% amino acid identity to identify likely homologs, to provide finer resolution. Contigs from draft genome assemblies or *Bx* XB1A were broken as needed to accommodate the inclusion of unique accessory genes, but only in circumstances where genes on both sides of the break could be aligned to homologs in one or more genomes with a contig that spanned that break point. After constructing a preliminary assembly, we analyzed the size distribution of putative homologous ORFs as a measure of assembly accuracy and to identify variations in genetic organization that might be attributable to real genetic differences such as frame shifts, which would result in two homologous gene calls of smaller size in the genome containing the frameshift. Any variation >50% of homologous ORF size was inspected manually using the "orthologous neighborhood viewer, by best Blast hit" function in the U. S. Dept. of Energy Integrated Microbial Genomes (IMG) website. Introduced contig breaks are documented in **Table S2** and **Fig. S6**. GenVision software (DNAstar, Madison, WI) was used to visualize and label selected functions in the pan-genome assembly and also display RNAseq data as a function of shared and unique PULs.

RNAseq analysis

For RNAseq, *B. xylanisolvens* and *B. ovatus* cells were grown to mid-exponential phase on either purified mucin *O*-linked glycans (purified in house from Sigma Type III porcine gastric mucin) or glucose as a reference as previously described (22). Total RNA was extracted using an RNeasy kit (Qiagen), treated with Turbo DNase I (Ambion), and mRNA was enriched using the Bacterial Ribo-Zero rRNA removal kit (Epicentre). Residual mRNA was converted to sequencing libraries using TruSeq barcoded adaptors (Illumina) and sequenced at the University of Michigan Sequencing Core in an Illumina HiSeq instrument with 24 samples multiplexed per lane. Bar-coded data were demultiplexed and analyzed using the Arraystar software package with Qseq (DNAstar). All RNAseq data are publicly available from the National Institutes of Health Gene Expression Omnibus Database under accession numbers GSM4714867-GSM4714890.

Core gene determination and detection of LGT events between *Bo* and *Bx* strains

The core gene alignment was generated with cognac (51). The alignment was then partitioned into the individual component genes and approximate maximum likelihood gene trees were generated with fastTree (52). Co-phylogenetic distances were calculated with APE (53). A distance threshold of greater than 0.1 to the same species and less than 0.1 to the opposite species was used to identify alleles bearing signatures of HGT. All analyses were performed in R (version 3.6.3) (54). All code developed for this project are available at https://github.com/rdcrawford/bacteroides_hgt.

Acknowledgements

This work is dedicated to the memory of Dr. Cherie Ziemer. We thank Thomas Schmidt (University of Michigan) for helpful advice on developing the phenotype clustering score. We thank Abigail Salyers (University of Illinois, Urbana-Champagne) who kindly provided a large portion of the strains used in this work. Additional support with strain culture and resources was provided by Nadja Shoemaker (University of Illinois, Urbana-Champagne), Emma Allen-Vercoe (University of Guelph), Laurie Comstock (Harvard University), Jin-Woo Bae (Kyung-Hee University, Korea), Tomomi Kuwahara (Kagawa University, Japan) and Jeffrey Gordon

(Washington University). This work was supported by funds from the U.S. National Institutes of Health (DK084214, DK118024, DK125445), the University of Michigan Biological Sciences Scholars Program and pilot/feasibility grants from the University of Michigan Center for Gastrointestinal Research (NIDDK DK034933).

Competing Interests: The authors declare no competing interests.

Figure legends

Figure 1. Glycan degradation abilities among gut Bacteroidetes. (**A.**) The number of species out of 29 tested that degrade each polysaccharide is listed in order of decreasing degradation frequency from left to right. Since not all strains within a given species necessarily have the metabolic potential to utilize each polysaccharide, colors illustrate the percentage of strains within each degrading species that possess the indicated ability. (**B.**) The number of polysaccharides that a given species degrades in decreasing order. The number of strains tested for each species is listed in parentheses and colors represent the percentage of strains in each indicated species that degrade each glycan counted towards the total.

Figure 2. Heat map of individual polysaccharide utilization traits. Species are clustered by glycan utilization phenotype based on normalized total growth level (**Fig. S4B**). The magnitude of growth is indicated by the heatmap scale at the bottom right. Columns at the left indicate the source (human, animal) and time period of isolation. The cladogram at the far left shows the results of unsupervised clustering of the data based the normalized growth data shown. The

species designations at the right are the results of 16S rRNA gene sequencing (>98% identity to the species type strain was used to assign species). All raw and normalized growth and rate data for individual strains may be found in **Table S1** see **Fig. S3** for an expanded heatmap with monosaccharide data and individual strain names labels.

Figure 3. Host mucin *O*-glycan metabolism within the *Bacteroides*. (A.) A phylogenetic tree based on housekeeping genes that compares mucin *O*-glycan utilization across species. The diameter of the black circles represents the number of strains tested within each species (sample depth), whereas the size of the overlaid red circle corresponds to the number of strains exhibiting *O*-glycan metabolism. Note that some species have either full or no penetrance of this phenotypic trait yet others like *B. ovatus*/*B. xylanisolvens* have more extensive variability among strains. **(B.)** Strains of *B. ovatus* (blue) and *B. xylanisolvens* (green) that show variable growth abilities on mucin *O*-glycan (n=2 growth assays per bar, error bars are range between values). Gray histogram bars are total growth controls on an aggregate of the monosaccharides that all strains of these two species grow on (**Table S1**) and are provided as a reference for overall growth ability on a non *O*-glycan substrate. Data from two established *O*-glycan degraders, *B. massiliensis* and *B. thetaiotaomicron,* are also shown for reference. Species with black arrows were used for pangenome analyses to compare genetic traits associated with mucin *O*-glycan metabolism. We performed RNA-seq on three strains included in this pangenome analyses (black boxes) positive for *O*-glycan utilization and an additional strain, *B. ovatus* NLAE-zl-H59 (red arrow, box), to see if there were unique genes/PULs present in strains that have the ability to grow on mucin *O*-glycans.

Figure 4. Distribution of all genes as well as core polysaccharide utilization functions in the *Bo/Bx* pangenome. (A.) The left panel shows the number of core genes (*i.e.*, those present in all seven strains used for pangenome construction) compared to genes present in 2-7 of the individual strains. The right panel shows the same distribution of genes assigned to PULs or particular degradative CAZyme families (GH, PL, CE, see **Tables S2** and **S3** for more detailed assignments. **(B.)** The distribution of genes between mucin-degrading (n=3) and non-degrading (n=4) strains used to construct the pangenome. Top numbers indicate total genes, while numbers in parentheses indicate the number of PULs (not individual PUL genes) in each category. **(C.)** Distribution of the genes that are unique to the three mucin-degrading strains within each genome. Genes/PULs are numbered as described for B. Note that no PULs are shared by all three strains.

Figure 5. (A.) A higher-resolution view of a region of the *Bo/Bx* pangenome shows the variable presence of at least six different PULs occurring between three genomic nodes (nodes 33-35 in this quarter of the total pangenome. Segment 2 of the physical pangenome map was selected because the first segment initiated with numerous small contigs and this segment contained previously validated genes for xyloglucan metabolism (49). Node genes are colored red, while *susC*-like and *susD*-like genes are colored purple and orange, respectively, and glycoside hydrolase genes in light blue. GH family numbers are given below select PULs starting from the top to indicate potential specificity and new numbers are only added going down the schematic if the family assignments are different, indicating a different PUL. A well-studied *B. ovatus* PUL for xyloglucan degradation (49) is shown in the center and occurs variably between two nodes and also has variable gene content. The two bottom genomes are from different species, *Bacteroides finegoldii* (*Bfin*) and *Bacteroides fragilis* (*Bfra*) and show less complex genome architecture with the *Bfra* region possessing no PULs. **(B.)** A broader view of the genome region shown in A. showing that the same mosaic pattern is common across the pangenome. Only PULs are illustrated, although many other genes were also variable in these regions. The numbers at the bottom delineate the presence of 35 different core gene nodes (as in A. some nodes contain multiple core genes) in this section of the genome and the presence of homologous or unique PULs is illustrated according to the color code at right (see **Fig. S6** for high resolution physical maps of the pan-genome with PUL annotations). Note that in some cases up to five different PULs were located at one location **(C.)** A schematic showing the proposed mechanism of genome exchange based on previous studies (42-44) and observations presented here. Genomic ICEs that are either partially active (excision deficient, but capable of initiating DNA strand breakage and conjugation) or activated *in trans* by the presence of an exogenous conjugative transposon, initiate genome mobilization from a donor into a recipient. If sufficient homology between node genes exists in the recipient, homologous recombination between two nodes can replace a section of the recipient with a segment from the donor. Note that genomic regions are shown as linear fragments for simplicity, but would be circular.

Figure 6. (A.) Schematic of the workflow to identify putative LGT core genes: align genes and build corresponding trees for each core gene,determine the median substitution distances distances for each allele of a core gene in a given strain to both species, and identify loci with an identical conserved structure between isolates of opposite species. **(B.)** Plot of median distances for all core genes identified in the 33 genomes analyzed. The boxes show the regions containing genes for which the median distance was $\geq$0.1 to the assigned species for a given strain and $\leq$ 0.1 for the opposite species to which a strain is assigned. These genes were determined to be high-confidence examples of core/node genes that had been replaced by an allele from the other species. **(C.)** A region of the *Bo/Bx* pangenome that contains a PUL involved in galactomannan (GalM) and glucomannan (GluM) degradation. This PUL is present in six strains of *Bx* and two strains of *Bo* and in the latter cases flanking node genes exhibit signatures of being derived from LGT with a *Bx* donor (the yellow box highlights potential recombination region). The columns at the left indicate the growth of each strain on GalM or GluM. The ability to grow on GalM is fully correlated with the presence of one of two different PULs, or both, that are transcriptionally activated during growth on this substrate (**Fig. S9**) (23). Notably, some strains (red "+") are able to grow weakly on GluM but do not possess either of the identified PULs, suggesting that additional, partially orthologous PULs exist that confer the ability to use only GluM.

Supplementary Figure and Table Legends

Figure S1. Schematics of the polysaccharides used in this study with sugar composition and linkages schematized according to the "Symbol nomenclature for glycans" standard format and based on the symbol key provided at the right. Linkages are labeled as α or β and the number provided represents the carbon position in the recipient sugar. The carbon in the donor sugar is carbon-1 in all cases except N-acetyl neuraminic acid and is not shown. Note that pectic galactan (potato and lupin), xylan (oat spelt and wheat arabinoxylan) and amylopectin (potato and maize) can have variable structures based on plant source. Abbreviations for several polysaccharides are provided in parentheses and used throughout the text and figures.

Figure S2. Correlation of replicate growth and rate measurements. Two replicate measurements were made for each of the two parameters recorded, total growth (**A.**) and growth rate (**B.**) for each species on each carbohydrate substrate. Data points are color-coded based on whether the two replicates exhibited variation between 0-5% (black), 5-10% (blue), 10-20% (green), >20% (orange) or growth in one assay and no growth in the other (red). (**C.**) A linear function was fitted (with red points omitted) to calculate an r^2 value for the data set associated with utilization of each individual substrate. Measurements on some substrates were more variable than on others due, at least in part, to the tendency of these substrates to partially precipitate or retrograde during growth, which yielded variable levels of background absorbance.

Figure S3. A heatmap identical to the one shown in **Fig. 2** main text, except that monosaccharide growth data is included. Strain names are also noted at the far right (best viewed in electronic PDF form with magnification) and animal strains are labeled in red font.

Figure S4. (A.) A scheme for evaluating which aspects of growth phenotype data are most influential for clustering strains that belong to the same species using hypothetical *B. theta* data as an illustrative example. A quantitative index was used in which the number of strains tested is divided by the minimum number of branches needed to encompass all of the strains for that species, with a perfect score being “1” (*e.g.*, eight *B. theta* strains divided by the minimum of eight branches needed to encompass all strains in the top example). **(B.)** Actual clustering index data for the raw and normalized growth and rate data gathered for 354 different Bacteroidetes strains. M and P stand for “monosaccharide” and “polysaccharide” growth, respectively. One of the two most optimal conditions, which incorporates normalized growth data on polysaccharides only, was used to construct **Figs. 2** and **S3**.

Figure S5. A Pearson correlation plot to determine if individual growth abilities co-occur in the same strains. Positive or negative correlations that are ≥0.40 are shown in the colors indicated.

Figure S6. High-resolution maps of the entire reconstructed pangenome. These maps are provided in four separate parts due to their large size (labeled as **Fig. S6a, b, c, d**) and correspond to the data table provided in **Table S2**. Note that a 5th file is provided with information about the gene, locus and strand breaking legend data.

Figure S7. Circular pangenome and corresponding mucin *O*-glycan transcriptomics from *Bx* D22, *Bo* 3_1_23 and *Bo* D2 .

Figure S8. Individual maps of high-confidence inter-genomic exchange events between Bo and Bx strains.

Figure S9. (**A.**) Schematics of PUL-A and PUL-B associated with GalM and GlcM utilization. In *Bo* ATCC8384, elimination of PUL-A eliminates both of these growth abilities. (**B.**). Expression analysis by qPCR of two sentinel genes from PUL-B in *Bo* strain D2 that lacks PUL-A but still exhibits robust growth on GalM.

Table S1. Strain designations, growth levels, growth rates, host species, isolation periods, growth media, 16S rRNA similarities and, if applicable, public genome sequence references for all Bacteroidetes strains used in this study.

Table S2. Data table of the reconstructed pangenome of seven *Bo/Bx* strains. Additional notes are provided directly on the table.

Table S3. PULs that were delineated in the seven strain pangenome with annotations based on whether they were unique to mucin non-degrading strains, unique to mucin-degraders or shared between strains in both categories. Additional notes are provided directly on the table.

Table S4. Gene expression changes detected using whole-genome transcriptional profiling by RNA-seq of *B. xylanisolvens* D22 grown on mucin *O*-glycan as a sole carbon source compared to glucose reference. Additional notes are provided directly on the table.

Table S5. Gene expression changes detected using whole-genome transcriptional profiling by RNA-seq of *B. ovatus* 3-1-23 grown on mucin *O*-glycan as a sole carbon source compared to glucose reference. Additional notes are provided directly on the table.

Table S6. Gene expression changes detected using whole-genome transcriptional profiling by RNA-seq of *B. ovatus* D2 grown on mucin *O*-glycan as a sole carbon source compared to glucose reference. Additional notes are provided directly on the table.

Table S7. Gene expression changes detected using whole-genome transcriptional profiling by RNA-seq of *B. ovatus* NLAE-zl-H59 grown on mucin *O*-glycan as a sole carbon source compared to glucose reference. Additional notes are provided directly on the table.

Table S8. Liquid media recipes (sheet **A**) and components (sheet **B**) for growing the Bacteroidetes used in this study.

Table S9. Mono- and polysaccharides used in the phenotypic growth arrays and corresponding supplier or purification details.

References

1. Koropatkin NM, Cameron EA, Martens EC. How glycan metabolism shapes the human gut microbiota. *Nat Rev Microbiol*. 2012; 10: 323-35.

2. Flint HJ, Scott KP, Duncan SH, Louis P, Forano E. Microbial degradation of complex carbohydrates in the gut. *Gut microbes*. 2012; 3:289-306.

3. Porter NT, Martens EC. The Critical Roles of Polysaccharides in Gut Microbial Ecology and Physiology. *Annual review of microbiology*. 2017; 71: 349-69.

4. El Kaoutari A, Armougom F, Gordon JI, Raoult D, Henrissat B. The abundance and variety of carbohydrate-active enzymes in the human gut microbiota. *Nature reviews Microbiology*. 2013; 11: 497-504.

5. McNeil NI. The contribution of the large intestine to energy supplies in man. *The American journal of clinical nutrition*. 1984; 39: 338-42.

6. Desai MS, Seekatz AM, Koropatkin NM, Kamada N, Hickey CA, Wolter M, et al. A Dietary Fiber-Deprived Gut Microbiota Degrades the Colonic Mucus Barrier and Enhances Pathogen Susceptibility. *Cell*. 2016; 167: 1339-53.

7. Sonnenburg ED, Smits SA, Tikhonov M, Higginbottom SK, Wingreen NS, Sonnenburg JL. Diet-induced extinctions in the gut microbiota compound over generations. *Nature*. 2016; 529: 212-5.

8. Sonnenburg ED, Sonnenburg JL. Starving our microbial self: the deleterious consequences of a diet deficient in microbiota-accessible carbohydrates. *Cell metabolism*. 2014; 20: 779-86.

9. Wrzosek L, Miquel S, Noordine ML, Bouet S, Joncquel Chevalier-Curt M, Robert V, et al. *Bacteroides thetaiotaomicron* and *Faecalibacterium prausnitzii* influence the production of mucus glycans and the development of goblet cells in the colonic epithelium of a gnotobiotic model rodent. *BMC Biol.* 2013; 11: 61.

10. Ganapathy V, Thangaraju M, Prasad PD, Martin PM, Singh N. Transporters and receptors for short-chain fatty acids as the molecular link between colonic bacteria and the host. *Current opinion in pharmacology*. 2013; 13: 869-74.

11. Cook SI, Sellin JH. Review article: short chain fatty acids in health and disease. *Aliment Pharmacol Ther.* 1998; 12: 499-507.

12. Smith PM, Howitt MR, Panikov N, Michaud M, Gallini CA, Bohlooly YM, et al. The microbial metabolites, short-chain fatty acids, regulate colonic Treg cell homeostasis. *Science*. 2013; 341: 569-73.

13. Kim M, Qie Y, Park J, Kim CH. Gut Microbial Metabolites Fuel Host Antibody Responses. *Cell Host Microbe*. 2016; 20: 202-14.

14. Xu J, Mahowald MA, Ley RE, Lozupone CA, Hamady M, Martens EC, et al. Evolution of Symbiotic Bacteria in the Distal Human Intestine. *Plos Biol*. 2007; 5: e156.

15. Cantarel BL, Coutinho PM, Rancurel C, Bernard T, Lombard V, Henrissat B. The Carbohydrate-Active EnZymes database (CAZy): an expert resource for Glycogenomics. *Nucleic acids research*. 2009; 37: D233-D8.

16. McNulty NP, Wu M, Erickson AR, Pan C, Erickson BK, Martens EC, et al. Effects of diet on resource utilization by a model human gut microbiota containing *Bacteroides cellulosilyticus* WH2, a symbiont with an extensive glycobiome. *Plos Biol*. 2013; 11: e1001637.

17. Salyers AA, Vercellotti JR, West SE, Wilkins TD. Fermentation of mucin and plant polysaccharides by strains of *Bacteroides* from the human colon. *Appl Environ Microbiol.* 1977; 33: 319-22.

18. Salyers AA, West SE, Vercellotti JR, Wilkins TD. Fermentation of mucins and plant polysaccharides by anaerobic bacteria from the human colon. *Appl Environ Microbiol.* 1977; 34: 529-33.

19. Qin J, Li R, Raes J, Arumugam M, Burgdorf KS, Manichanh C, et al. A human gut microbial gene catalogue established by metagenomic sequencing. *Nature*. 2010; 464: 59-65.

20. Ley RE, Hamady M, Lozupone C, Turnbaugh PJ, Ramey RR, Bircher JS, et al. Evolution of mammals and their gut microbes. *Science*. 2008; 320: 1647-51.

21. Eckburg PB, Bik EM, Bernstein CN, Purdom E, Dethlefsen L, Sargent M, et al. Diversity of the human intestinal microbial flora. *Science*. 2005; 308: 1635-8.

22. Martens EC, Chiang HC, Gordon JI. Mucosal Glycan Foraging Enhances Fitness and Transmission of a Saccharolytic Human Gut Bacterial Symbiont. *Cell Host Microbe*. 2008; 4: 447-57.

23. Martens EC, Lowe EC, Chiang H, Pudlo NA, Wu M, McNulty NP, et al. Recognition and Degradation of Plant Cell Wall Polysaccharides by Two Human Gut Symbionts. *Plos Biol.* 2011; 9: e1001221.

24. Bloom SM, Bijanki VN, Nava GM, Sun L, Malvin NP, Donermeyer DL, et al. Commensal *Bacteroides* species induce colitis in host-genotype-specific fashion in a mouse model of inflammatory bowel disease. *Cell Host Microbe*. 2011; 9: 390-403.

25. Hickey CA, Kuhn KA, Donermeyer DL, Porter NT, Jin C, Cameron EA, et al. Colitogenic *Bacteroides thetaiotaomicron* Antigens Access Host Immune Cells in a Sulfatase-Dependent Manner via Outer Membrane Vesicles. *Cell Host Microbe*. 2015; 17: 672-80.

26. Mazmanian SK, Round JL, Kasper DL. A microbial symbiosis factor prevents intestinal inflammatory disease. *Nature*. 2008; 453: 620-5.

27. Lagkouvardos I, Pukall R, Abt B, Foesel BU, Meier-Kolthoff JP, Kumar N, et al. The Mouse Intestinal Bacterial Collection (miBC) provides host-specific insight into cultured diversity and functional potential of the gut microbiota. *Nat Microbiol*. 2016; 1: 16131.

28. Browne HP, Forster SC, Anonye BO, Kumar N, Neville BA, Stares MD, et al. Culturing of 'unculturable' human microbiota reveals novel taxa and extensive sporulation. *Nature*. 2016; 533: 543-6.

29. Lagier JC, Khelaifia S, Alou MT, Ndongo S, Dione N, Hugon P, et al. Culture of previously uncultured members of the human gut microbiota by culturomics. *Nat Microbiol*. 2016; 1: 16203.

30. Tramontano M, Andrejev S, Pruteanu M, Klunemann M, Kuhn M, Galardini M, et al. Nutritional preferences of human gut bacteria reveal their metabolic idiosyncrasies. *Nat Microbiol.* 2018; 3: 514-22.

31. Hehemann JH, Kelly AG, Pudlo NA, Martens EC, Boraston AB. Bacteria of the human gut microbiome catabolize red seaweed glycans with carbohydrate-active enzyme updates from extrinsic microbes. *Proceedings of the National Academy of Sciences of the United States of America*. 2012; 109: 19786-91.

32. Tamura K, Hemsworth GR, Dejean G, Rogers TE, Pudlo NA, Urs K, et al. Molecular mechanism by which prominent human gut Bacteroidetes utilize mixed-linkage β-glucans, major health-promoting cereal polysaccharides. Cell Reports. 2017; 21: 417-430.

33. Shipman JA, Berleman JE, Salyers AA. Characterization of four outer membrane proteins involved in binding starch to the cell surface of *Bacteroides thetaiotaomicron*. *J Bacteriol.* 2000; 182: 5365-72.

34. Déjean G, Tamura K, Cabrera A, Jain N, Pudlo N, Holm Viborg A, et al. Synergy between cell-surface glycosidases and glycan-binding proteins dictates the utilization of specific beta(1,3)-glucans by human gut *Bacteroides*. *mBio*. 2020; 11: e00095-20.

35. Pudlo NA, Urs K, Kumar SS, German JB, Mills DA, Martens EC. Symbiotic Human Gut Bacteria with Variable Metabolic Priorities for Host Mucosal Glycans. mBio. 2015; 6: e01282-15.

36. Despres J, Forano E, Lepercq P, Comtet-Marre S, Jubelin G, Chambon C, et al. Xylan degradation by the human gut *Bacteroides xylanisolvens* XB1A(T) involves two distinct gene clusters that are linked at the transcriptional level. *BMC genomics*. 2016; 17: 326.

37. Sonnenburg ED, Zheng H, Joglekar P, Higginbottom SK, Firbank SJ, Bolam DN, et al. Specificity of polysaccharide use in intestinal *Bacteroides* species determines diet-induced microbiota alterations. *Cell*. 2010; 141: 1241-52.

38. Terrapon N, Lombard V, Drula E, Lapebie P, Al-Masaudi S, Gilbert HJ, et al. PULDB: the expanded database of Polysaccharide Utilization Loci. *Nucleic Acids Res*. 2018; 46:D677-D83.

39. Johansson ME, Holmen Larsson JM, Hansson GC. Microbes and Health Sackler Colloquium: The two mucus layers of colon are organized by the MUC2 mucin, whereas the outer layer is a legislator of host-microbial interactions. *Proceedings of the National Academy of Sciences of the United States of America*. 2011; 108 Suppl 1: 4659-65.

40. Pudlo NA, Vasconcelos-Pereira G, Parnami J, Cid M, Markert S, Tingley JP, et al. Extensive transfer of genes for edible seaweed digestion from marine to human gut bacteria. *Preprint.* 2021; BIORXIV/2020/142968.

41. Martens EC, Kelly AG, Tauzin AS, Brumer H. The devil lies in the details: how variations in polysaccharide fine-structure impact the physiology and evolution of gut microbes. *Journal of molecular biology*. 2014; 426: 3851-65.

42. Moon K, Sonnenburg J, Salyers AA. Unexpected effect of a *Bacteroides* conjugative transposon, CTnDOT, on chromosomal gene expression in its bacterial host. *Mol Microbiol.* 2007; 64: 1562-71.

43. Husain F, Tang K, Veeranagouda Y, Boente R, Patrick S, Blakely G, et al. Novel large-scale chromosomal transfer in *Bacteroides fragilis* contributes to its pan-genome and rapid environmental adaptation. *Microb Genom*. 2017; 3:e000136.

44. Whittle G, Hamburger N, Shoemaker NB, Salyers AA. A Bacteroides conjugative transposon, CTnERL, can transfer a portion of itself by conjugation without excising from the chromosome. *J Bacteriol*. 2006; 188: 1169-74.

45. Reddy SK, Bagenholm V, Pudlo NA, Bouraoui H, Koropatkin NM, Martens EC, et al. A beta-mannan utilization locus in *Bacteroides ovatus* involves a GH36 alpha-galactosidase active on galactomannans. *FEBS Lett*. 2016; 590: 2106-18.

46. Schloss PD, Westcott SL, Ryabin T, Hall JR, Hartmann M, Hollister EB, et al. Introducing mothur: open-source, platform-independent, community-supported software for describing and comparing microbial communities. *Appl Environ Microbiol*. 2009; 75: 7537-41.

47. Altschul SF, Gish W, Miller W, Myers EW, Lipman DJ. Basic Local Alignment Search Tool. *J Mol Biol*. 1990; 215: 403-10.

48. Holdeman LV, Cato ED, Moore WEC. Anaerobe Laboratory Manual. Moore WEC, editor. Blacksburg, Va.: Virginia Polytechnic Institute and State University Anaerobe Laboratory; 1977.

49. Larsbrink J, Rogers TE, Hemsworth GR, McKee LS, Tauzin AS, Spadiut O, et al. A discrete genetic locus confers xyloglucan metabolism in select human gut Bacteroidetes. *Nature*. 2014;506(7489):498-502.

50. Darling AC, Mau B, Blattner FR, Perna NT. Mauve: multiple alignment of conserved genomic sequence with rearrangements. *Genome Res*. 2004; 14: 1394-403.

51. Crawford RD, Snitkin ES. cognac: rapid generation of concatenated gene alignments for phylogenetic inference from large, bacterial whole genome sequencing datasets. *BMC Bioinformatics*. 2021; 22: 70.

52. Price MN, Dehal PS, Arkin AP. FastTree: computing large minimum evolution trees with profiles instead of a distance matrix. *Mol Biol Evol.* 2009; 26: 1641-50.

53. Popescu AA, Huber KT, Paradis E. ape 3.0: New tools for distance-based phylogenetics and evolutionary analysis in R. *Bioinformatics*. 2012; 28: 1536-7.

54. R Core Team. R: A language and environment for statistical computing. R Foundation for Statistical Computing, Vienna, Austria. 2017; URL https://www.R-project.org/.

Figure 1

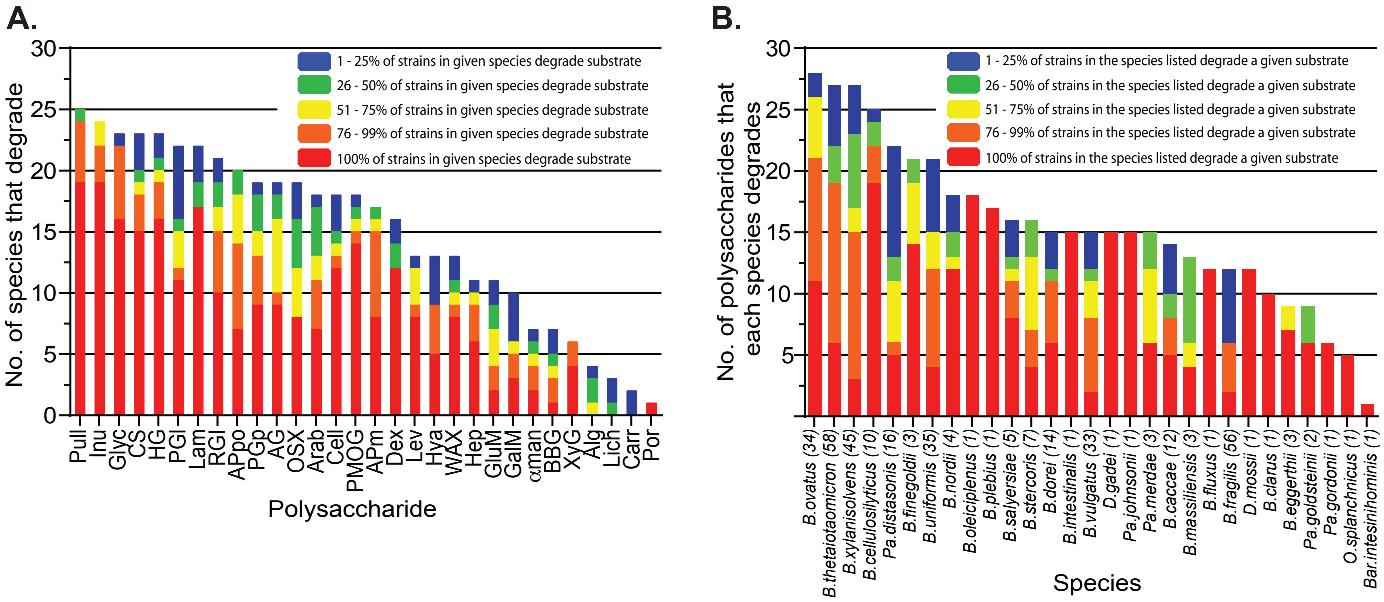
A.
30
25
20
15
10
5
0
No. of species that degrade
🟦 1 - 25% of strains in given species degrade substrate
🟩 26 - 50% of strains in given species degrade substrate
🟨 51 - 75% of strains in given species degrade substrate
🟧 76 - 99% of strains in given species degrade substrate
🟥 100% of strains in given species degrade substrate
Pull
Inu
Glyc
CS
HG
PGl
Lam
RGI
APpo
PGp
AG
OSX
Arab
Cell
PMOG
APm
Dex
Lev
Hya
WAX
Hep
GluM
GalM
αman
BBG
XyG
Alg
Lich
Carr
Por
Polysaccharide
B.
30
25
20
15
10
5
No. of polysaccharides that each species degrades
🟦 1 - 25% of strains in the species listed degrade a given substrate
🟩 26 - 50% of strains in the species listed degrade a given substrate
🟨 51 - 75% of strains in the species listed degrade a given substrate
🟧 76 - 99% of strains in the species listed degrade a given substrate
🟥 100% of strains in the species listed degrade a given substrate
B.ovatus (34)
B.thetaiotaomicron (58)
B.xylanisolvens (45)
B.cellulosilyticus (10)
Pa.distasonis (16)
B.finegoldii (3)
B.uniformis (35)
B.nordii (4)
B.oleiciplenus (1)
B.plebius (1)
B.salyersiae (5)
B.stercoris (7)
B.dorei (14)
B.intestinalis (1)
B.vulgatus (33)
D.gadei (1)
Pa.johnsonii (1)
Pa.merdae (3)
B.caccae (12)
B.massiliensis (3)
B.fluxus (1)
B.fragilis (56)
D.mossii (1)
B.clarus (1)
B.eggerthii (3)
Pa.goldsteinii (2)
Pa.gordonii (1)
O.splanchnicus (1)
Bar.intesinihominis (1)
Species

Figure 2

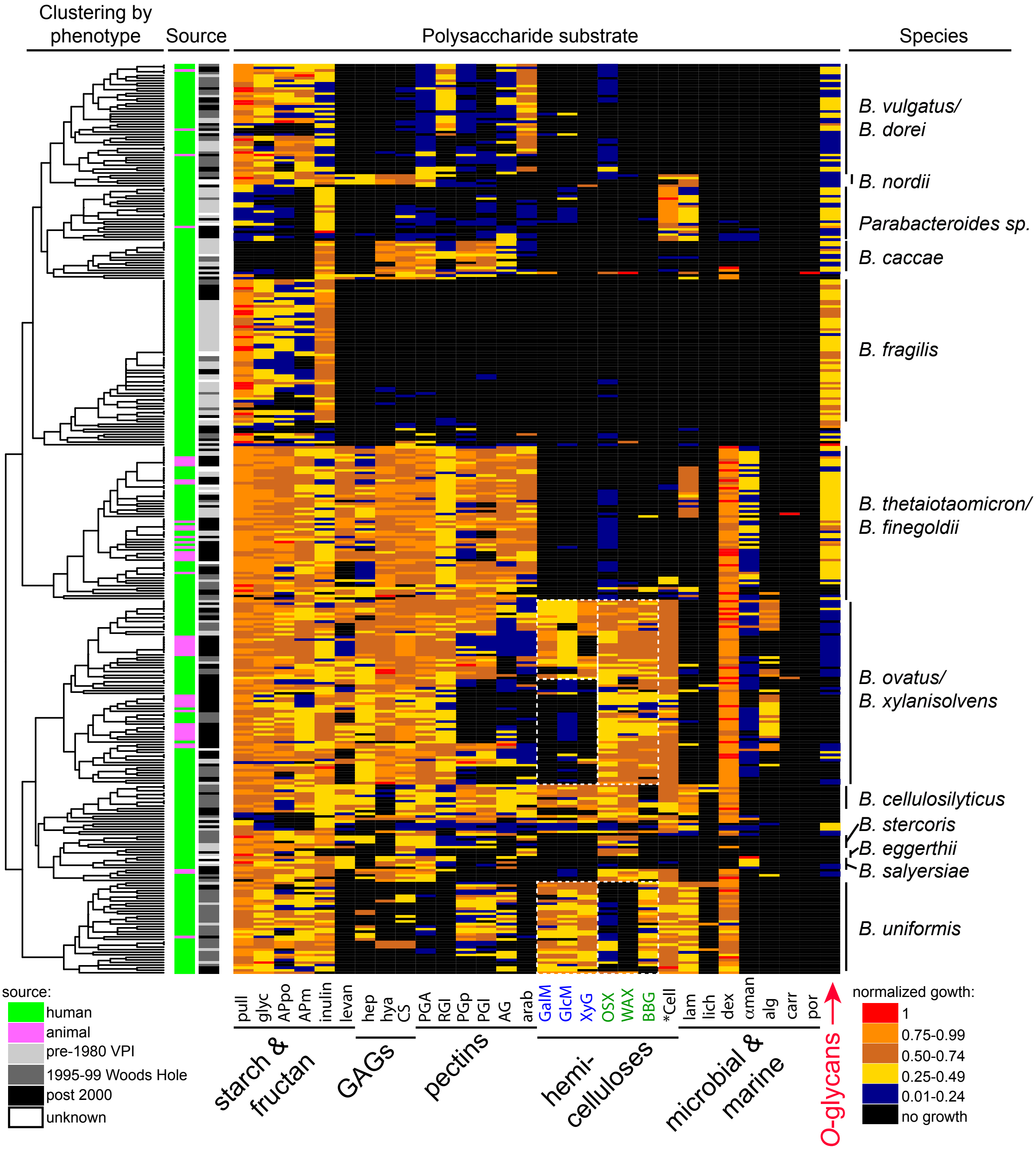
Clustering by phenotype
Source
Polysaccharide substrate
Species
B. vulgatus/
B. dorei
B. nordii
Parabacteroides sp.
B. caccae
B. fragilis
B. thetaiotaomicron/
B. finegoldii
B. ovatus/
B. xylanisolvens
B. cellulosilyticus
B. stercoris
B. eggerthii
B. salyersiae
B. uniformis
source:
human
animal
pre-1980 VPI
1995-99 Woods Hole
post 2000
unknown
pull
glyc
APpo
APm
inulin
levan
hep
hya
CS
PGA
RGI
PGp
PGI
AG
arab
GalM
GlcM
XyG
OSX
WAX
BBG
*Cell
lam
lich
dex
αman
alg
carr
por
starch & fructan
GAGs
pectins
hemi-celluloses
microbial & marine
O-glycans
normalized gowth:
1
0.75-0.99
0.50-0.74
0.25-0.49
0.01-0.24
no growth

Figure 3

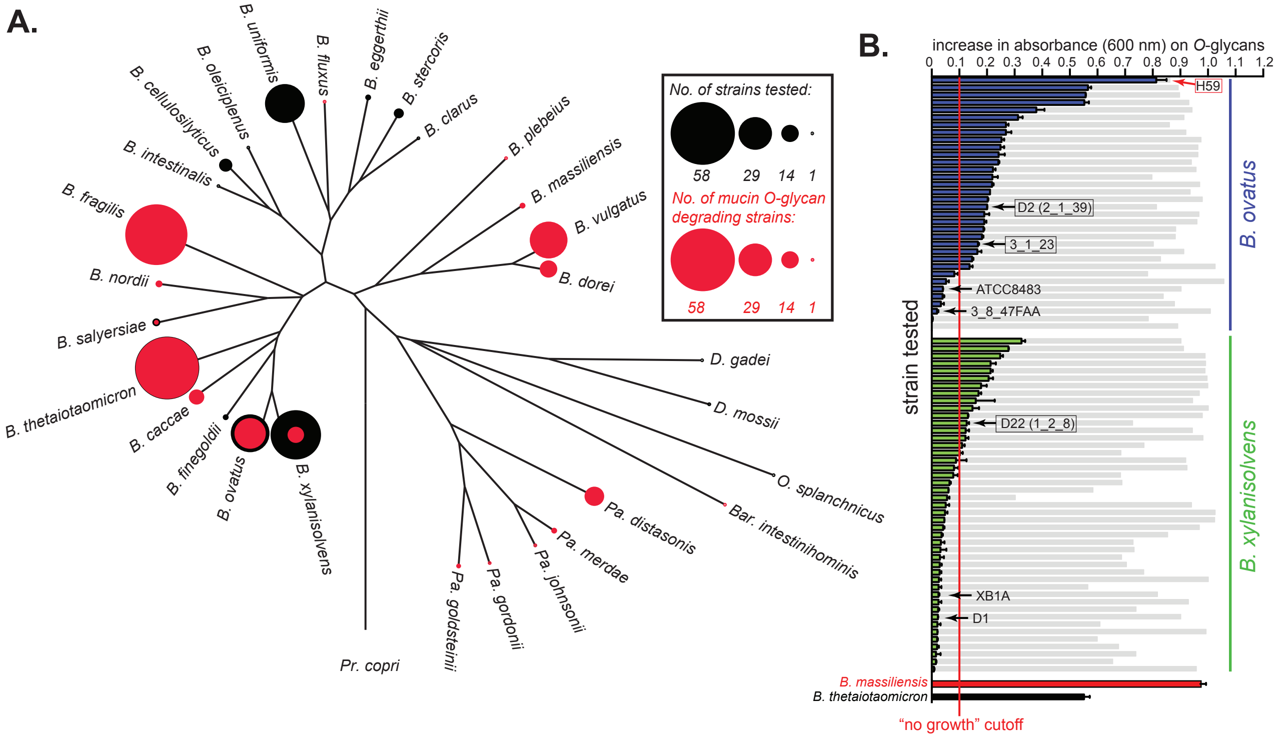
A.
B. uniformis
B. fluxus
B. eggerthii
B. stercoris
B. clarus
B. oleiciplenus
B. cellulosilyticus
B. intestinalis
B. fragilis
B. nordii
B. salyersiae
B. thetaiotaomicron
B. caccae
B. finegoldii
B. ovatus
B. xylanisolvens
B. plebeius
B. massiliensis
B. vulgatus
B. dorei
D. gadei
D. mossii
O. splanchnicus
Bar. intestinihominis
Pa. distasonis
Pa. merdae
Pa. johnsonii
Pa. gordonii
Pa. goldsteinii
Pr. copri
No. of strains tested:
58
29
14
1
No. of mucin O-glycan degrading strains:
58
29
14
1
B.
increase in absorbance (600 nm) on O-glycans
0
0.1
0.2
0.3
0.4
0.5
0.6
0.7
0.8
0.9
1.0
1.1
1.2
H59
D2 (2_1_39)
3_1_23
ATCC8483
3_8_47FAA
D22 (1_2_8)
XB1A
D1
strain tested
B. ovatus
B. xylanisolvens
B. massiliensis
B. thetaiotaomicron
"no growth" cutoff

Figure 4

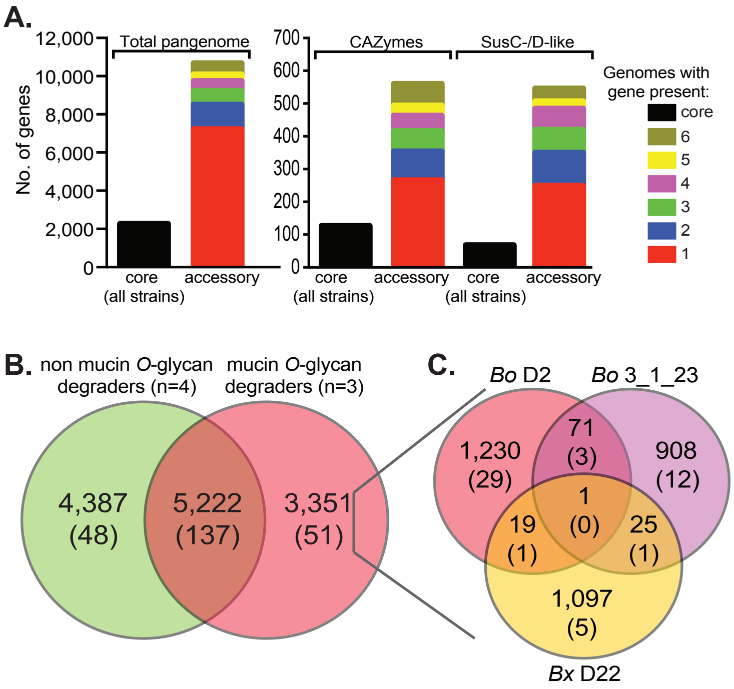
A.
Total pangenome
CAZymes
SusC-/D-like
No. of genes
12,000
10,000
8,000
6,000
4,000
2,000
0
700
600
500
400
300
200
100
0
core (all strains)
accessory
Genomes with gene present:
core
6
5
4
3
2
1
B.
non mucin O-glycan degraders (n=4)
mucin O-glycan degraders (n=3)
4,387 (48)
5,222 (137)
3,351 (51)
C.
Bo D2
Bo 3_1_23
Bx D22
1,230 (29)
71 (3)
908 (12)
1 (0)
19 (1)
25 (1)
1,097 (5)

Figure 5

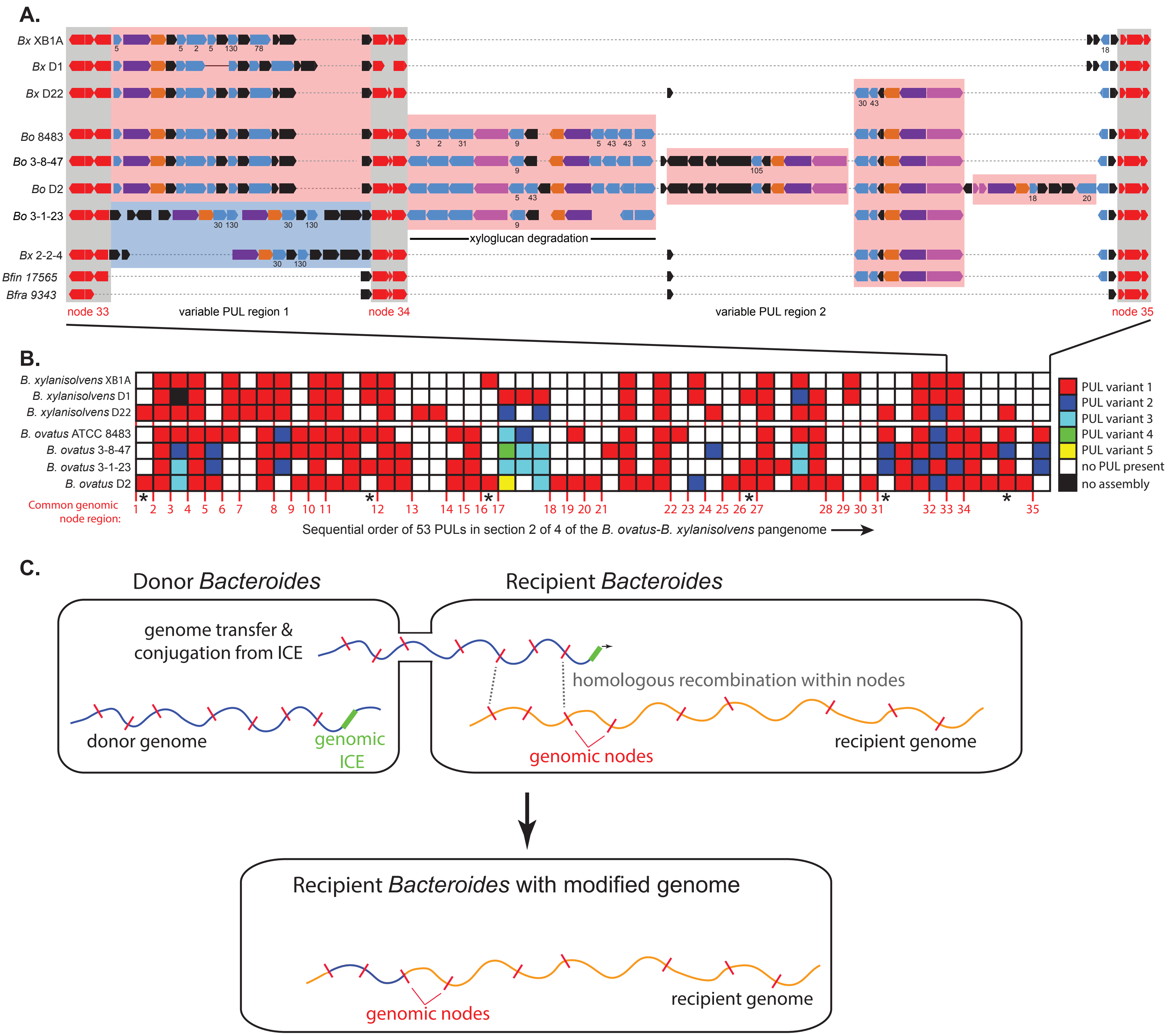
A.
Bx XB1A
Bx D1
Bx D22
Bo 8483
Bo 3-8-47
Bo D2
Bo 3-1-23
Bx 2-2-4
Bfin 17565
Bfra 9343
5
5 2 5 130 78
18
30 43
3 2 31 9 5 43 43 3
9
105
5 43
18 20
30 130 30 130
9
30 130
xyloglucan degradation
node 33
variable PUL region 1
node 34
variable PUL region 2
node 35
B.
B. xylanisolvens XB1A
B. xylanisolvens D1
B. xylanisolvens D22
B. ovatus ATCC 8483
B. ovatus 3-8-47
B. ovatus 3-1-23
B. ovatus D2
PUL variant 1
PUL variant 2
PUL variant 3
PUL variant 4
PUL variant 5
no PUL present
no assembly
Common genomic node region:
1 2 3 4 5 6 7 8 9 10 11 12 13 14 15 16 17 18 19 20 21 22 23 24 25 26 27 28 29 30 31 32 33 34 35
*
Sequential order of 53 PULs in section 2 of 4 of the B. ovatus-B. xylanisolvens pangenome
C.
Donor Bacteroides
Recipient Bacteroides
genome transfer & conjugation from ICE
homologous recombination within nodes
donor genome
genomic ICE
genomic nodes
recipient genome
Recipient Bacteroides with modified genome
genomic nodes
recipient genome

Figure 6

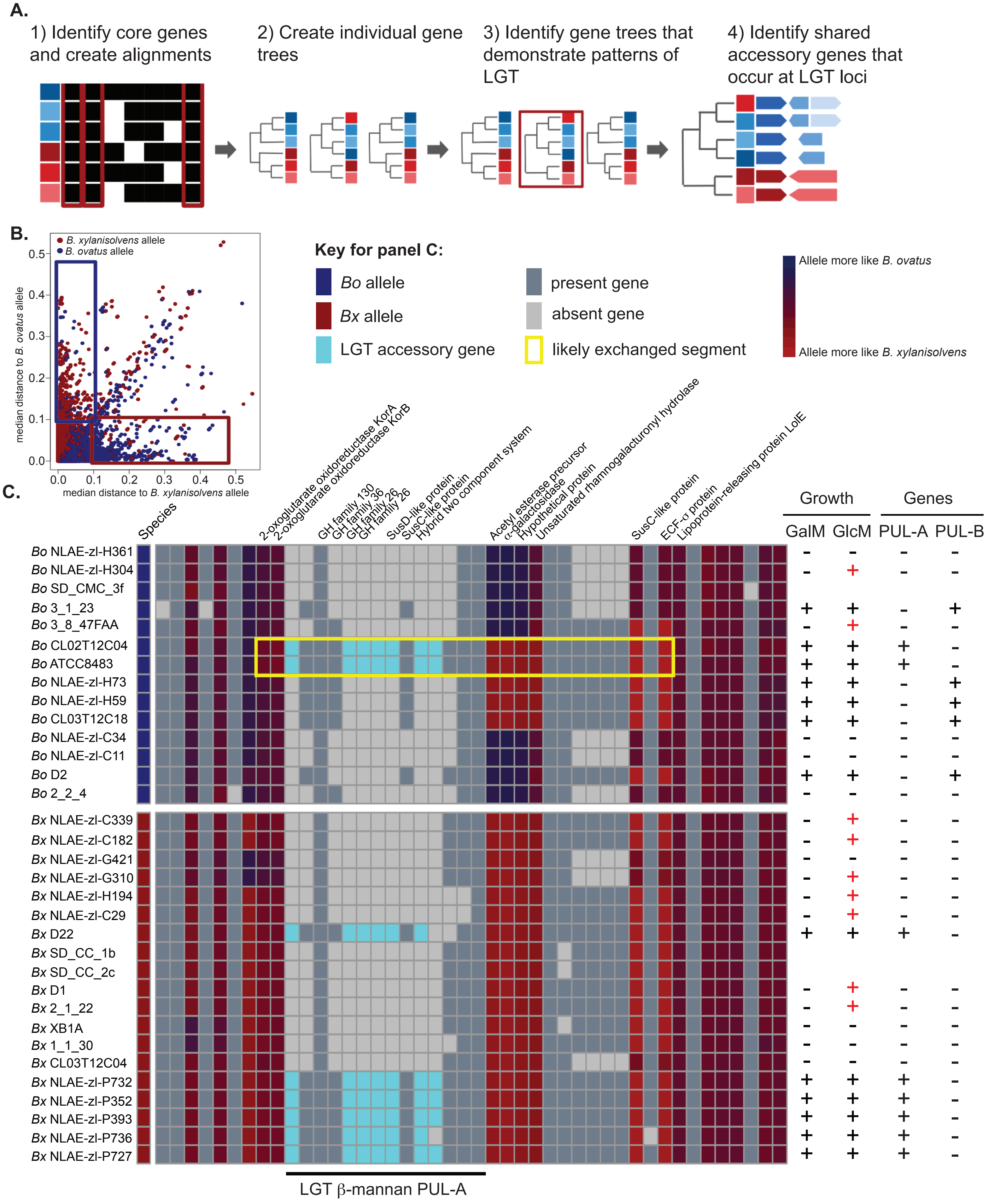
A.
1) Identify core genes and create alignments
2) Create individual gene trees
3) Identify gene trees that demonstrate patterns of LGT
4) Identify shared accessory genes that occur at LGT loci
B.
B. xylanisolvens allele
B. ovatus allele
median distance to B. ovatus allele
median distance to B. xylanisolvens allele
0.0
0.1
0.2
0.3
0.4
0.5
Key for panel C:
Bo allele
Bx allele
LGT accessory gene
present gene
absent gene
likely exchanged segment
Allele more like B. ovatus
Allele more like B. xylanisolvens
C.
Species
2-oxoglutarate oxidoreductase KorA
2-oxoglutarate oxidoreductase KorB
GH family 130
GH family 36
GH family 26
GH family 26
SusD-like protein
SusC-like protein
Hybrid two component system
Acetyl esterase precursor
α-galactosidase
Hypothetical protein
Unsaturated rhamnogalacturonyl hydrolase
SusC-like protein
ECF-σ protein
Lipoprotein-releasing protein LolE
Growth
Genes
GalM GlcM PUL-A PUL-B
Bo NLAE-zl-H361 - - - -
Bo NLAE-zl-H304 - + - -
Bo SD_CMC_3f
Bo 3_1_23 + + - +
Bo 3_8_47FAA - + - -
Bo CL02T12C04 + + + -
Bo ATCC8483 + + + -
Bo NLAE-zl-H73 + + - +
Bo NLAE-zl-H59 + + - +
Bo CL03T12C18 + + - +
Bo NLAE-zl-C34 - - - -
Bo NLAE-zl-C11 - - - -
Bo D2 + + - +
Bo 2_2_4 - - - -
Bx NLAE-zl-C339 - + - -
Bx NLAE-zl-C182 - + - -
Bx NLAE-zl-G421 - - - -
Bx NLAE-zl-G310 - + - -
Bx NLAE-zl-H194 - + - -
Bx NLAE-zl-C29 - + - -
Bx D22 + + + -
Bx SD_CC_1b
Bx SD_CC_2c
Bx D1 - + - -
Bx 2_1_22 - + - -
Bx XB1A - - - -
Bx 1_1_30 - - - -
Bx CL03T12C04 - - - -
Bx NLAE-zl-P732 + + + -
Bx NLAE-zl-P352 + + + -
Bx NLAE-zl-P393 + + + -
Bx NLAE-zl-P736 + + + -
Bx NLAE-zl-P727 + + + -
LGT β-mannan PUL-A

Figure S1

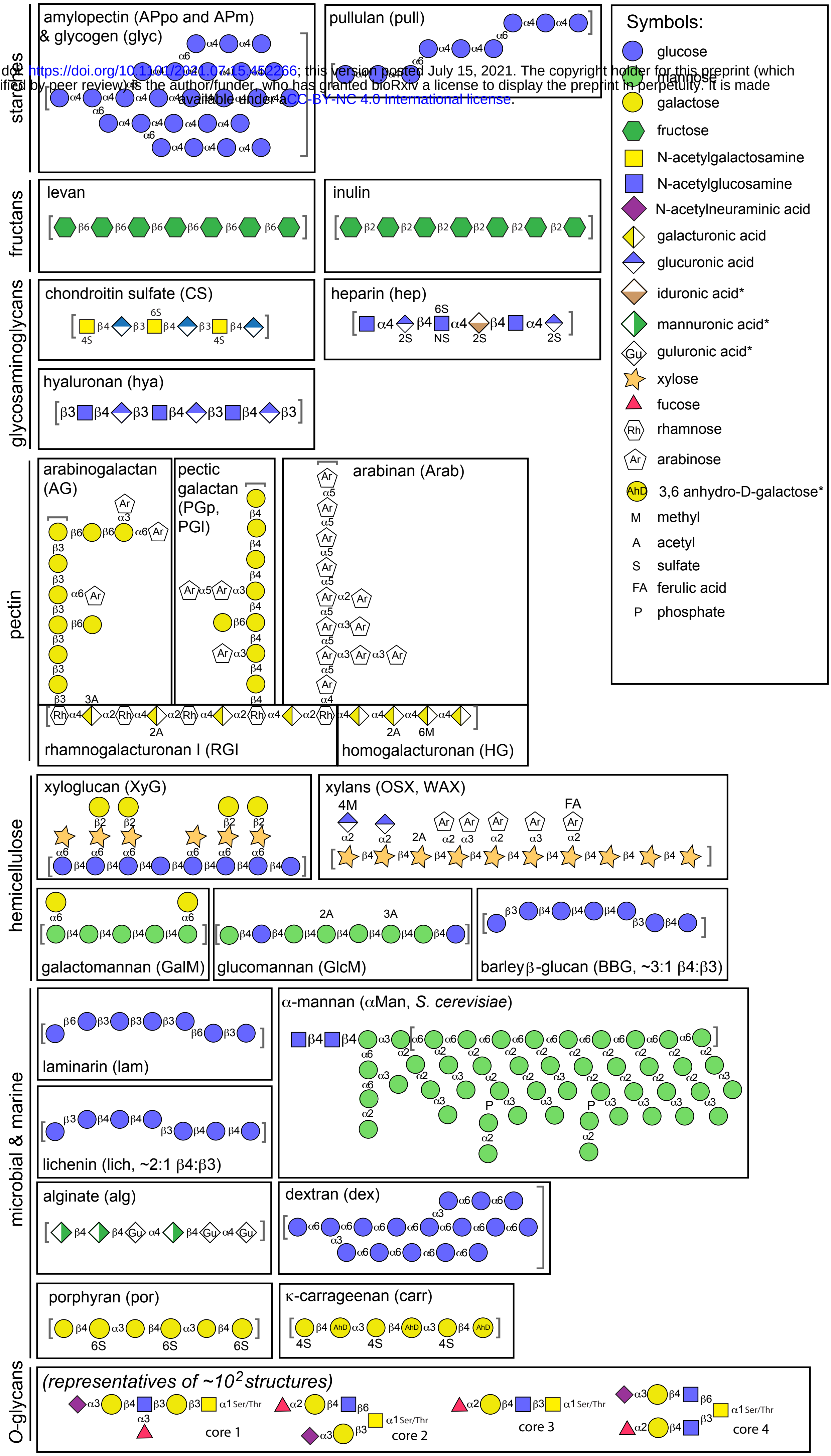
starches
amylopectin (APpo and APm)
& glycogen (glyc)
pullulan (pull)
fructans
levan
inulin
glycosaminoglycans
chondroitin sulfate (CS)
heparin (hep)
hyaluronan (hya)
pectin
arabinogalactan (AG)
pectic galactan (PGp, PGI)
arabinan (Arab)
rhamnogalacturonan I (RGI
homogalacturonan (HG)
hemicellulose
xyloglucan (XyG)
xylans (OSX, WAX)
galactomannan (GalM)
glucomannan (GlcM)
barley β-glucan (BBG, ~3:1 β4:β3)
microbial & marine
laminarin (lam)
lichenin (lich, ~2:1 β4:β3)
α-mannan (αMan, S. cerevisiae)
alginate (alg)
dextran (dex)
porphyran (por)
κ-carrageenan (carr)
O-glycans
(representatives of ~10² structures)
Ser/Thr
core 1
core 2
core 3
core 4
Symbols:
glucose
mannose
galactose
fructose
N-acetylgalactosamine
N-acetylglucosamine
N-acetylneuraminic acid
galacturonic acid
glucuronic acid
iduronic acid*
mannuronic acid*
Gu
guluronic acid*
xylose
fucose
Rh
rhamnose
Ar
arabinose
AhD
3,6 anhydro-D-galactose*
M
methyl
A
acetyl
S
sulfate
FA
ferulic acid
P
phosphate

Figure S2

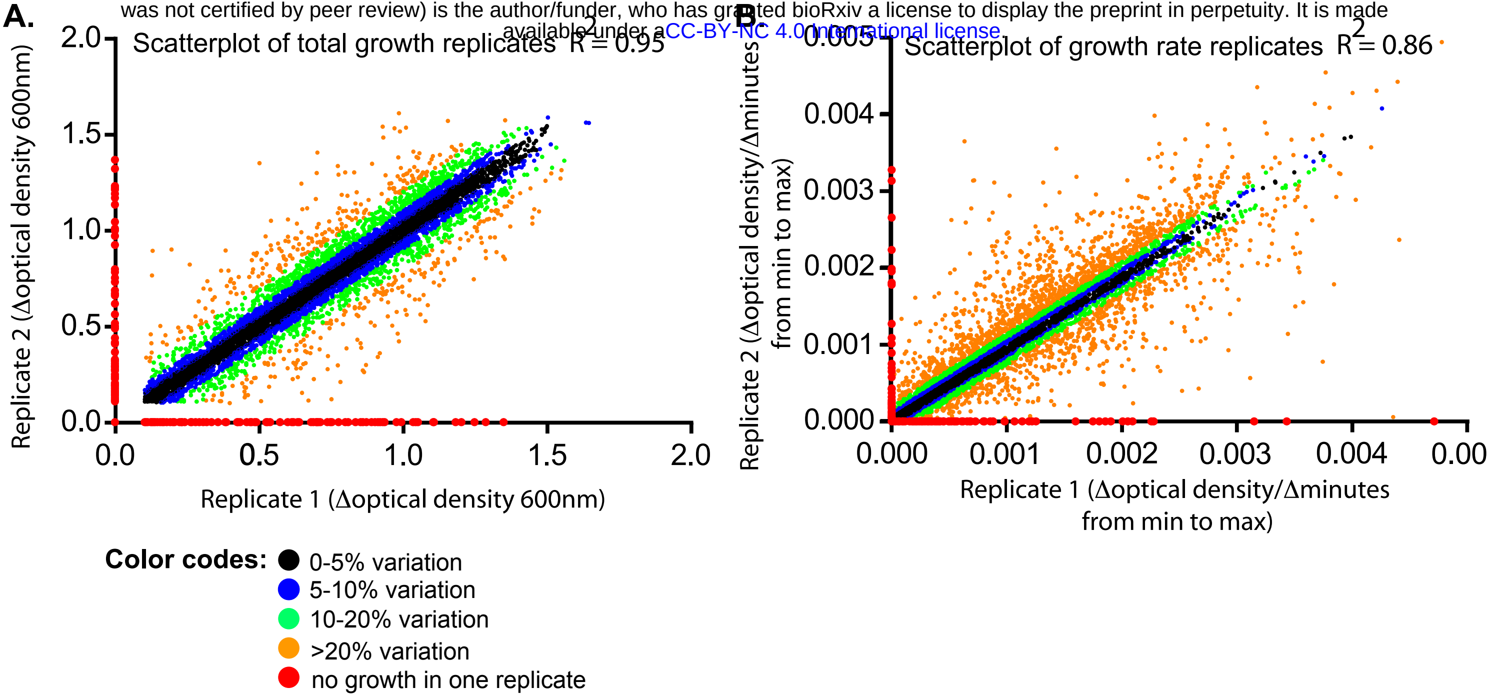

C.

Polysaccharides:

Substrate	R^2 between growth values	R^2 between rate values
AG	0.99	0.89
alg	0.96	0.96
α-mann	0.93	0.76
APm	0.94	0.92
APpo	0.96	0.91
arab	0.98	0.96
BBG	0.95	0.70
carr	0.93	0.96
Cell	0.96	0.81
CS	0.96	0.91
dex	0.96	0.87
GalM	0.96	0.98
GlcM	0.93	0.85
glyc	0.96	0.94
hep	0.96	0.85
hya	0.91	0.88
inulin	0.92	0.89
lam	0.96	0.96
levan	0.96	0.88
lich	0.80	0.45
MOG	0.98	0.97
OSX	0.93	0.83
PGA	0.97	0.89
PGI	0.95	0.96
PGp	0.92	0.92
por	0.85	0.85
pull	0.84	0.78
RGI	0.96	0.98
WAX	0.97	0.42
XyG	0.92	0.72

Monosaccharides:

Substrate	R^2 between growth values
Ara	0.90
Fru	0.90
Fuc	0.93
Gal	0.60
GalA	0.86
GalNAc	0.93
Glc	0.69
GlcA	0.87
GlcNAc	0.72
GlcNH3	0.93
Man	0.88
NeuNAc	0.86
Rha	0.96
Rib	0.94
Xyl	0.85

Figure S3

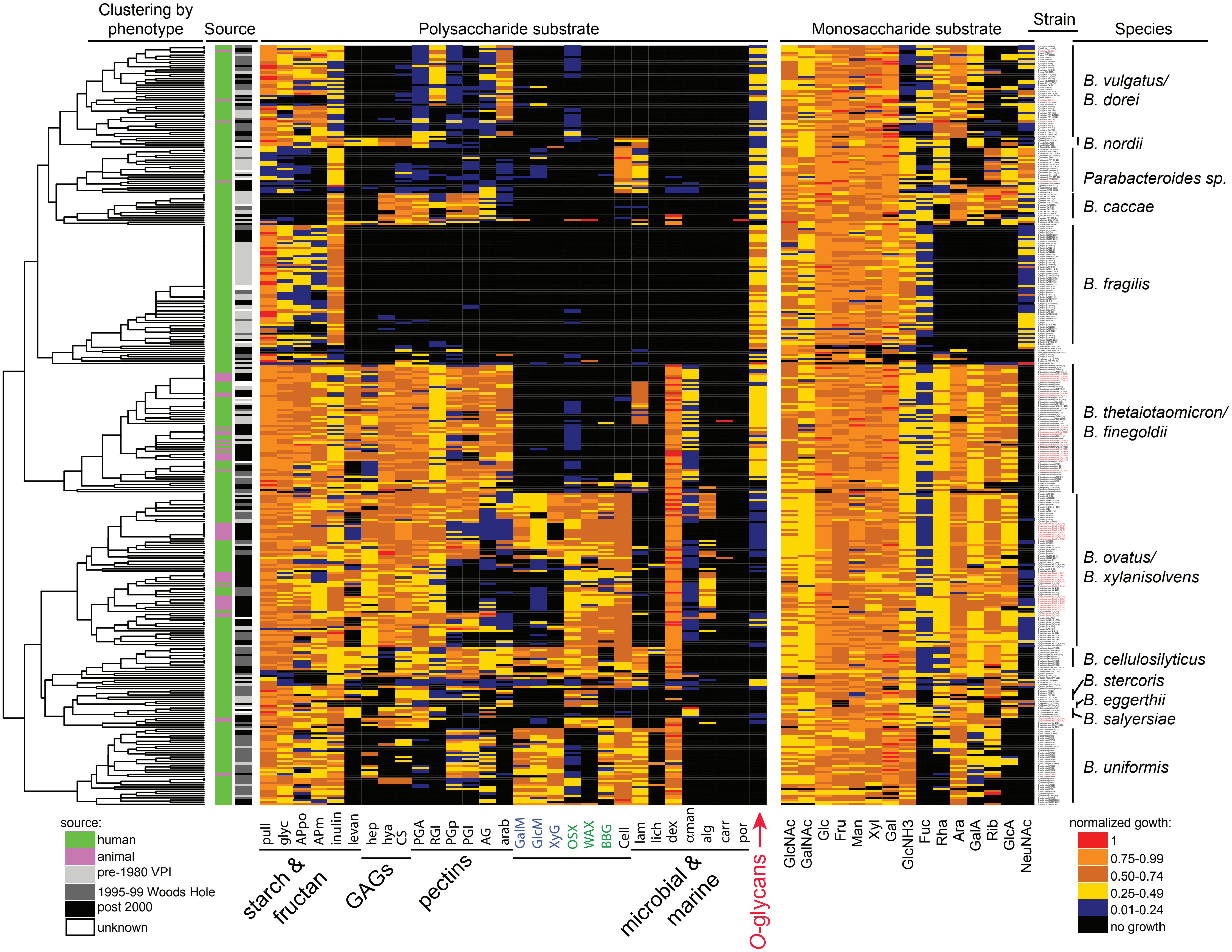
Clustering by phenotype
Source
Polysaccharide substrate
Monosaccharide substrate
Strain
Species
B. vulgatus/
B. dorei
B. nordii
Parabacteroides sp.
B. caccae
B. fragilis
B. thetaiotaomicron/
B. finegoldii
B. ovatus/
B. xylanisolvens
B. cellulosilyticus
B. stercoris
B. eggerthii
B. salyersiae
B. uniformis
source:
human
animal
pre-1980 VPI
1995-99 Woods Hole
post 2000
unknown
pull
glyc
APpo
APm
inulin
levan
hep
hya
CS
PGA
RGI
PGp
PGI
AG
arab
GalM
GlcM
XyG
OSX
WAX
BBG
Cell
lam
lich
dex
αman
alg
carr
por
starch &
fructan
GAGs
pectins
microbial &
marine
O-glycans
GlcNAc
GalNAc
Glc
Fru
Man
Xyl
Gal
GlcNH3
Fuc
Rha
Ara
GalA
Rib
GlcA
NeuNAc
normalized gowth:
1
0.75-0.99
0.50-0.74
0.25-0.49
0.01-0.24
no growth

Figure S4

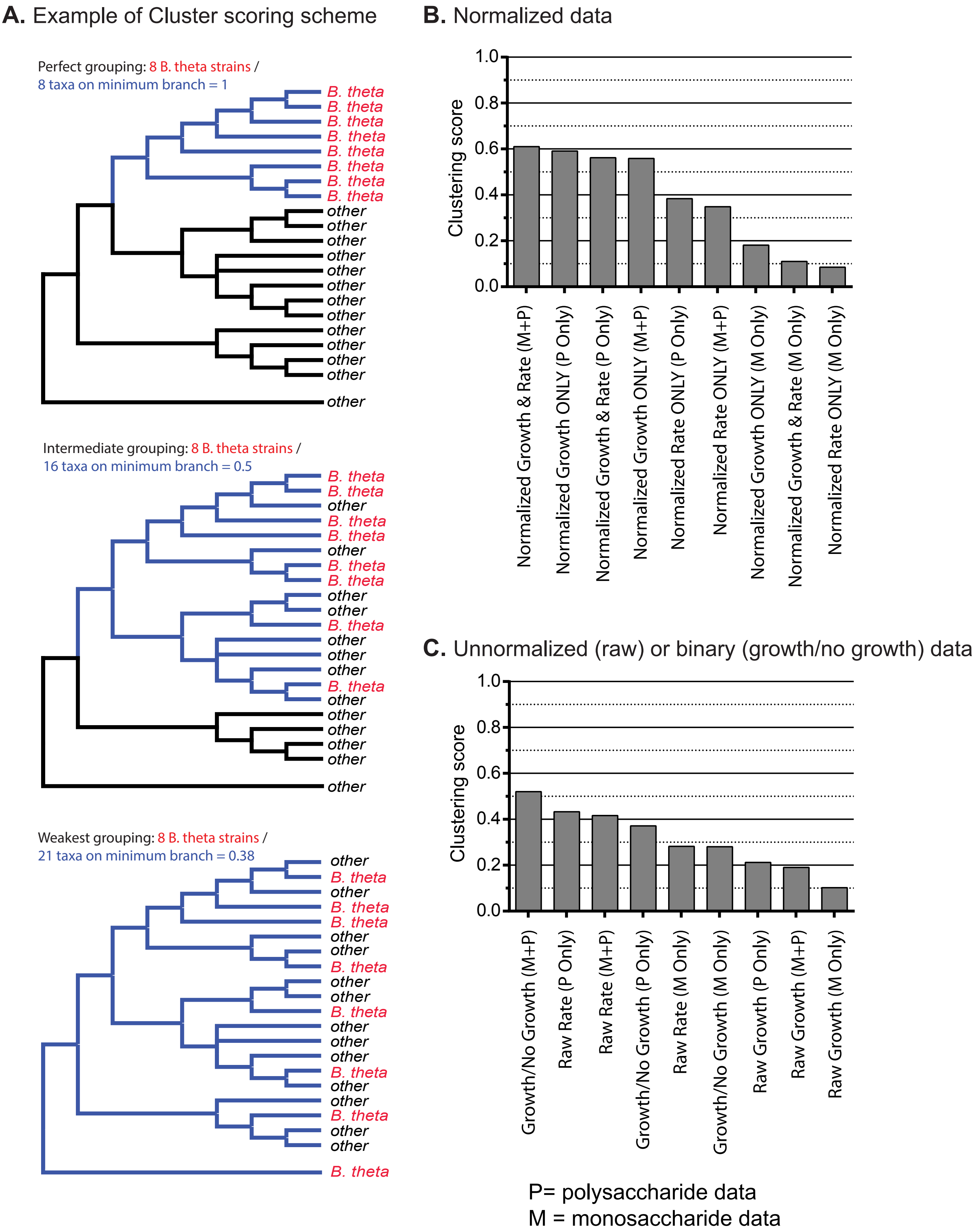

A. Example of Cluster scoring scheme

B. Normalized data

C. Unnormalized (raw) or binary (growth/no growth) data

P= polysaccharide data
M = monosaccharide data

	starches				fructans		GAGs			pectins						hemi-celluloses							microbial & marine							O-glycans ↓
	Pull	Glyc	APp	APm	Inulin	Levan	Hep	Hya	CS	PGA	RGI	PGp	PGl	AG	Arab	GalM	GlcM	XyG	OSX	WAX	BBG	Cell	Lam	Lich	Dex	αmann	Alg	Carr	Porph	MOG
Pull	1.00	0.60	0.43	0.51	0.10	0.11	0.14	-0.03	-0.06	-0.04	0.10	-0.07	-0.12	0.03	0.07	0.05	0.04	0.04	0.07	0.02	0.10	-0.12	-0.14	0.02	0.12	0.08	0.09	0.02	-0.12	-0.05
Glyc	0.60	1.00	0.52	0.68	0.04	0.39	0.47	0.35	0.38	0.37	0.41	0.26	0.23	0.33	0.25	0.21	0.22	0.23	0.38	0.31	0.32	0.14	0.04	0.14	0.50	0.32	0.18	0.03	-0.09	-0.16
App	0.43	0.52	1.00	0.72	0.02	0.35	0.30	0.30	0.37	0.30	0.37	0.17	0.14	0.28	0.27	0.07	0.06	0.03	0.23	0.17	0.28	0.01	-0.13	0.01	0.36	0.28	0.19	0.05	-0.07	-0.05
Apm	0.51	0.68	0.72	1.00	-0.04	0.25	0.41	0.31	0.33	0.37	0.39	0.25	0.20	0.32	0.30	0.21	0.16	0.17	0.30	0.21	0.32	0.07	-0.05	0.11	0.43	0.29	0.13	0.01	-0.08	-0.22
Inulin	0.10	0.04	0.02	-0.04	1.00	-0.03	0.09	0.16	0.08	0.08	0.00	-0.07	-0.01	-0.02	-0.23	-0.01	0.00	-0.02	0.06	0.09	0.08	0.10	0.00	0.08	0.05	0.03	0.09	0.03	0.07	0.05
Levan	0.11	0.39	0.35	0.25	-0.03	1.00	0.62	0.55	0.63	0.64	0.58	0.44	0.43	0.53	0.37	0.08	0.09	0.14	0.31	0.29	0.20	0.09	0.12	-0.04	0.55	0.47	0.33	0.10	-0.04	-0.07
Hep	0.14	0.47	0.30	0.41	0.09	0.62	1.00	0.65	0.69	0.66	0.66	0.38	0.36	0.35	0.26	0.18	0.17	0.16	0.54	0.52	0.47	0.35	0.04	0.00	0.70	0.37	0.34	0.06	-0.04	-0.22
Hya	-0.03	0.35	0.30	0.31	0.16	0.55	0.65	1.00	0.83	0.77	0.69	0.44	0.45	0.44	0.26	0.05	0.02	0.04	0.40	0.38	0.40	0.23	-0.09	-0.08	0.64	0.56	0.37	0.07	0.05	-0.10
CS	-0.06	0.38	0.37	0.33	0.08	0.63	0.69	0.83	1.00	0.83	0.68	0.50	0.51	0.48	0.32	0.08	0.06	0.04	0.46	0.45	0.38	0.23	-0.02	-0.06	0.67	0.54	0.30	0.10	0.03	-0.13
PGA	-0.04	0.37	0.30	0.37	0.08	0.64	0.66	0.77	0.83	1.00	0.72	0.55	0.55	0.55	0.46	0.03	-0.01	0.02	0.44	0.44	0.24	0.14	-0.07	-0.06	0.62	0.56	0.28	0.10	0.06	-0.10
RGI	0.10	0.41	0.37	0.39	0.00	0.58	0.66	0.69	0.68	0.72	1.00	0.43	0.39	0.39	0.46	0.12	0.07	0.07	0.57	0.52	0.44	0.25	-0.19	-0.06	0.56	0.45	0.41	0.04	0.10	-0.14
PGp	-0.07	0.26	0.17	0.25	-0.07	0.44	0.38	0.44	0.50	0.55	0.43	1.00	0.92	0.53	0.40	0.30	0.23	0.44	0.24	0.23	0.23	0.17	0.22	0.05	0.57	0.41	0.19	0.11	-0.01	-0.07
PGl	-0.12	0.23	0.14	0.20	-0.01	0.43	0.36	0.45	0.51	0.55	0.39	0.92	1.00	0.53	0.36	0.29	0.22	0.42	0.22	0.21	0.22	0.19	0.22	0.06	0.56	0.43	0.21	0.11	-0.01	-0.02
AG	0.03	0.33	0.28	0.32	-0.02	0.53	0.35	0.44	0.48	0.55	0.39	0.53	0.53	1.00	0.54	-0.03	-0.07	-0.02	-0.05	-0.08	-0.06	-0.13	0.15	-0.03	0.48	0.66	0.04	0.05	0.02	0.22
Arab	0.07	0.25	0.27	0.30	-0.23	0.37	0.26	0.26	0.32	0.46	0.46	0.40	0.36	0.54	1.00	-0.03	-0.14	-0.04	0.05	0.02	-0.22	-0.25	0.04	-0.02	0.24	0.45	-0.02	0.03	0.05	0.20
GalM	0.05	0.21	0.07	0.21	-0.01	0.08	0.18	0.05	0.08	0.03	0.12	0.30	0.29	-0.03	-0.03	1.00	0.81	0.74	0.42	0.41	0.52	0.51	0.30	0.24	0.38	-0.13	0.18	0.05	0.16	-0.42
GlcM	0.04	0.22	0.06	0.16	0.00	0.09	0.17	0.02	0.06	-0.01	0.07	0.23	0.22	-0.07	-0.14	0.81	1.00	0.71	0.42	0.39	0.58	0.62	0.35	0.30	0.41	-0.17	0.22	0.02	-0.03	-0.49
XyG	0.04	0.23	0.03	0.17	-0.02	0.14	0.16	0.04	0.04	0.02	0.07	0.44	0.42	-0.02	-0.04	0.74	0.71	1.00	0.42	0.38	0.50	0.53	0.34	0.21	0.41	-0.04	0.29	0.02	-0.03	-0.44
OSX	0.07	0.38	0.23	0.30	0.06	0.31	0.54	0.40	0.46	0.44	0.57	0.24	0.22	-0.05	0.05	0.42	0.42	0.42	1.00	0.92	0.69	0.63	-0.08	0.07	0.51	0.01	0.51	0.03	0.14	-0.53
WAX	0.02	0.31	0.17	0.21	0.09	0.29	0.52	0.38	0.45	0.44	0.52	0.23	0.21	-0.08	0.02	0.41	0.39	0.38	0.92	1.00	0.62	0.62	-0.07	0.04	0.47	-0.01	0.50	-0.01	0.13	-0.50
BBG	0.10	0.32	0.28	0.32	0.08	0.20	0.47	0.40	0.38	0.24	0.44	0.23	0.22	-0.06	-0.22	0.52	0.58	0.50	0.69	0.62	1.00	0.70	-0.03	0.13	0.57	-0.01	0.48	0.02	-0.03	-0.55
Cell	-0.12	0.14	0.01	0.07	0.10	0.09	0.35	0.23	0.23	0.14	0.25	0.17	0.19	-0.13	-0.25	0.51	0.62	0.53	0.63	0.62	0.70	1.00	0.27	0.14	0.47	-0.09	0.39	-0.01	-0.05	-0.55
Lam	-0.14	0.04	-0.13	-0.05	0.00	0.12	0.04	-0.09	-0.02	-0.07	-0.19	0.22	0.22	0.15	0.04	0.30	0.35	0.34	-0.08	-0.07	-0.03	0.27	1.00	0.17	0.21	0.01	-0.19	0.07	0.13	-0.20
Lich	0.02	0.14	0.01	0.11	0.08	-0.04	0.00	-0.08	-0.06	-0.06	-0.06	0.05	0.06	-0.03	-0.02	0.24	0.30	0.21	0.07	0.04	0.13	0.14	0.17	1.00	0.10	-0.07	-0.05	-0.01	-0.01	-0.16
Dex	0.12	0.50	0.36	0.43	0.05	0.55	0.70	0.64	0.67	0.62	0.56	0.57	0.56	0.48	0.24	0.38	0.41	0.41	0.51	0.47	0.57	0.47	0.21	0.10	1.00	0.42	0.32	0.08	-0.06	-0.36
αmann	0.08	0.32	0.28	0.29	0.03	0.47	0.37	0.56	0.54	0.56	0.45	0.41	0.43	0.66	0.45	-0.13	-0.17	-0.04	0.01	-0.01	-0.01	-0.09	0.01	-0.07	0.42	1.00	0.11	0.13	-0.03	0.19
Alg	0.09	0.18	0.19	0.13	0.09	0.33	0.34	0.37	0.30	0.28	0.41	0.19	0.21	0.04	-0.02	0.18	0.22	0.29	0.51	0.50	0.48	0.39	-0.19	-0.05	0.32	0.11	1.00	-0.03	-0.02	-0.24
Carr	0.02	0.03	0.05	0.01	0.03	0.10	0.06	0.07	0.10	0.10	0.04	0.11	0.11	0.05	0.03	0.05	0.02	0.02	0.03	-0.01	0.02	-0.01	0.07	-0.01	0.08	0.13	-0.03	1.00	0.00	-0.01
Porph	-0.12	-0.09	-0.07	-0.08	0.07	-0.04	-0.04	0.05	0.03	0.06	0.10	-0.01	-0.01	0.02	0.05	0.16	-0.03	-0.03	0.14	0.13	-0.03	-0.05	0.13	-0.01	-0.06	-0.03	-0.02	0.00	1.00	0.00
MOG	-0.05	-0.16	-0.05	-0.22	0.05	-0.07	-0.22	-0.10	-0.13	-0.10	-0.14	-0.07	-0.02	0.22	0.20	-0.42	-0.49	-0.44	-0.53	-0.50	-0.55	-0.55	-0.20	-0.16	-0.36	0.19	-0.24	-0.01	0.00	1.00

Color key:

🟥	perfect correlation (1.0)
🟥	+0.7 to 1.0
🟪	+0.40 to 0.7
□	-0.40 to 0.40
🟦	less than -0.40

Figure S6

Please note that Figure S6 is provided as a zipped folder containing 4 separate quarters of the pangenome assembly along with a corresponding legend that explains the color coding scheme. The four maps correspond to **Table S2**.

Each map contains 5 vertically stacked panes of pangenome map starting in the upper left. Each horizontal pane has 8 rows with the top row representing the pangenome and the corresponding 7 individual genome regions shown below.

The example below shows a small region of pangenome section 2 in which *Bo* 3-1-23 is missing an ECF-σ regulated PUL. The small text above genes in individual genomes correspond to the contig and the green dashed line represents a region that was broken to accomodate accessory genes.

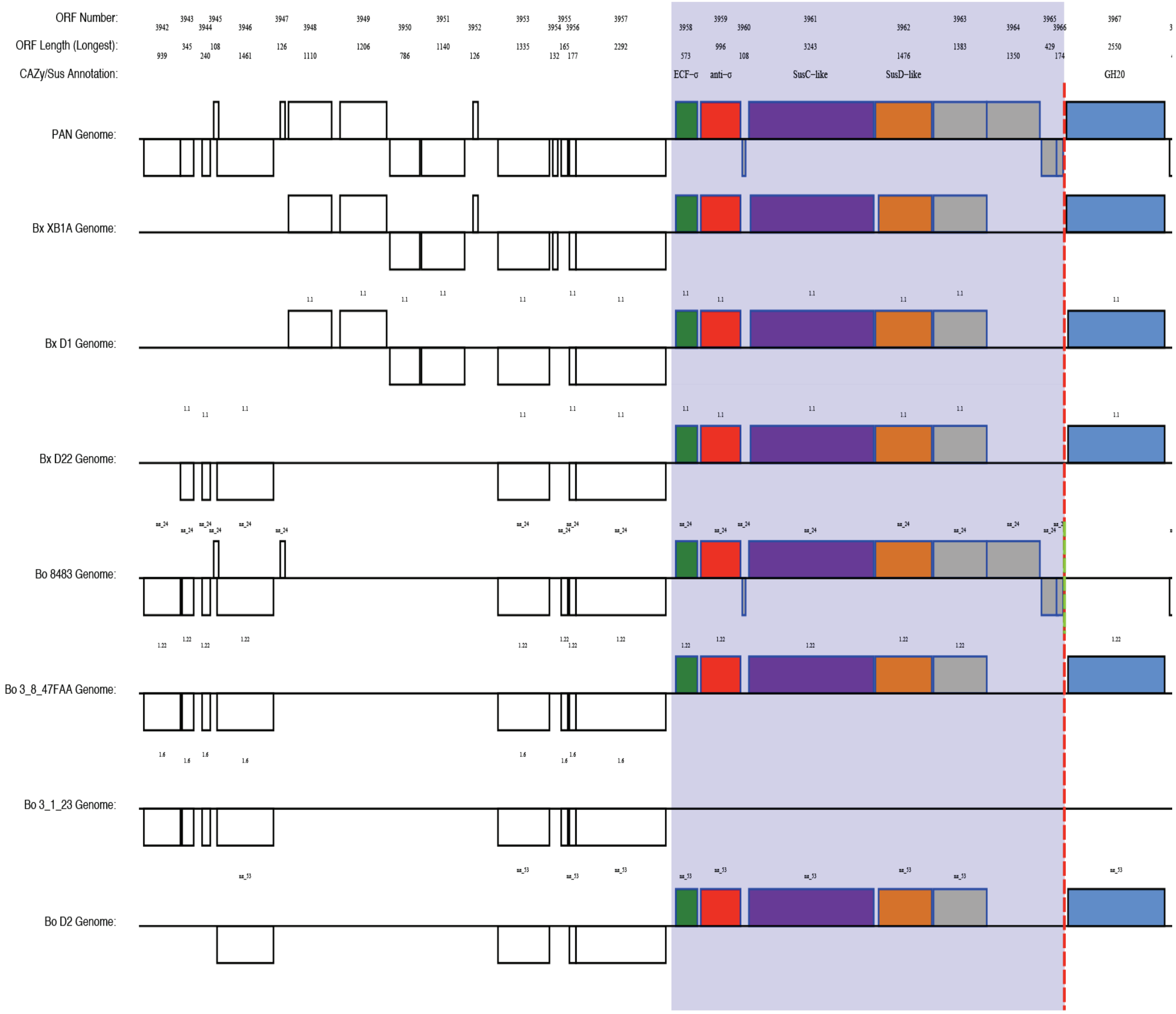

Figure S7

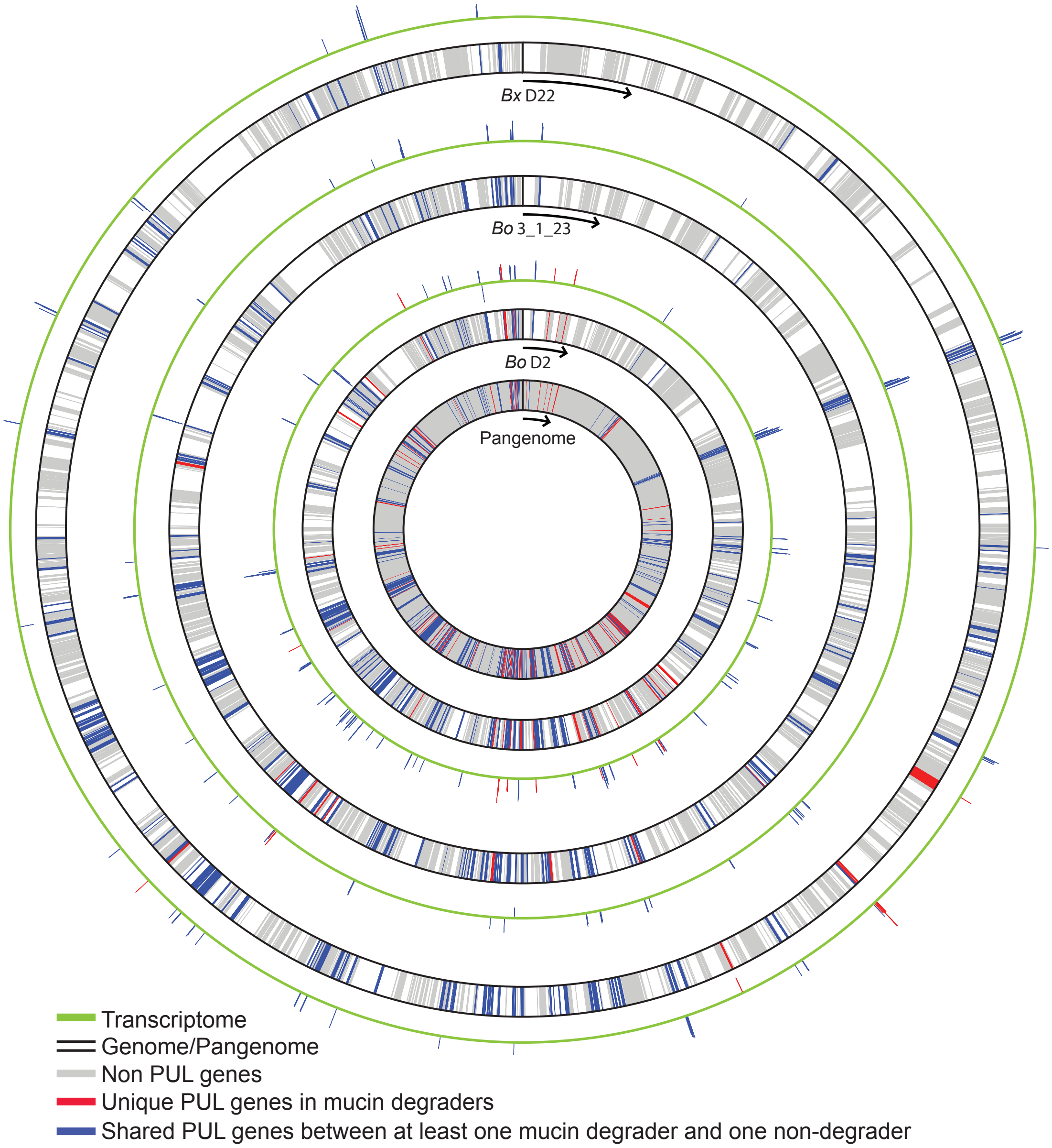
Bx D22
Bo 3_1_23
Bo D2
Pangenome
Transcriptome
Genome/Pangenome
Non PUL genes
Unique PUL genes in mucin degraders
Shared PUL genes between at least one mucin degrader and one non-degrader

Figure S8. Bacteroides LGT Loci

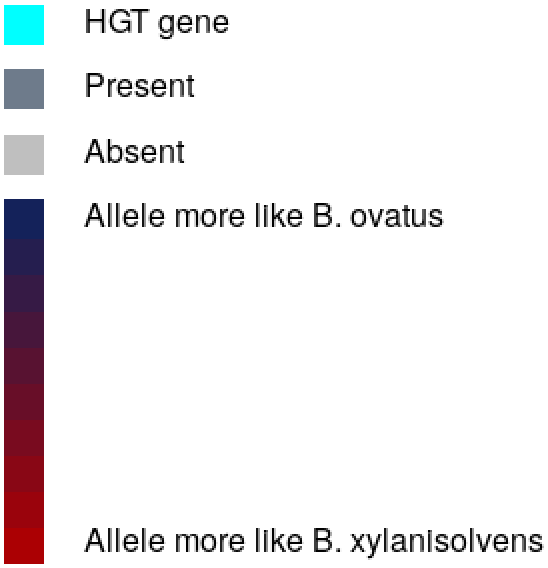

PUL LGT Events

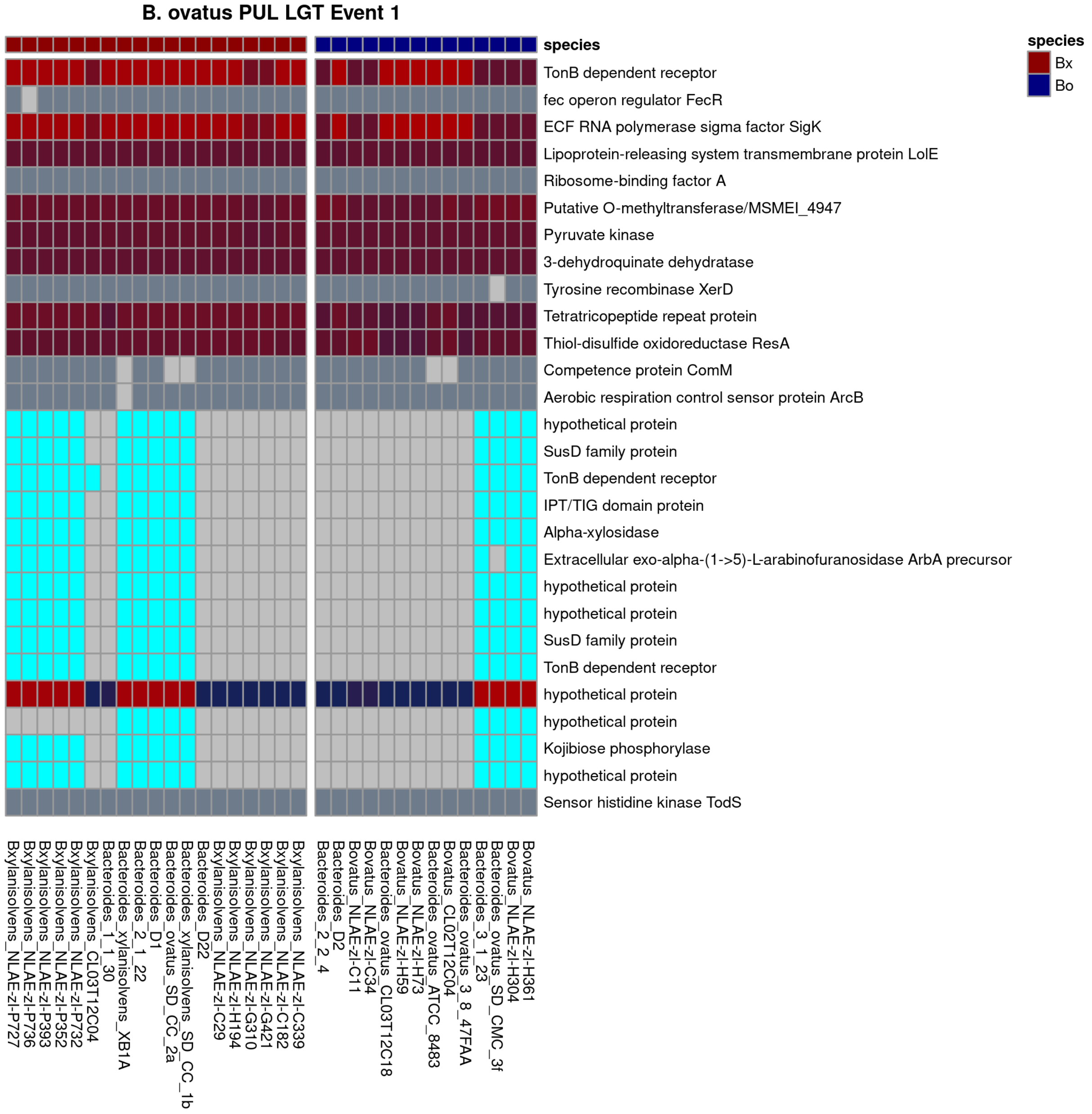

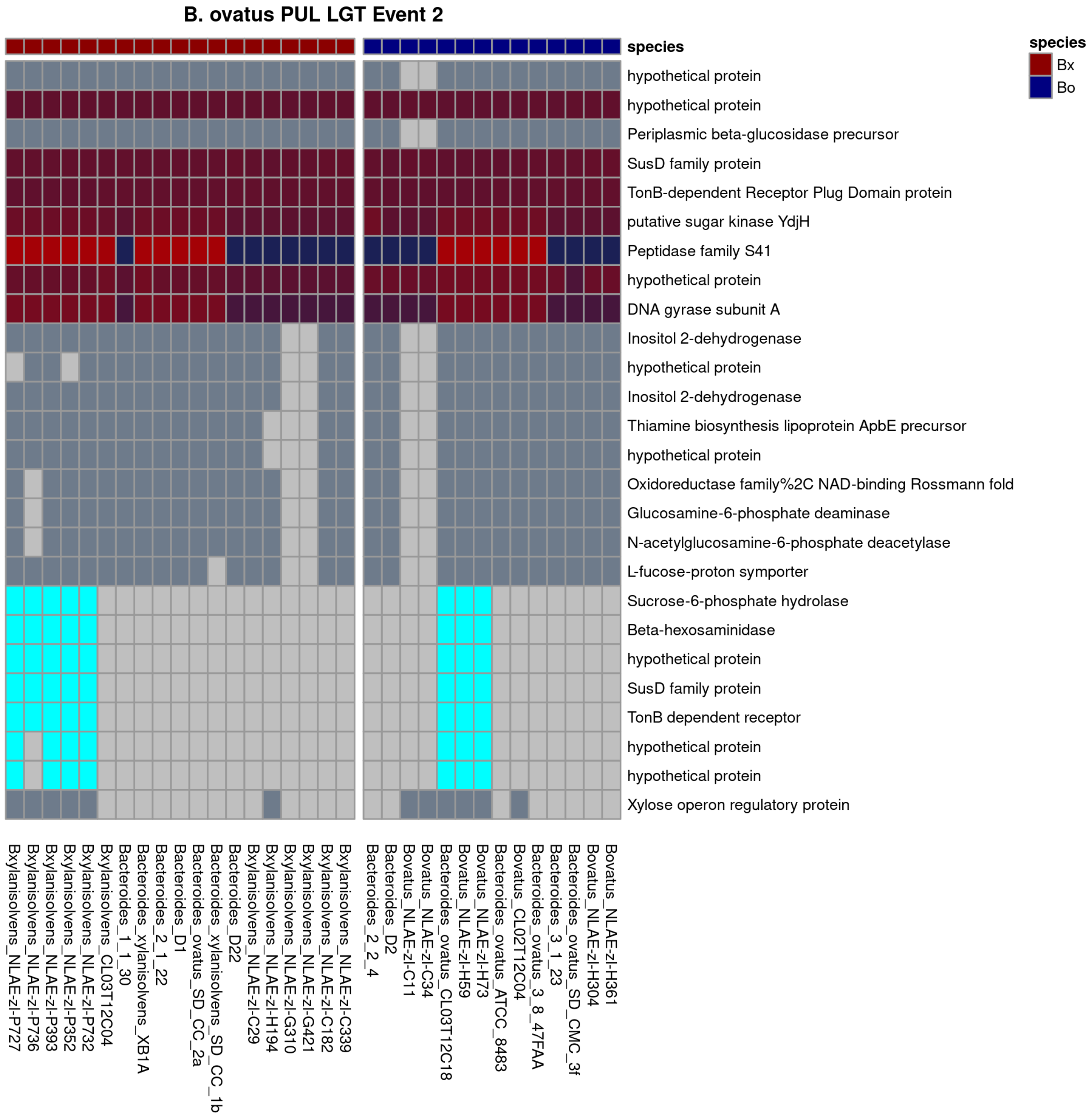
B. ovatus PUL LGT Event 2
species
hypothetical protein
hypothetical protein
Periplasmic beta-glucosidase precursor
SusD family protein
TonB-dependent Receptor Plug Domain protein
putative sugar kinase YdjH
Peptidase family S41
hypothetical protein
DNA gyrase subunit A
Inositol 2-dehydrogenase
hypothetical protein
Inositol 2-dehydrogenase
Thiamine biosynthesis lipoprotein ApbE precursor
hypothetical protein
Oxidoreductase family%2C NAD-binding Rossmann fold
Glucosamine-6-phosphate deaminase
N-acetylglucosamine-6-phosphate deacetylase
L-fucose-proton symporter
Sucrose-6-phosphate hydrolase
Beta-hexosaminidase
hypothetical protein
SusD family protein
TonB dependent receptor
hypothetical protein
hypothetical protein
Xylose operon regulatory protein
species
Bx
Bo
Bxylanisolvens_NLAE-zl-P727
Bxylanisolvens_NLAE-zl-P736
Bxylanisolvens_NLAE-zl-P393
Bxylanisolvens_NLAE-zl-P352
Bxylanisolvens_NLAE-zl-P732
Bxylanisolvens_CL03T12C04
Bacteroides_1_1_30
Bacteroides_xylanisolvens_XB1A
Bacteroides_2_1_22
Bacteroides_D1
Bacteroides_ovatus_SD_CC_2a
Bacteroides_xylanisolvens_SD_CC_1b
Bacteroides_D22
Bxylanisolvens_NLAE-zl-C29
Bxylanisolvens_NLAE-zl-H194
Bxylanisolvens_NLAE-zl-G310
Bxylanisolvens_NLAE-zl-G421
Bxylanisolvens_NLAE-zl-C182
Bxylanisolvens_NLAE-zl-C339
Bacteroides_2_2_4
Bacteroides_D2
Bovatus_NLAE-zl-C11
Bovatus_NLAE-zl-C34
Bacteroides_ovatus_CL03T12C18
Bovatus_NLAE-zl-H59
Bovatus_NLAE-zl-H73
Bacteroides_ovatus_ATCC_8483
Bovatus_CL02T12C04
Bacteroides_ovatus_3_8_47FAA
Bacteroides_3_1_23
Bacteroides_ovatus_SD_CMC_3f
Bovatus_NLAE-zl-H304
Bovatus_NLAE-zl-H361

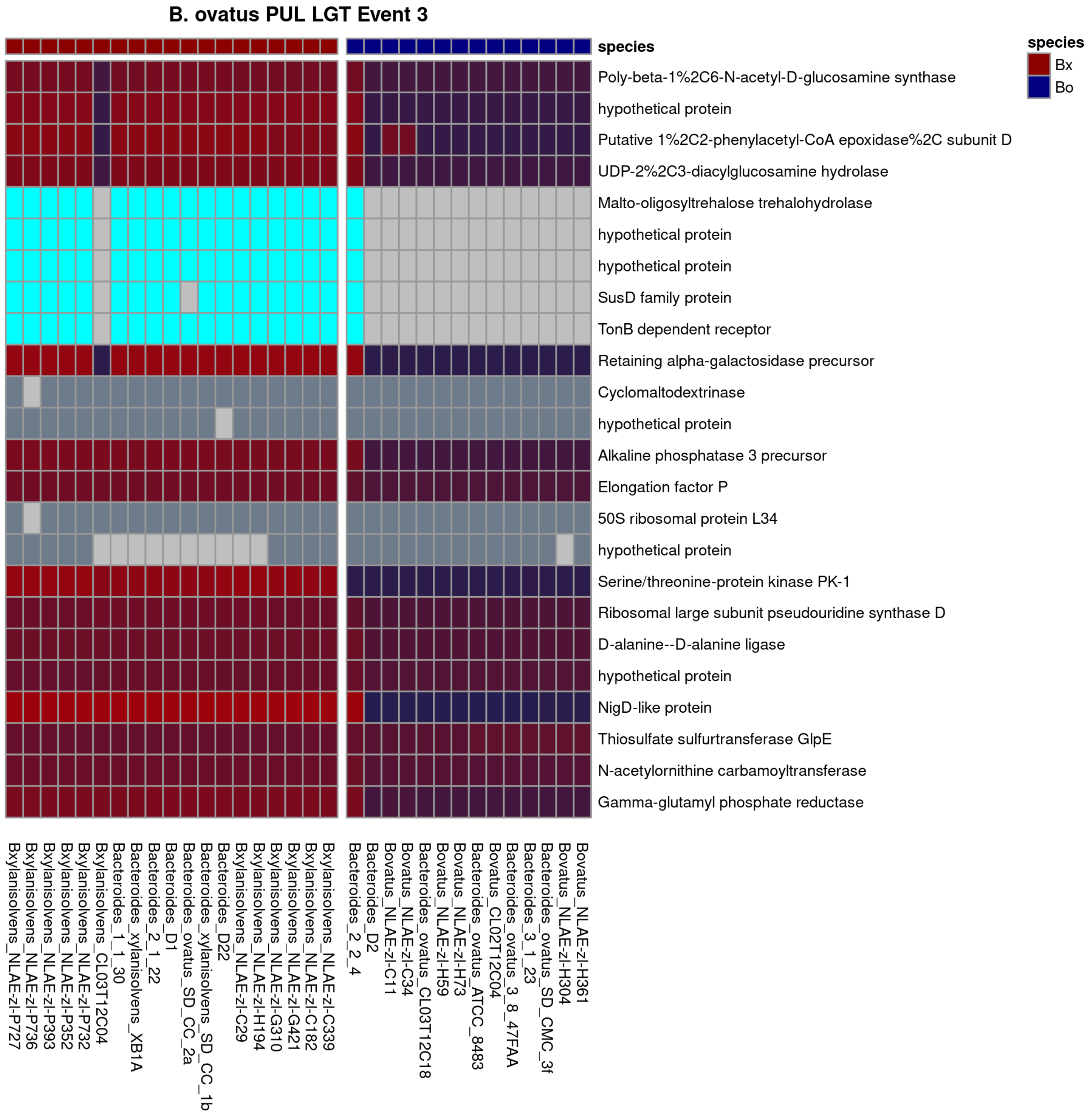
B. ovatus PUL LGT Event 3
species
species
Bx
Bo
Poly-beta-1%2C6-N-acetyl-D-glucosamine synthase
hypothetical protein
Putative 1%2C2-phenylacetyl-CoA epoxidase%2C subunit D
UDP-2%2C3-diacylglucosamine hydrolase
Malto-oligosyltrehalose trehalohydrolase
hypothetical protein
hypothetical protein
SusD family protein
TonB dependent receptor
Retaining alpha-galactosidase precursor
Cyclomaltodextrinase
hypothetical protein
Alkaline phosphatase 3 precursor
Elongation factor P
50S ribosomal protein L34
hypothetical protein
Serine/threonine-protein kinase PK-1
Ribosomal large subunit pseudouridine synthase D
D-alanine--D-alanine ligase
hypothetical protein
NigD-like protein
Thiosulfate sulfurtransferase GlpE
N-acetylornithine carbamoyltransferase
Gamma-glutamyl phosphate reductase
Bxylanisolvens_NLAE-zl-P727
Bxylanisolvens_NLAE-zl-P736
Bxylanisolvens_NLAE-zl-P393
Bxylanisolvens_NLAE-zl-P352
Bxylanisolvens_NLAE-zl-P732
Bxylanisolvens_CL03T12C04
Bacteroides_1_1_30
Bacteroides_xylanisolvens_XB1A
Bacteroides_2_1_22
Bacteroides_D1
Bacteroides_ovatus_SD_CC_2a
Bacteroides_xylanisolvens_SD_CC_1b
Bacteroides_D22
Bxylanisolvens_NLAE-zl-C29
Bxylanisolvens_NLAE-zl-H194
Bxylanisolvens_NLAE-zl-G310
Bxylanisolvens_NLAE-zl-G421
Bxylanisolvens_NLAE-zl-C182
Bxylanisolvens_NLAE-zl-C339
Bacteroides_2_2_4
Bacteroides_D2
Bovatus_NLAE-zl-C11
Bovatus_NLAE-zl-C34
Bacteroides_ovatus_CL03T12C18
Bovatus_NLAE-zl-H59
Bovatus_NLAE-zl-H73
Bacteroides_ovatus_ATCC_8483
Bovatus_CL02T12C04
Bacteroides_ovatus_3_8_47FAA
Bacteroides_3_1_23
Bacteroides_ovatus_SD_CMC_3f
Bovatus_NLAE-zl-H304
Bovatus_NLAE-zl-H361

)

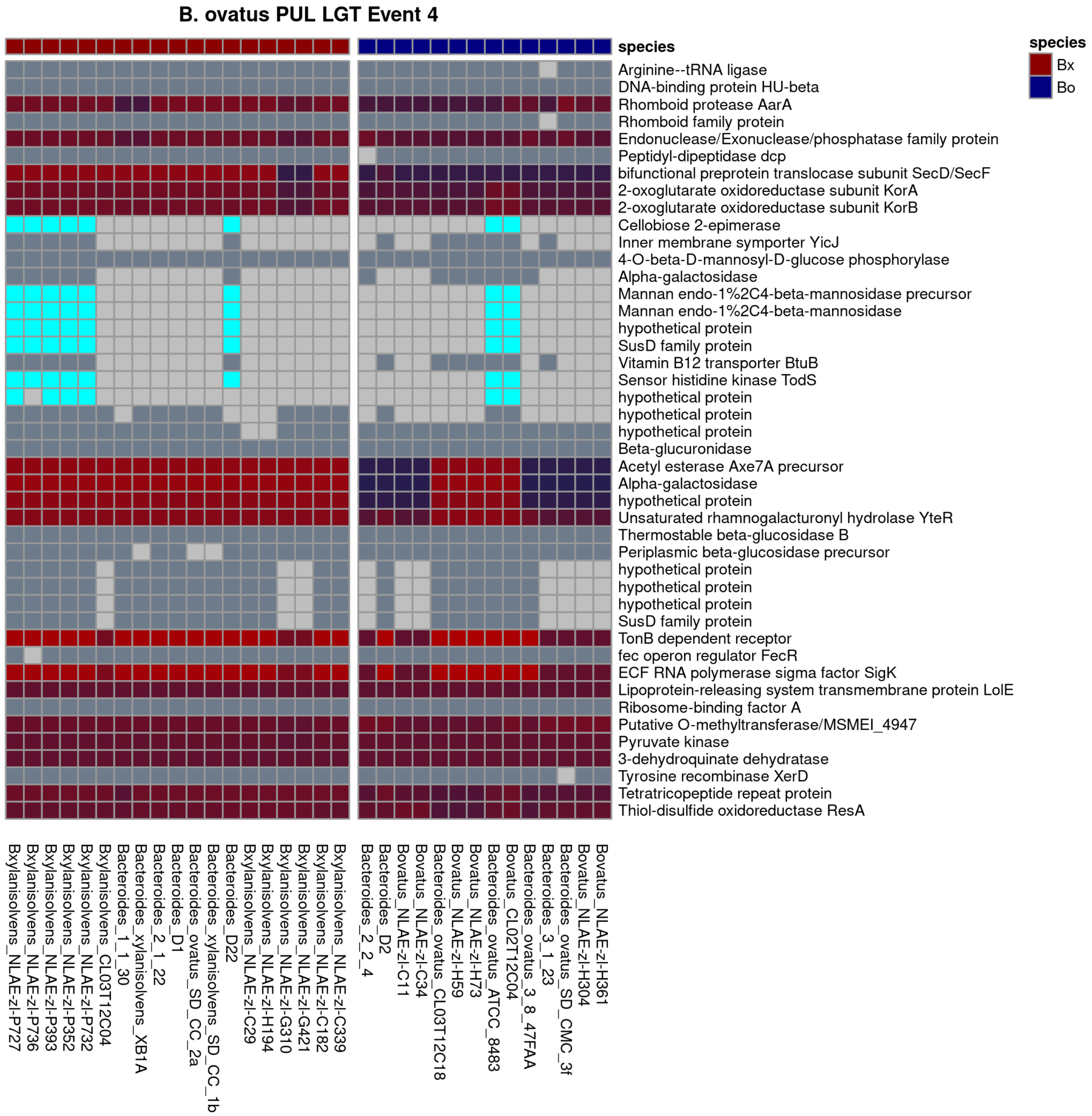
B. ovatus PUL LGT Event 4
species
species
Bx
Bo
Arginine--tRNA ligase
DNA-binding protein HU-beta
Rhomboid protease AarA
Rhomboid family protein
Endonuclease/Exonuclease/phosphatase family protein
Peptidyl-dipeptidase dcp
bifunctional preprotein translocase subunit SecD/SecF
2-oxoglutarate oxidoreductase subunit KorA
2-oxoglutarate oxidoreductase subunit KorB
Cellobiose 2-epimerase
Inner membrane symporter YicJ
4-O-beta-D-mannosyl-D-glucose phosphorylase
Alpha-galactosidase
Mannan endo-1%2C4-beta-mannosidase precursor
Mannan endo-1%2C4-beta-mannosidase
hypothetical protein
SusD family protein
Vitamin B12 transporter BtuB
Sensor histidine kinase TodS
hypothetical protein
hypothetical protein
hypothetical protein
Beta-glucuronidase
Acetyl esterase Axe7A precursor
Alpha-galactosidase
hypothetical protein
Unsaturated rhamnogalacturonyl hydrolase YteR
Thermostable beta-glucosidase B
Periplasmic beta-glucosidase precursor
hypothetical protein
hypothetical protein
hypothetical protein
SusD family protein
TonB dependent receptor
fec operon regulator FecR
ECF RNA polymerase sigma factor SigK
Lipoprotein-releasing system transmembrane protein LolE
Ribosome-binding factor A
Putative O-methyltransferase/MSMEI_4947
Pyruvate kinase
3-dehydroquinate dehydratase
Tyrosine recombinase XerD
Tetratricopeptide repeat protein
Thiol-disulfide oxidoreductase ResA
Bxylanisolvens_NLAE-zl-P727
Bxylanisolvens_NLAE-zl-P736
Bxylanisolvens_NLAE-zl-P393
Bxylanisolvens_NLAE-zl-P352
Bxylanisolvens_NLAE-zl-P732
Bxylanisolvens_CL03T12C04
Bacteroides_1_1_30
Bacteroides_xylanisolvens_XB1A
Bacteroides_2_1_22
Bacteroides_D1
Bacteroides_ovatus_SD_CC_2a
Bacteroides_xylanisolvens_SD_CC_1b
Bacteroides_D22
Bxylanisolvens_NLAE-zl-C29
Bxylanisolvens_NLAE-zl-H194
Bxylanisolvens_NLAE-zl-G310
Bxylanisolvens_NLAE-zl-G421
Bxylanisolvens_NLAE-zl-C182
Bxylanisolvens_NLAE-zl-C339
Bacteroides_2_2_4
Bacteroides_D2
Bovatus_NLAE-zl-C11
Bovatus_NLAE-zl-C34
Bacteroides_ovatus_CL03T12C18
Bovatus_NLAE-zl-H59
Bovatus_NLAE-zl-H73
Bacteroides_ovatus_ATCC_8483
Bovatus_CL02T12C04
Bacteroides_ovatus_3_8_47FAA
Bacteroides_3_1_23
Bacteroides_ovatus_SD_CMC_3f
Bovatus_NLAE-zl-H304
Bovatus_NLAE-zl-H361

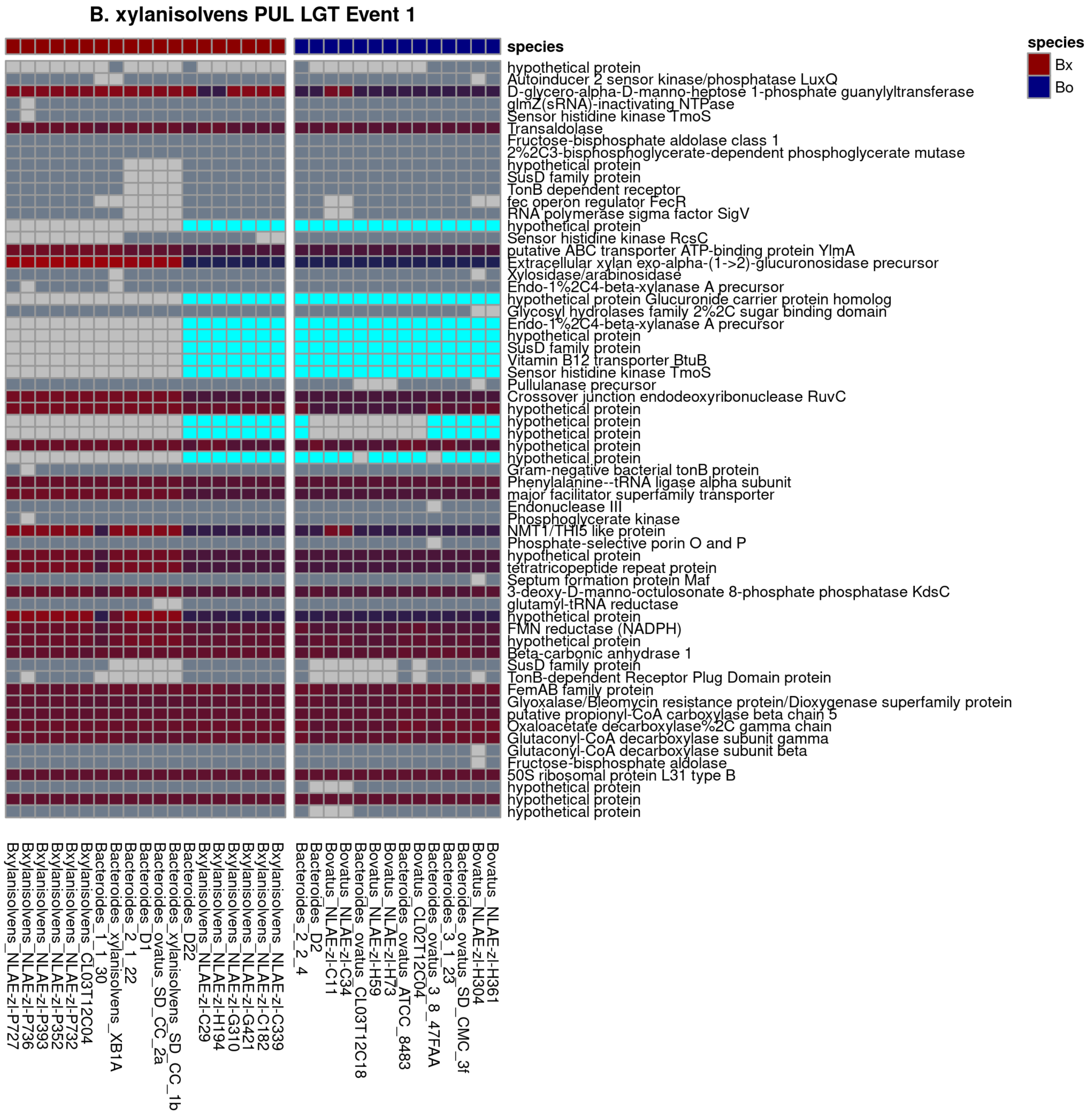
B. xylanisolvens PUL LGT Event 1
species
species
Bx
Bo
hypothetical protein
Autoinducer 2 sensor kinase/phosphatase LuxQ
D-glycero-alpha-D-manno-heptose 1-phosphate guanylyltransferase
glmZ(sRNA)-inactivating NTPase
Sensor histidine kinase TmoS
Transaldolase
Fructose-bisphosphate aldolase class 1
2%2C3-bisphosphoglycerate-dependent phosphoglycerate mutase
hypothetical protein
SusD family protein
TonB dependent receptor
fec operon regulator FecR
RNA polymerase sigma factor SigV
hypothetical protein
Sensor histidine kinase RcsC
putative ABC transporter ATP-binding protein YlmA
Extracellular xylan exo-alpha-(1->2)-glucuronosidase precursor
Xylosidase/arabinosidase
Endo-1%2C4-beta-xylanase A precursor
hypothetical protein Glucuronide carrier protein homolog
Glycosyl hydrolases family 2%2C sugar binding domain
Endo-1%2C4-beta-xylanase A precursor
hypothetical protein
SusD family protein
Vitamin B12 transporter BtuB
Sensor histidine kinase TmoS
Pullulanase precursor
Crossover junction endodeoxyribonuclease RuvC
hypothetical protein
hypothetical protein
hypothetical protein
hypothetical protein
hypothetical protein
Gram-negative bacterial tonB protein
Phenylalanine--tRNA ligase alpha subunit
major facilitator superfamily transporter
Endonuclease III
Phosphoglycerate kinase
NMT1/THI5 like protein
Phosphate-selective porin O and P
hypothetical protein
tetratricopeptide repeat protein
Septum formation protein Maf
3-deoxy-D-manno-octulosonate 8-phosphate phosphatase KdsC
glutamyl-tRNA reductase
hypothetical protein
FMN reductase (NADPH)
hypothetical protein
Beta-carbonic anhydrase 1
SusD family protein
TonB-dependent Receptor Plug Domain protein
FemAB family protein
Glyoxalase/Bleomycin resistance protein/Dioxygenase superfamily protein
putative propionyl-CoA carboxylase beta chain 5
Oxaloacetate decarboxylase%2C gamma chain
Glutaconyl-CoA decarboxylase subunit gamma
Glutaconyl-CoA decarboxylase subunit beta
Fructose-bisphosphate aldolase
50S ribosomal protein L31 type B
hypothetical protein
hypothetical protein
hypothetical protein
Bxylanisolvens_NLAE-zl-P727
Bxylanisolvens_NLAE-zl-P736
Bxylanisolvens_NLAE-zl-P393
Bxylanisolvens_NLAE-zl-P352
Bxylanisolvens_NLAE-zl-P732
Bxylanisolvens_CL03T12C04
Bacteroides_1_1_30
Bacteroides_xylanisolvens_XB1A
Bacteroides_2_1_22
Bacteroides_D1
Bacteroides_ovatus_SD_CC_2a
Bacteroides_xylanisolvens_SD_CC_1b
Bacteroides_D22
Bxylanisolvens_NLAE-zl-C29
Bxylanisolvens_NLAE-zl-H194
Bxylanisolvens_NLAE-zl-G310
Bxylanisolvens_NLAE-zl-G421
Bxylanisolvens_NLAE-zl-C182
Bxylanisolvens_NLAE-zl-C339
Bacteroides_2_2_4
Bacteroides_D2
Bovatus_NLAE-zl-C11
Bovatus_NLAE-zl-C34
Bacteroides_ovatus_CL03T12C18
Bovatus_NLAE-zl-H59
Bovatus_NLAE-zl-H73
Bacteroides_ovatus_ATCC_8483
Bovatus_CL02T12C04
Bacteroides_ovatus_3_8_47FAA
Bacteroides_3_1_23
Bacteroides_ovatus_SD_CMC_3f
Bovatus_NLAE-zl-H304
Bovatus_NLAE-zl-H361

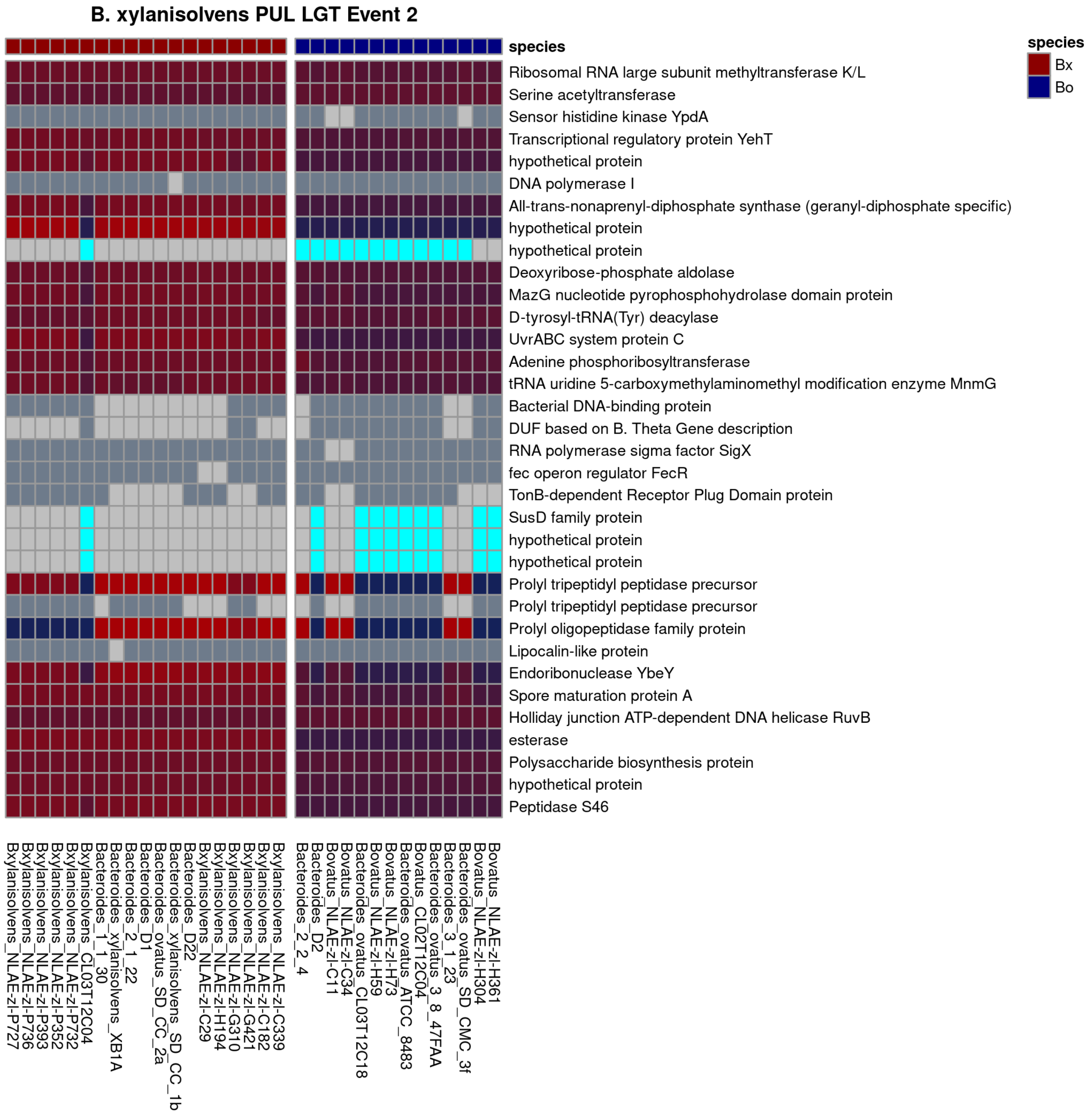
B. xylanisolvens PUL LGT Event 2
species
Bx
Bo
species
Ribosomal RNA large subunit methyltransferase K/L
Serine acetyltransferase
Sensor histidine kinase YpdA
Transcriptional regulatory protein YehT
hypothetical protein
DNA polymerase I
All-trans-nonaprenyl-diphosphate synthase (geranyl-diphosphate specific)
hypothetical protein
hypothetical protein
Deoxyribose-phosphate aldolase
MazG nucleotide pyrophosphohydrolase domain protein
D-tyrosyl-tRNA(Tyr) deacylase
UvrABC system protein C
Adenine phosphoribosyltransferase
tRNA uridine 5-carboxymethylaminomethyl modification enzyme MnmG
Bacterial DNA-binding protein
DUF based on B. Theta Gene description
RNA polymerase sigma factor SigX
fec operon regulator FecR
TonB-dependent Receptor Plug Domain protein
SusD family protein
hypothetical protein
hypothetical protein
Prolyl tripeptidyl peptidase precursor
Prolyl tripeptidyl peptidase precursor
Prolyl oligopeptidase family protein
Lipocalin-like protein
Endoribonuclease YbeY
Spore maturation protein A
Holliday junction ATP-dependent DNA helicase RuvB
esterase
Polysaccharide biosynthesis protein
hypothetical protein
Peptidase S46
Bxylanisolvens_NLAE-zl-P727
Bxylanisolvens_NLAE-zl-P736
Bxylanisolvens_NLAE-zl-P393
Bxylanisolvens_NLAE-zl-P352
Bxylanisolvens_NLAE-zl-P732
Bxylanisolvens_CL03T12C04
Bacteroides_1_1_30
Bacteroides_xylanisolvens_XB1A
Bacteroides_2_1_22
Bacteroides_D1
Bacteroides_ovatus_SD_CC_2a
Bacteroides_xylanisolvens_SD_CC_1b
Bacteroides_D22
Bxylanisolvens_NLAE-zl-C29
Bxylanisolvens_NLAE-zl-H194
Bxylanisolvens_NLAE-zl-G310
Bxylanisolvens_NLAE-zl-G421
Bxylanisolvens_NLAE-zl-C182
Bxylanisolvens_NLAE-zl-C339
Bacteroides_2_2_4
Bacteroides_D2
Bovatus_NLAE-zl-C11
Bovatus_NLAE-zl-C34
Bacteroides_ovatus_CL03T12C18
Bovatus_NLAE-zl-H59
Bovatus_NLAE-zl-H73
Bacteroides_ovatus_ATCC_8483
Bovatus_CL02T12C04
Bacteroides_ovatus_3_8_47FAA
Bacteroides_3_1_23
Bacteroides_ovatus_SD_CMC_3f
Bovatus_NLAE-zl-H304
Bovatus_NLAE-zl-H361

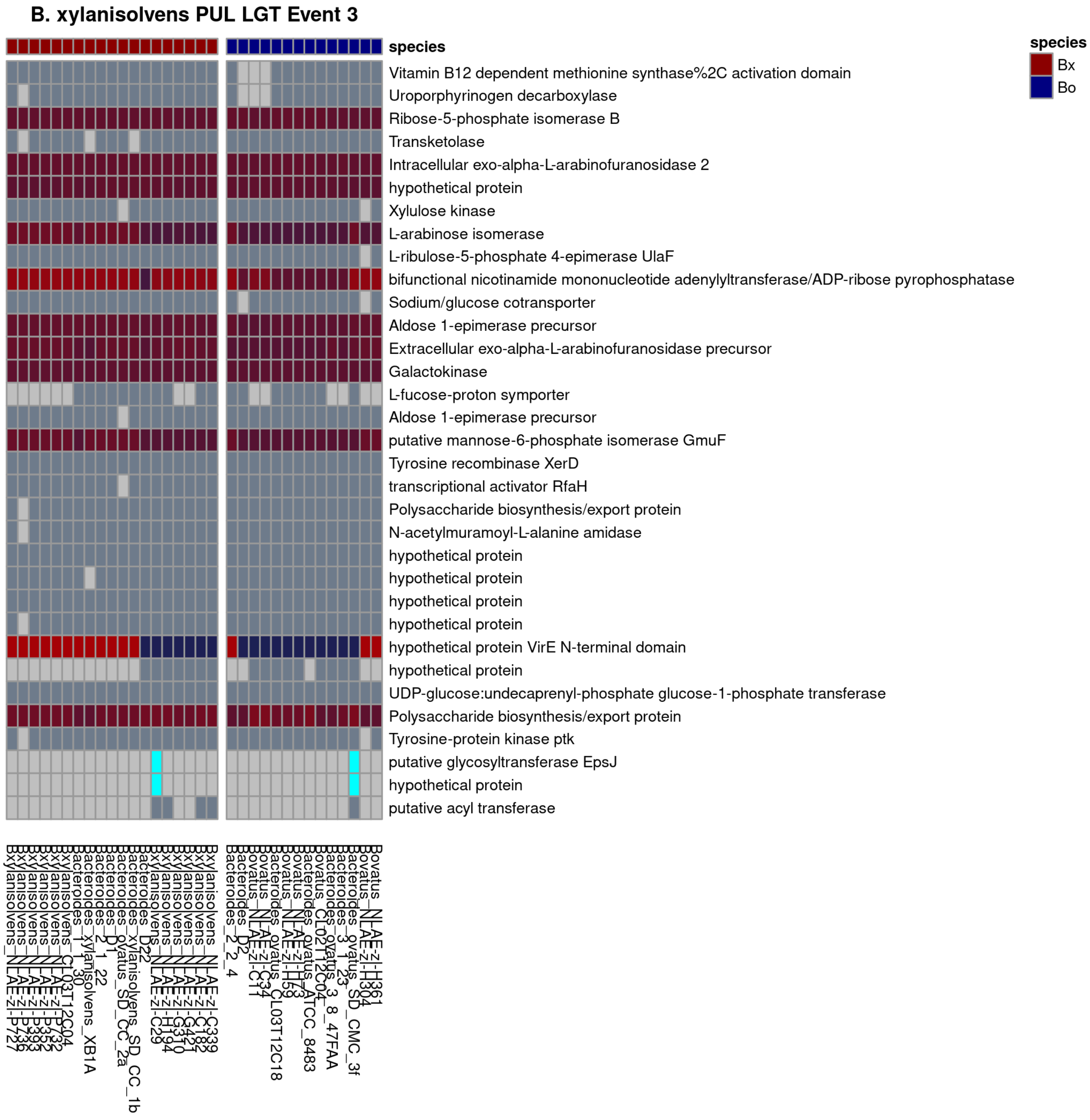
B. xylanisolvens PUL LGT Event 3
species
Bx
Bo
species
Vitamin B12 dependent methionine synthase%2C activation domain
Uroporphyrinogen decarboxylase
Ribose-5-phosphate isomerase B
Transketolase
Intracellular exo-alpha-L-arabinofuranosidase 2
hypothetical protein
Xylulose kinase
L-arabinose isomerase
L-ribulose-5-phosphate 4-epimerase UlaF
bifunctional nicotinamide mononucleotide adenylyltransferase/ADP-ribose pyrophosphatase
Sodium/glucose cotransporter
Aldose 1-epimerase precursor
Extracellular exo-alpha-L-arabinofuranosidase precursor
Galactokinase
L-fucose-proton symporter
Aldose 1-epimerase precursor
putative mannose-6-phosphate isomerase GmuF
Tyrosine recombinase XerD
transcriptional activator RfaH
Polysaccharide biosynthesis/export protein
N-acetylmuramoyl-L-alanine amidase
hypothetical protein
hypothetical protein
hypothetical protein
hypothetical protein
hypothetical protein VirE N-terminal domain
hypothetical protein
UDP-glucose:undecaprenyl-phosphate glucose-1-phosphate transferase
Polysaccharide biosynthesis/export protein
Tyrosine-protein kinase ptk
putative glycosyltransferase EpsJ
hypothetical protein
putative acyl transferase
Bxylanisolvens_NLAE-zl-P727
Bxylanisolvens_NLAE-zl-P736
Bxylanisolvens_NLAE-zl-P393
Bxylanisolvens_NLAE-zl-P352
Bxylanisolvens_NLAE-zl-P732
Bxylanisolvens_CL03T12C04
Bacteroides_1_1_30
Bacteroides_xylanisolvens_XB1A
Bacteroides_2_1_22
Bacteroides_D1
Bacteroides_ovatus_SD_CC_2a
Bacteroides_xylanisolvens_SD_CC_1b
Bacteroides_D22
Bxylanisolvens_NLAE-zl-C29
Bxylanisolvens_NLAE-zl-H194
Bxylanisolvens_NLAE-zl-G310
Bxylanisolvens_NLAE-zl-G421
Bxylanisolvens_NLAE-zl-C182
Bxylanisolvens_NLAE-zl-C339
Bacteroides_2_2_4
Bacteroides_D2
Bovatus_NLAE-zl-C11
Bovatus_NLAE-zl-C34
Bacteroides_ovatus_CL03T12C18
Bovatus_NLAE-zl-H59
Bovatus_NLAE-zl-H73
Bacteroides_ovatus_ATCC_8483
Bovatus_CL02T12C04
Bacteroides_ovatus_3_8_47FAA
Bacteroides_3_1_23
Bacteroides_ovatus_SD_CMC_3f
Bovatus_NLAE-zl-H304
Bovatus_NLAE-zl-H361

non-PUL LGT Events

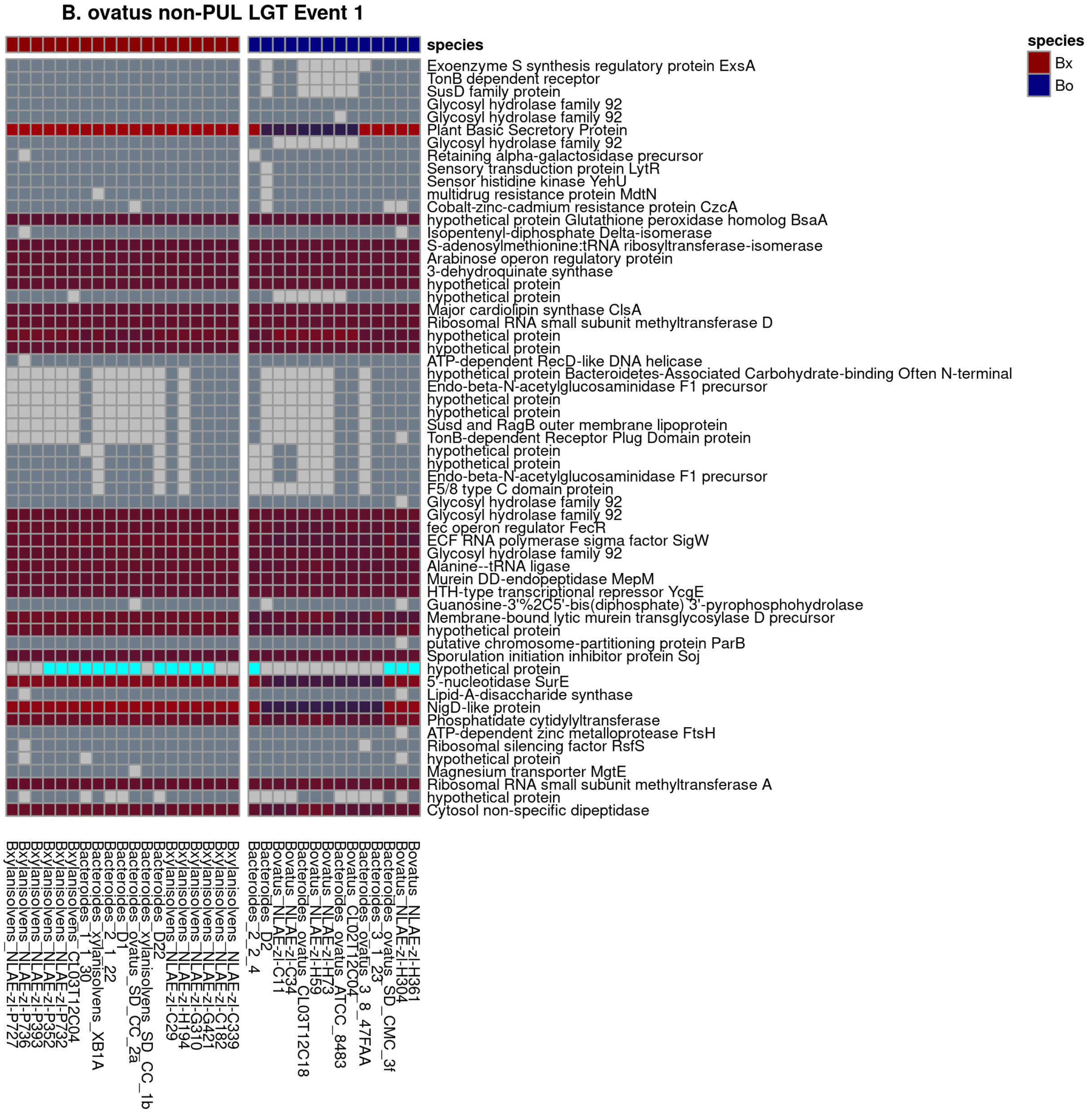

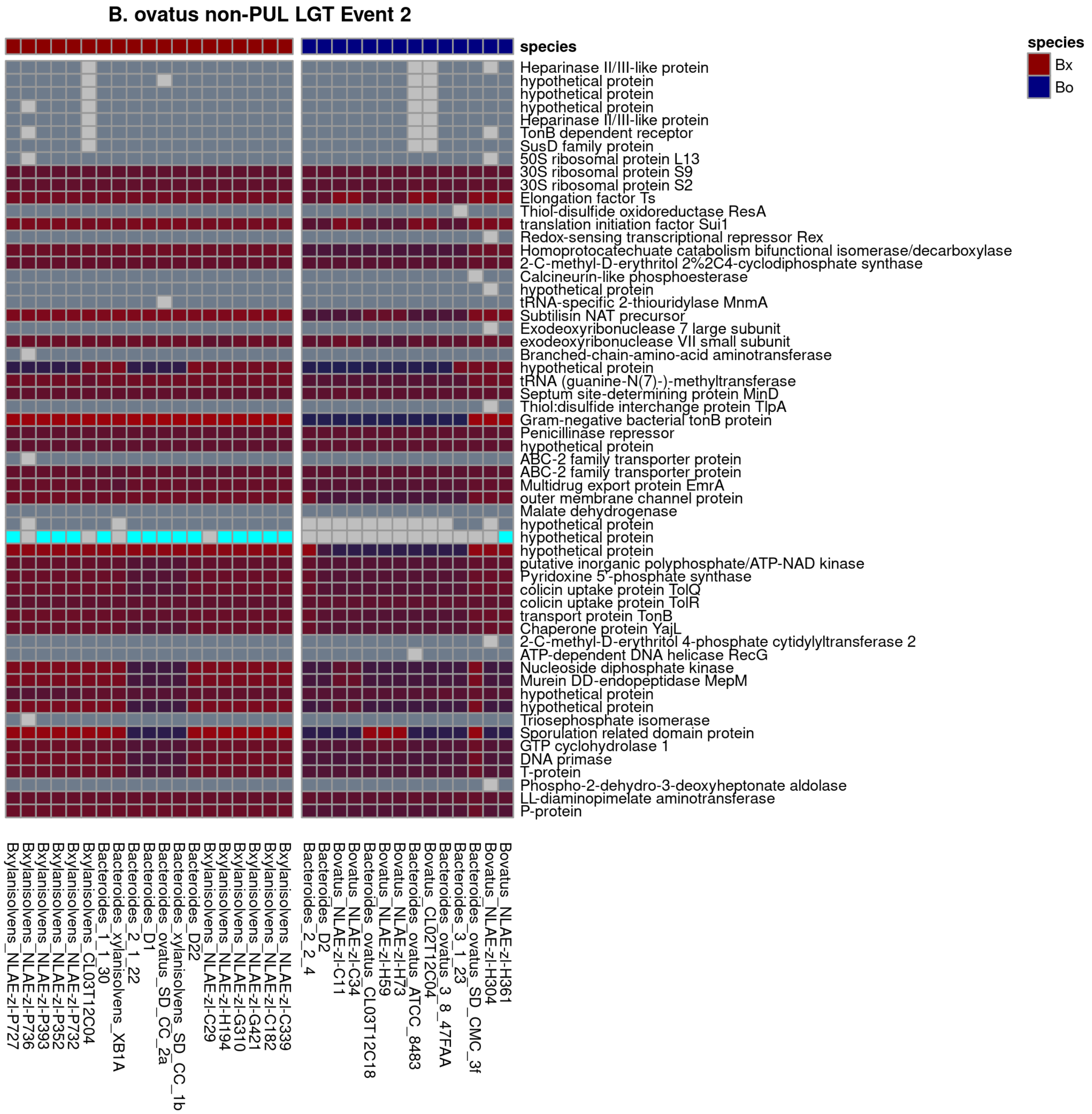
B. ovatus non-PUL LGT Event 2
species
species
Bx
Bo
Heparinase II/III-like protein
hypothetical protein
hypothetical protein
hypothetical protein
Heparinase II/III-like protein
TonB dependent receptor
SusD family protein
50S ribosomal protein L13
30S ribosomal protein S9
30S ribosomal protein S2
Elongation factor Ts
Thiol-disulfide oxidoreductase ResA
translation initiation factor Sui1
Redox-sensing transcriptional repressor Rex
Homoprotocatechuate catabolism bifunctional isomerase/decarboxylase
2-C-methyl-D-erythritol 2%2C4-cyclodiphosphate synthase
Calcineurin-like phosphoesterase
hypothetical protein
tRNA-specific 2-thiouridylase MnmA
Subtilisin NAT precursor
Exodeoxyribonuclease 7 large subunit
exodeoxyribonuclease VII small subunit
Branched-chain-amino-acid aminotransferase
hypothetical protein
tRNA (guanine-N(7)-)-methyltransferase
Septum site-determining protein MinD
Thiol:disulfide interchange protein TlpA
Gram-negative bacterial tonB protein
Penicillinase repressor
hypothetical protein
ABC-2 family transporter protein
ABC-2 family transporter protein
Multidrug export protein EmrA
outer membrane channel protein
Malate dehydrogenase
hypothetical protein
hypothetical protein
hypothetical protein
putative inorganic polyphosphate/ATP-NAD kinase
Pyridoxine 5'-phosphate synthase
colicin uptake protein TolQ
colicin uptake protein TolR
transport protein TonB
Chaperone protein YajL
2-C-methyl-D-erythritol 4-phosphate cytidylyltransferase 2
ATP-dependent DNA helicase RecG
Nucleoside diphosphate kinase
Murein DD-endopeptidase MepM
hypothetical protein
hypothetical protein
Triosephosphate isomerase
Sporulation related domain protein
GTP cyclohydrolase 1
DNA primase
T-protein
Phospho-2-dehydro-3-deoxyheptonate aldolase
LL-diaminopimelate aminotransferase
P-protein
Bxylanisolvens_NLAE-zl-P727
Bxylanisolvens_NLAE-zl-P736
Bxylanisolvens_NLAE-zl-P393
Bxylanisolvens_NLAE-zl-P352
Bxylanisolvens_NLAE-zl-P732
Bxylanisolvens_CL03T12C04
Bacteroides_1_1_30
Bacteroides_xylanisolvens_XB1A
Bacteroides_2_1_22
Bacteroides_D1
Bacteroides_ovatus_SD_CC_2a
Bacteroides_xylanisolvens_SD_CC_1b
Bacteroides_D22
Bxylanisolvens_NLAE-zl-C29
Bxylanisolvens_NLAE-zl-H194
Bxylanisolvens_NLAE-zl-G310
Bxylanisolvens_NLAE-zl-G421
Bxylanisolvens_NLAE-zl-C182
Bxylanisolvens_NLAE-zl-C339
Bacteroides_2_2_4
Bacteroides_D2
Bovatus_NLAE-zl-C11
Bovatus_NLAE-zl-C34
Bacteroides_ovatus_CL03T12C18
Bovatus_NLAE-zl-H59
Bovatus_NLAE-zl-H73
Bacteroides_ovatus_ATCC_8483
Bovatus_CL02T12C04
Bacteroides_ovatus_3_8_47FAA
Bacteroides_3_1_23
Bacteroides_ovatus_SD_CMC_3f
Bovatus_NLAE-zl-H304
Bovatus_NLAE-zl-H361

B. ovatus non-PUL LGT Event 3

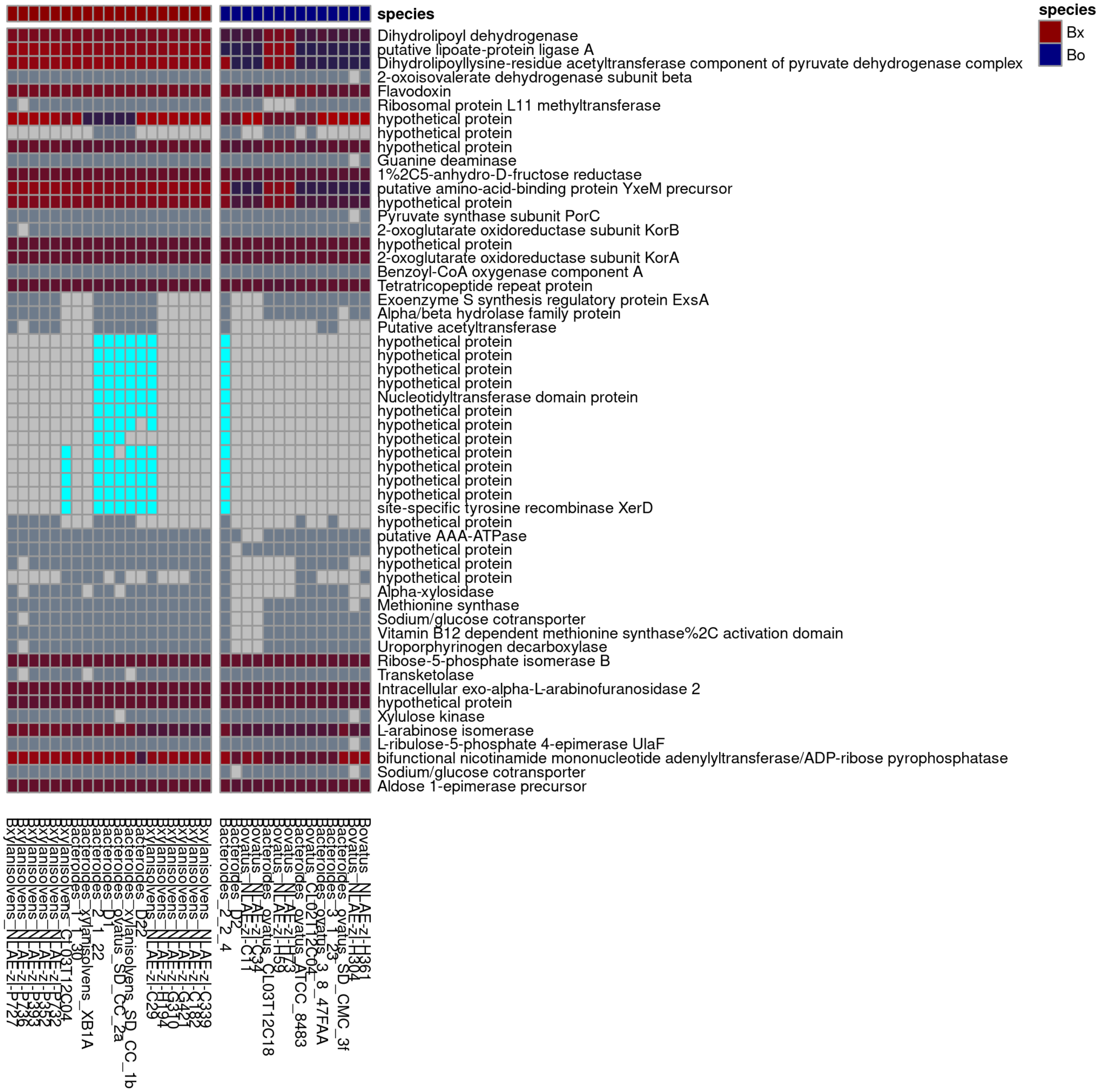

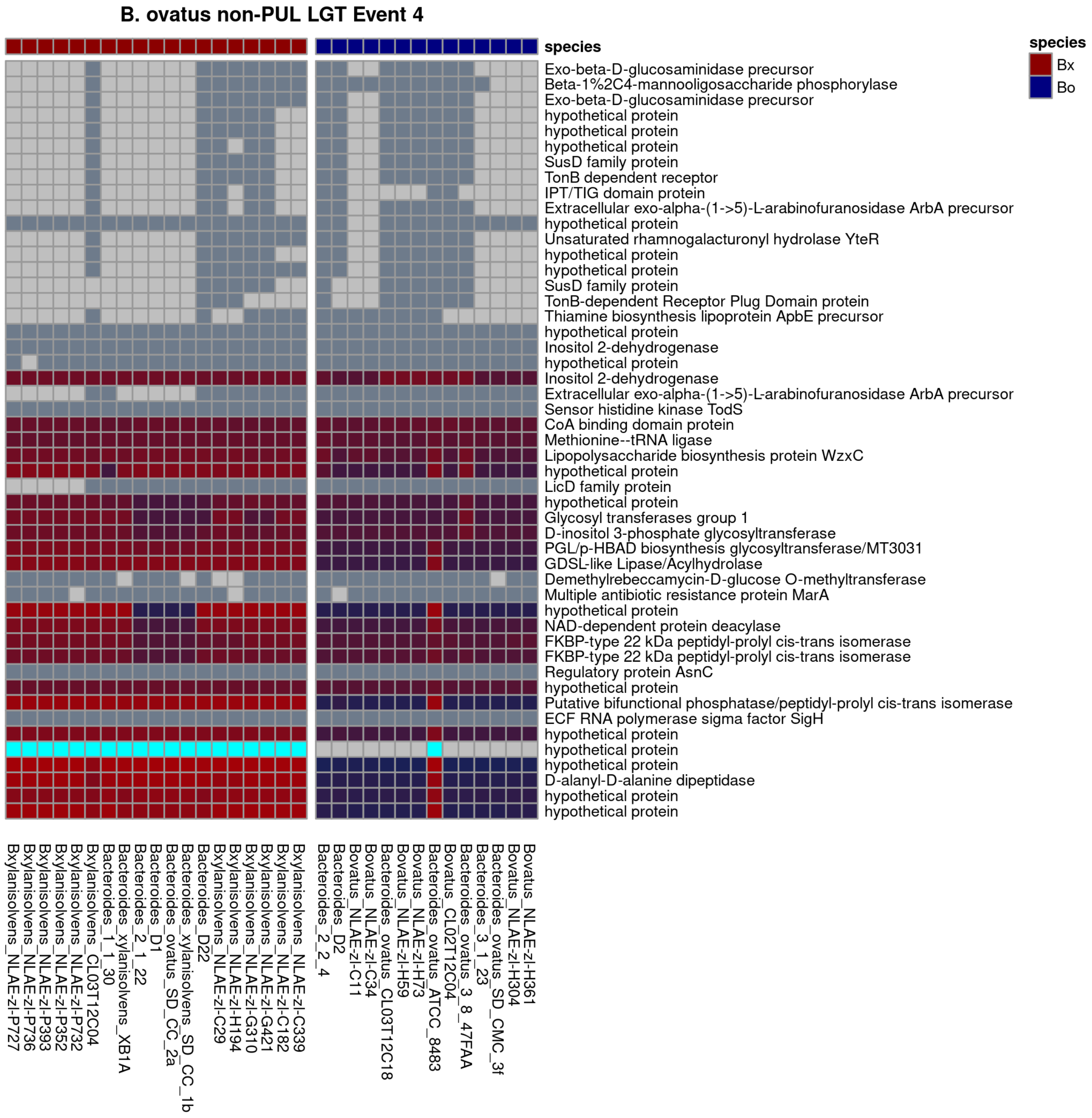
B. ovatus non-PUL LGT Event 4
species
species
Bx
Bo
Exo-beta-D-glucosaminidase precursor
Beta-1%2C4-mannooligosaccharide phosphorylase
Exo-beta-D-glucosaminidase precursor
hypothetical protein
hypothetical protein
hypothetical protein
SusD family protein
TonB dependent receptor
IPT/TIG domain protein
Extracellular exo-alpha-(1->5)-L-arabinofuranosidase ArbA precursor
hypothetical protein
Unsaturated rhamnogalacturonyl hydrolase YteR
hypothetical protein
hypothetical protein
SusD family protein
TonB-dependent Receptor Plug Domain protein
Thiamine biosynthesis lipoprotein ApbE precursor
hypothetical protein
Inositol 2-dehydrogenase
hypothetical protein
Inositol 2-dehydrogenase
Extracellular exo-alpha-(1->5)-L-arabinofuranosidase ArbA precursor
Sensor histidine kinase TodS
CoA binding domain protein
Methionine--tRNA ligase
Lipopolysaccharide biosynthesis protein WzxC
hypothetical protein
LicD family protein
hypothetical protein
Glycosyl transferases group 1
D-inositol 3-phosphate glycosyltransferase
PGL/p-HBAD biosynthesis glycosyltransferase/MT3031
GDSL-like Lipase/Acylhydrolase
Demethylrebeccamycin-D-glucose O-methyltransferase
Multiple antibiotic resistance protein MarA
hypothetical protein
NAD-dependent protein deacylase
FKBP-type 22 kDa peptidyl-prolyl cis-trans isomerase
FKBP-type 22 kDa peptidyl-prolyl cis-trans isomerase
Regulatory protein AsnC
hypothetical protein
Putative bifunctional phosphatase/peptidyl-prolyl cis-trans isomerase
ECF RNA polymerase sigma factor SigH
hypothetical protein
hypothetical protein
hypothetical protein
D-alanyl-D-alanine dipeptidase
hypothetical protein
hypothetical protein
Bxylanisolvens_NLAE-zl-P727
Bxylanisolvens_NLAE-zl-P736
Bxylanisolvens_NLAE-zl-P393
Bxylanisolvens_NLAE-zl-P352
Bxylanisolvens_NLAE-zl-P732
Bxylanisolvens_CL03T12C04
Bacteroides_1_1_30
Bacteroides_xylanisolvens_XB1A
Bacteroides_2_1_22
Bacteroides_D1
Bacteroides_ovatus_SD_CC_2a
Bacteroides_xylanisolvens_SD_CC_1b
Bacteroides_D22
Bxylanisolvens_NLAE-zl-C29
Bxylanisolvens_NLAE-zl-H194
Bxylanisolvens_NLAE-zl-G310
Bxylanisolvens_NLAE-zl-G421
Bxylanisolvens_NLAE-zl-C182
Bxylanisolvens_NLAE-zl-C339
Bacteroides_2_2_4
Bacteroides_D2
Bovatus_NLAE-zl-C11
Bovatus_NLAE-zl-C34
Bacteroides_ovatus_CL03T12C18
Bovatus_NLAE-zl-H59
Bovatus_NLAE-zl-H73
Bacteroides_ovatus_ATCC_8483
Bovatus_CL02T12C04
Bacteroides_ovatus_3_8_47FAA
Bacteroides_3_1_23
Bacteroides_ovatus_SD_CMC_3f
Bovatus_NLAE-zl-H304
Bovatus_NLAE-zl-H361

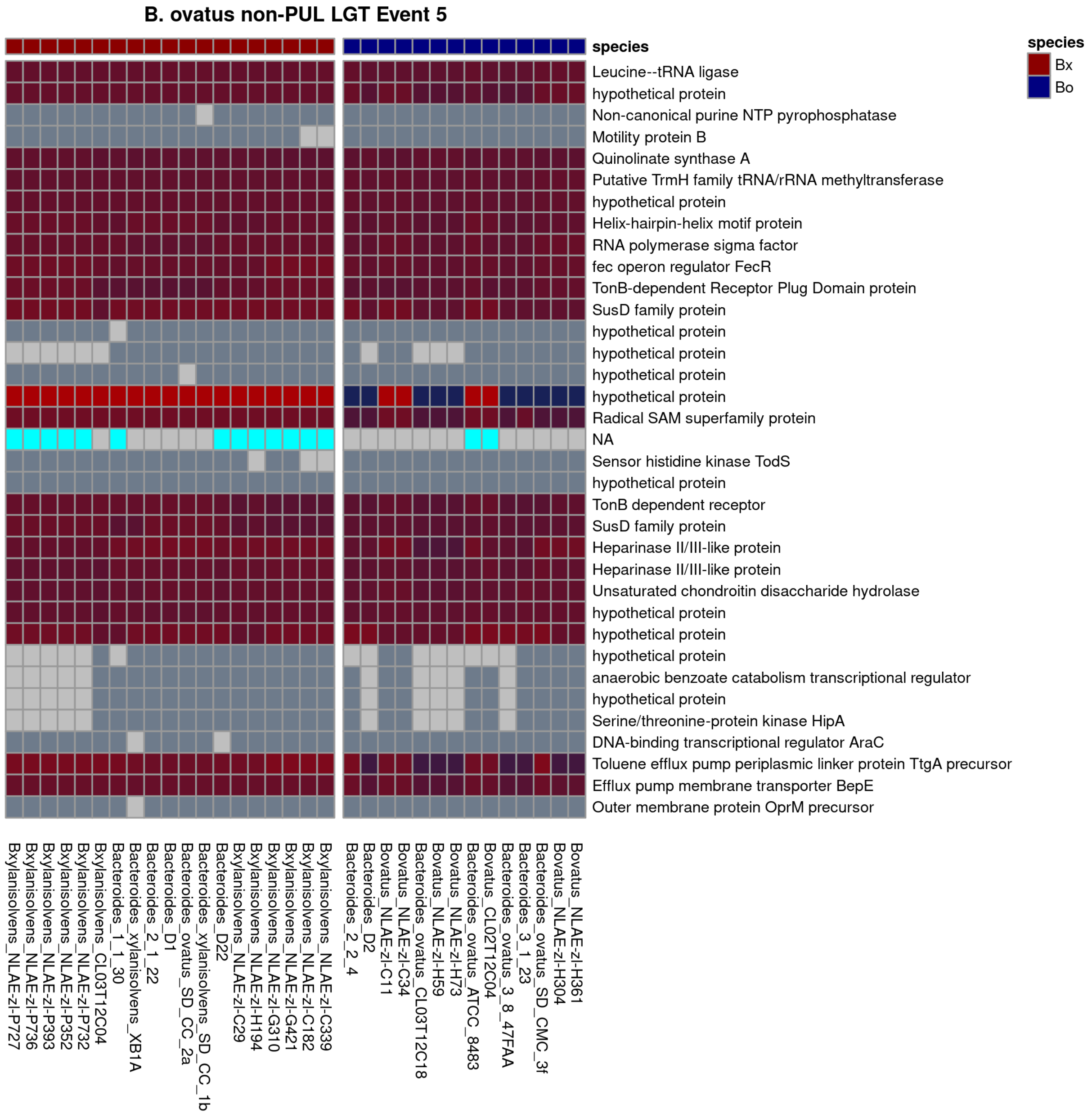
B. ovatus non-PUL LGT Event 5
species
species
Bx
Bo
Leucine--tRNA ligase
hypothetical protein
Non-canonical purine NTP pyrophosphatase
Motility protein B
Quinolinate synthase A
Putative TrmH family tRNA/rRNA methyltransferase
hypothetical protein
Helix-hairpin-helix motif protein
RNA polymerase sigma factor
fec operon regulator FecR
TonB-dependent Receptor Plug Domain protein
SusD family protein
hypothetical protein
hypothetical protein
hypothetical protein
hypothetical protein
Radical SAM superfamily protein
NA
Sensor histidine kinase TodS
hypothetical protein
TonB dependent receptor
SusD family protein
Heparinase II/III-like protein
Heparinase II/III-like protein
Unsaturated chondroitin disaccharide hydrolase
hypothetical protein
hypothetical protein
hypothetical protein
anaerobic benzoate catabolism transcriptional regulator
hypothetical protein
Serine/threonine-protein kinase HipA
DNA-binding transcriptional regulator AraC
Toluene efflux pump periplasmic linker protein TtgA precursor
Efflux pump membrane transporter BepE
Outer membrane protein OprM precursor
Bxylanisolvens_NLAE-zl-P727
Bxylanisolvens_NLAE-zl-P736
Bxylanisolvens_NLAE-zl-P393
Bxylanisolvens_NLAE-zl-P352
Bxylanisolvens_NLAE-zl-P732
Bxylanisolvens_CL03T12C04
Bacteroides_1_1_30
Bacteroides_xylanisolvens_XB1A
Bacteroides_2_1_22
Bacteroides_D1
Bacteroides_ovatus_SD_CC_2a
Bacteroides_xylanisolvens_SD_CC_1b
Bacteroides_D22
Bxylanisolvens_NLAE-zl-C29
Bxylanisolvens_NLAE-zl-H194
Bxylanisolvens_NLAE-zl-G310
Bxylanisolvens_NLAE-zl-G421
Bxylanisolvens_NLAE-zl-C182
Bxylanisolvens_NLAE-zl-C339
Bacteroides_2_2_4
Bacteroides_D2
Bovatus_NLAE-zl-C11
Bovatus_NLAE-zl-C34
Bacteroides_ovatus_CL03T12C18
Bovatus_NLAE-zl-H59
Bovatus_NLAE-zl-H73
Bacteroides_ovatus_ATCC_8483
Bovatus_CL02T12C04
Bacteroides_ovatus_3_8_47FAA
Bacteroides_3_1_23
Bacteroides_ovatus_SD_CMC_3f
Bovatus_NLAE-zl-H304
Bovatus_NLAE-zl-H361

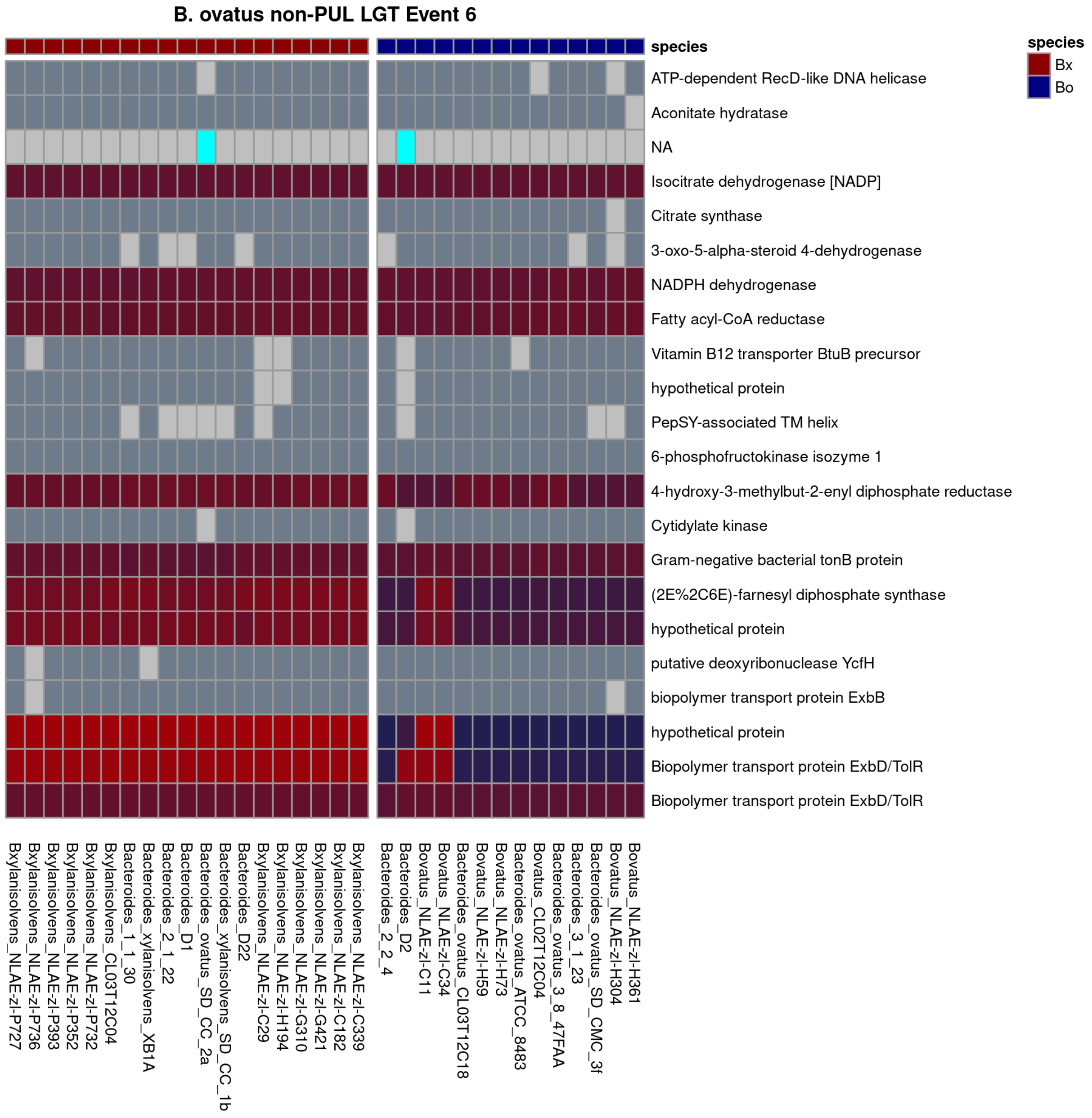
B. ovatus non-PUL LGT Event 6
species
species
Bx
Bo
ATP-dependent RecD-like DNA helicase
Aconitate hydratase
NA
Isocitrate dehydrogenase [NADP]
Citrate synthase
3-oxo-5-alpha-steroid 4-dehydrogenase
NADPH dehydrogenase
Fatty acyl-CoA reductase
Vitamin B12 transporter BtuB precursor
hypothetical protein
PepSY-associated TM helix
6-phosphofructokinase isozyme 1
4-hydroxy-3-methylbut-2-enyl diphosphate reductase
Cytidylate kinase
Gram-negative bacterial tonB protein
(2E%2C6E)-farnesyl diphosphate synthase
hypothetical protein
putative deoxyribonuclease YcfH
biopolymer transport protein ExbB
hypothetical protein
Biopolymer transport protein ExbD/TolR
Biopolymer transport protein ExbD/TolR
Bxylanisolvens_NLAE-zl-P727
Bxylanisolvens_NLAE-zl-P736
Bxylanisolvens_NLAE-zl-P393
Bxylanisolvens_NLAE-zl-P352
Bxylanisolvens_NLAE-zl-P732
Bxylanisolvens_CL03T12C04
Bacteroides_1_1_30
Bacteroides_xylanisolvens_XB1A
Bacteroides_2_1_22
Bacteroides_D1
Bacteroides_ovatus_SD_CC_2a
Bacteroides_xylanisolvens_SD_CC_1b
Bacteroides_D22
Bxylanisolvens_NLAE-zl-C29
Bxylanisolvens_NLAE-zl-H194
Bxylanisolvens_NLAE-zl-G310
Bxylanisolvens_NLAE-zl-G421
Bxylanisolvens_NLAE-zl-C182
Bxylanisolvens_NLAE-zl-C339
Bacteroides_2_2_4
Bacteroides_D2
Bovatus_NLAE-zl-C11
Bovatus_NLAE-zl-C34
Bacteroides_ovatus_CL03T12C18
Bovatus_NLAE-zl-H59
Bovatus_NLAE-zl-H73
Bacteroides_ovatus_ATCC_8483
Bovatus_CL02T12C04
Bacteroides_ovatus_3_8_47FAA
Bacteroides_3_1_23
Bacteroides_ovatus_SD_CMC_3f
Bovatus_NLAE-zl-H304
Bovatus_NLAE-zl-H361

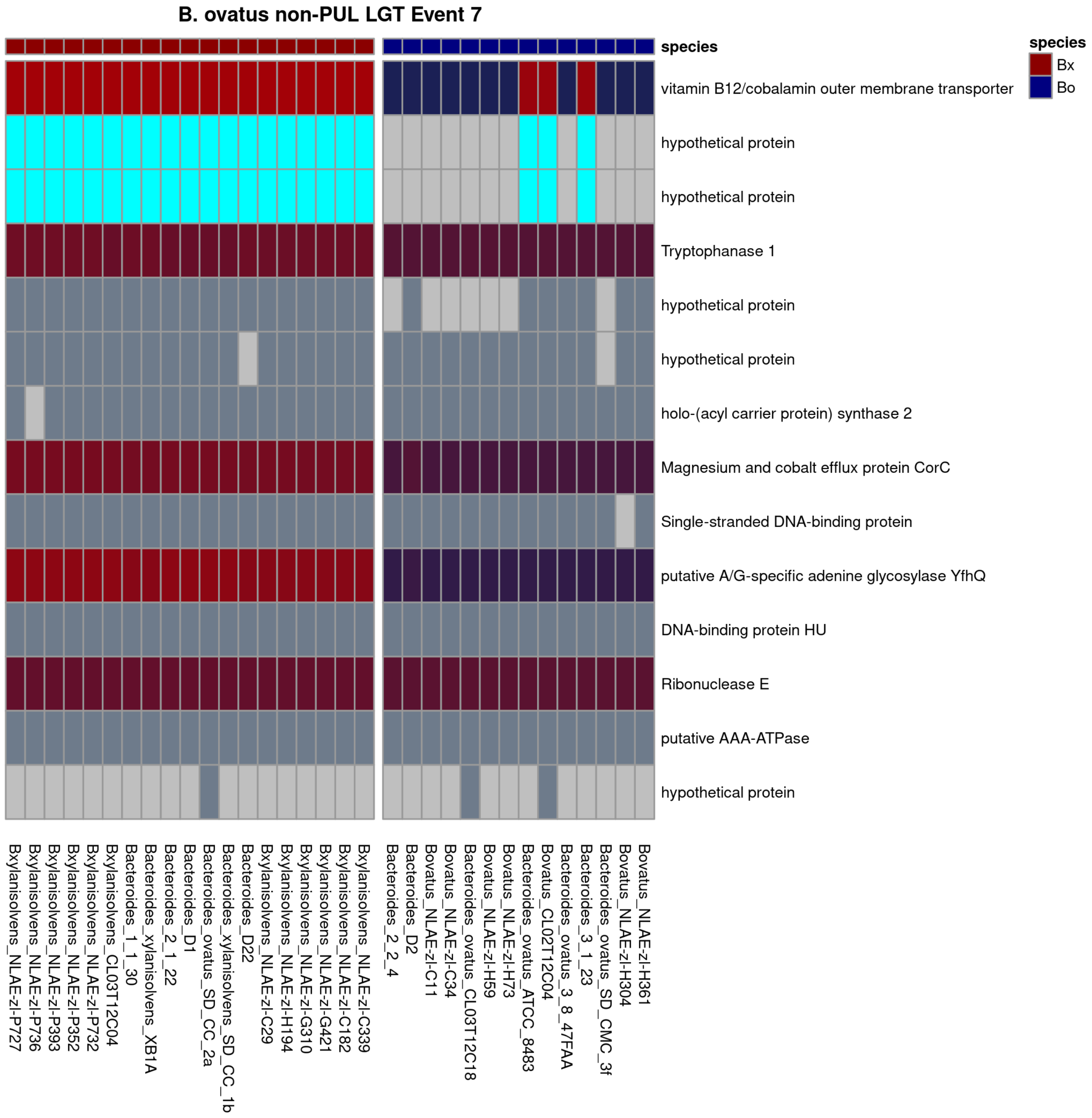
B. ovatus non-PUL LGT Event 7
species
vitamin B12/cobalamin outer membrane transporter
hypothetical protein
hypothetical protein
Tryptophanase 1
hypothetical protein
hypothetical protein
holo-(acyl carrier protein) synthase 2
Magnesium and cobalt efflux protein CorC
Single-stranded DNA-binding protein
putative A/G-specific adenine glycosylase YfhQ
DNA-binding protein HU
Ribonuclease E
putative AAA-ATPase
hypothetical protein
species
Bx
Bo
Bxylanisolvens_NLAE-zl-P727
Bxylanisolvens_NLAE-zl-P736
Bxylanisolvens_NLAE-zl-P393
Bxylanisolvens_NLAE-zl-P352
Bxylanisolvens_NLAE-zl-P732
Bxylanisolvens_CL03T12C04
Bacteroides_1_1_30
Bacteroides_xylanisolvens_XB1A
Bacteroides_2_1_22
Bacteroides_D1
Bacteroides_ovatus_SD_CC_2a
Bacteroides_xylanisolvens_SD_CC_1b
Bacteroides_D22
Bxylanisolvens_NLAE-zl-C29
Bxylanisolvens_NLAE-zl-H194
Bxylanisolvens_NLAE-zl-G310
Bxylanisolvens_NLAE-zl-G421
Bxylanisolvens_NLAE-zl-C182
Bxylanisolvens_NLAE-zl-C339
Bacteroides_2_2_4
Bacteroides_D2
Bovatus_NLAE-zl-C11
Bovatus_NLAE-zl-C34
Bacteroides_ovatus_CL03T12C18
Bovatus_NLAE-zl-H59
Bovatus_NLAE-zl-H73
Bacteroides_ovatus_ATCC_8483
Bovatus_CL02T12C04
Bacteroides_ovatus_3_8_47FAA
Bacteroides_3_1_23
Bacteroides_ovatus_SD_CMC_3f
Bovatus_NLAE-zl-H304
Bovatus_NLAE-zl-H361

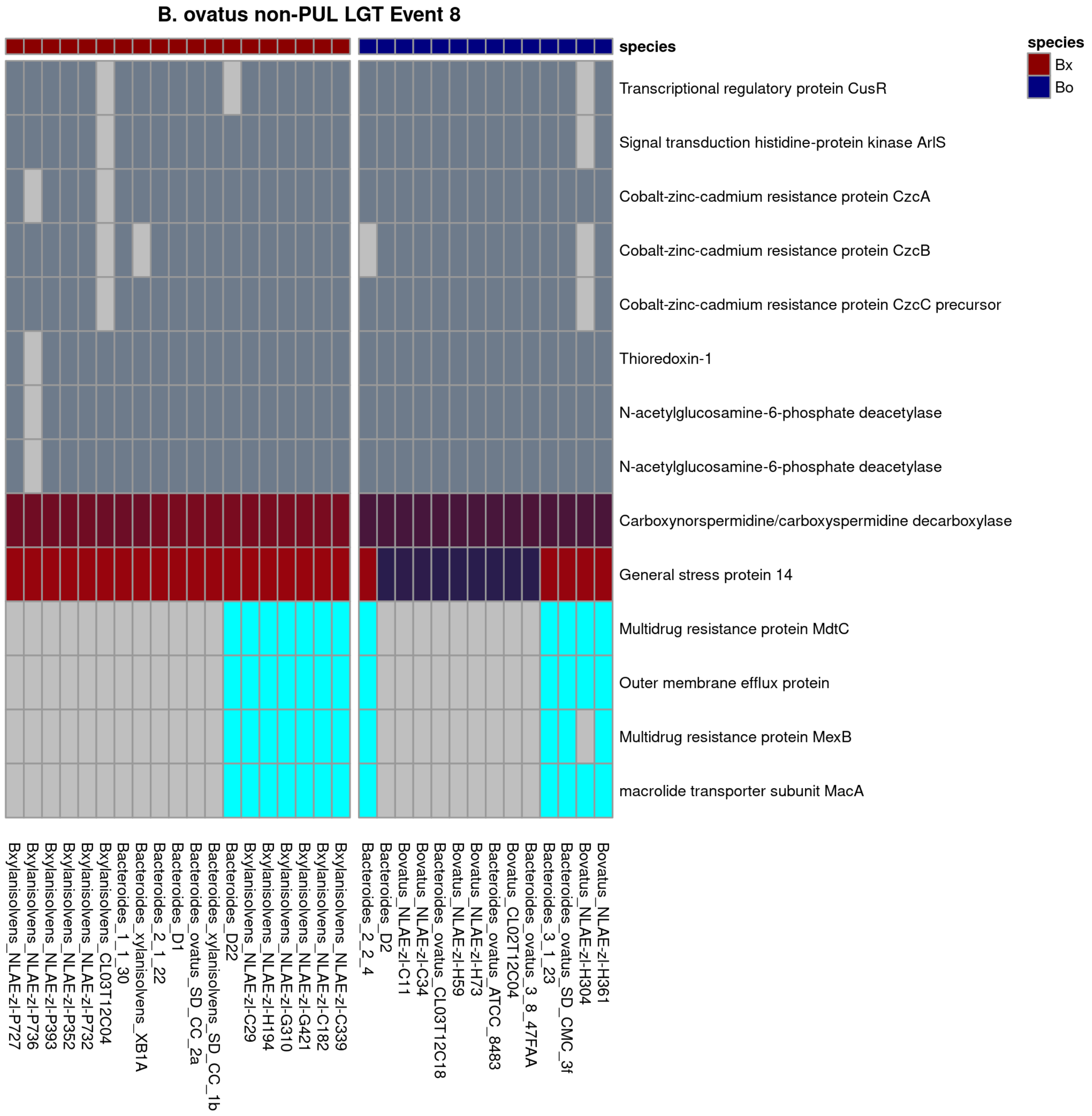
B. ovatus non-PUL LGT Event 8
species
species
Bx
Bo
Transcriptional regulatory protein CusR
Signal transduction histidine-protein kinase ArlS
Cobalt-zinc-cadmium resistance protein CzcA
Cobalt-zinc-cadmium resistance protein CzcB
Cobalt-zinc-cadmium resistance protein CzcC precursor
Thioredoxin-1
N-acetylglucosamine-6-phosphate deacetylase
N-acetylglucosamine-6-phosphate deacetylase
Carboxynorspermidine/carboxyspermidine decarboxylase
General stress protein 14
Multidrug resistance protein MdtC
Outer membrane efflux protein
Multidrug resistance protein MexB
macrolide transporter subunit MacA
Bxylanisolvens_NLAE-zl-P727
Bxylanisolvens_NLAE-zl-P736
Bxylanisolvens_NLAE-zl-P393
Bxylanisolvens_NLAE-zl-P352
Bxylanisolvens_NLAE-zl-P732
Bxylanisolvens_CL03T12C04
Bacteroides_1_1_30
Bacteroides_xylanisolvens_XB1A
Bacteroides_2_1_22
Bacteroides_D1
Bacteroides_ovatus_SD_CC_2a
Bacteroides_xylanisolvens_SD_CC_1b
Bacteroides_D22
Bxylanisolvens_NLAE-zl-C29
Bxylanisolvens_NLAE-zl-H194
Bxylanisolvens_NLAE-zl-G310
Bxylanisolvens_NLAE-zl-G421
Bxylanisolvens_NLAE-zl-C182
Bxylanisolvens_NLAE-zl-C339
Bacteroides_2_2_4
Bacteroides_D2
Bovatus_NLAE-zl-C11
Bovatus_NLAE-zl-C34
Bacteroides_ovatus_CL03T12C18
Bovatus_NLAE-zl-H59
Bovatus_NLAE-zl-H73
Bacteroides_ovatus_ATCC_8483
Bovatus_CL02T12C04
Bacteroides_ovatus_3_8_47FAA
Bacteroides_3_1_23
Bacteroides_ovatus_SD_CMC_3f
Bovatus_NLAE-zl-H304
Bovatus_NLAE-zl-H361

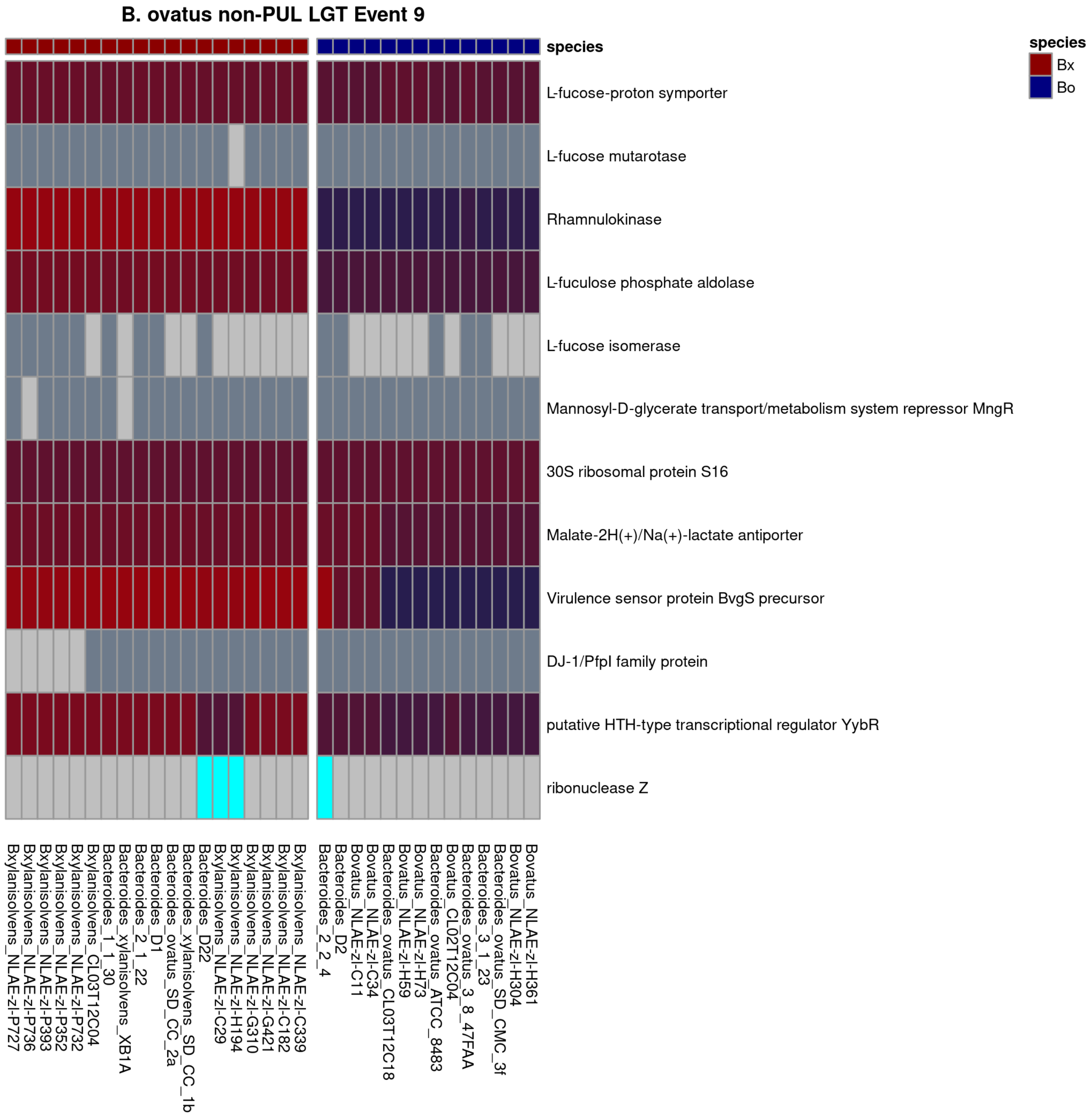
B. ovatus non-PUL LGT Event 9
species
species
Bx
Bo
L-fucose-proton symporter
L-fucose mutarotase
Rhamnulokinase
L-fuculose phosphate aldolase
L-fucose isomerase
Mannosyl-D-glycerate transport/metabolism system repressor MngR
30S ribosomal protein S16
Malate-2H(+)/Na(+)-lactate antiporter
Virulence sensor protein BvgS precursor
DJ-1/PfpI family protein
putative HTH-type transcriptional regulator YybR
ribonuclease Z
Bxylanisolvens_NLAE-zl-P727
Bxylanisolvens_NLAE-zl-P736
Bxylanisolvens_NLAE-zl-P393
Bxylanisolvens_NLAE-zl-P352
Bxylanisolvens_NLAE-zl-P732
Bxylanisolvens_CL03T12C04
Bacteroides_1_1_30
Bacteroides_xylanisolvens_XB1A
Bacteroides_2_1_22
Bacteroides_D1
Bacteroides_ovatus_SD_CC_2a
Bacteroides_xylanisolvens_SD_CC_1b
Bacteroides_D22
Bxylanisolvens_NLAE-zl-C29
Bxylanisolvens_NLAE-zl-H194
Bxylanisolvens_NLAE-zl-G310
Bxylanisolvens_NLAE-zl-G421
Bxylanisolvens_NLAE-zl-C182
Bxylanisolvens_NLAE-zl-C339
Bacteroides_2_2_4
Bacteroides_D2
Bovatus_NLAE-zl-C11
Bovatus_NLAE-zl-C34
Bacteroides_ovatus_CL03T12C18
Bovatus_NLAE-zl-H59
Bovatus_NLAE-zl-H73
Bacteroides_ovatus_ATCC_8483
Bovatus_CL02T12C04
Bacteroides_ovatus_3_8_47FAA
Bacteroides_3_1_23
Bacteroides_ovatus_SD_CMC_3f
Bovatus_NLAE-zl-H304
Bovatus_NLAE-zl-H361

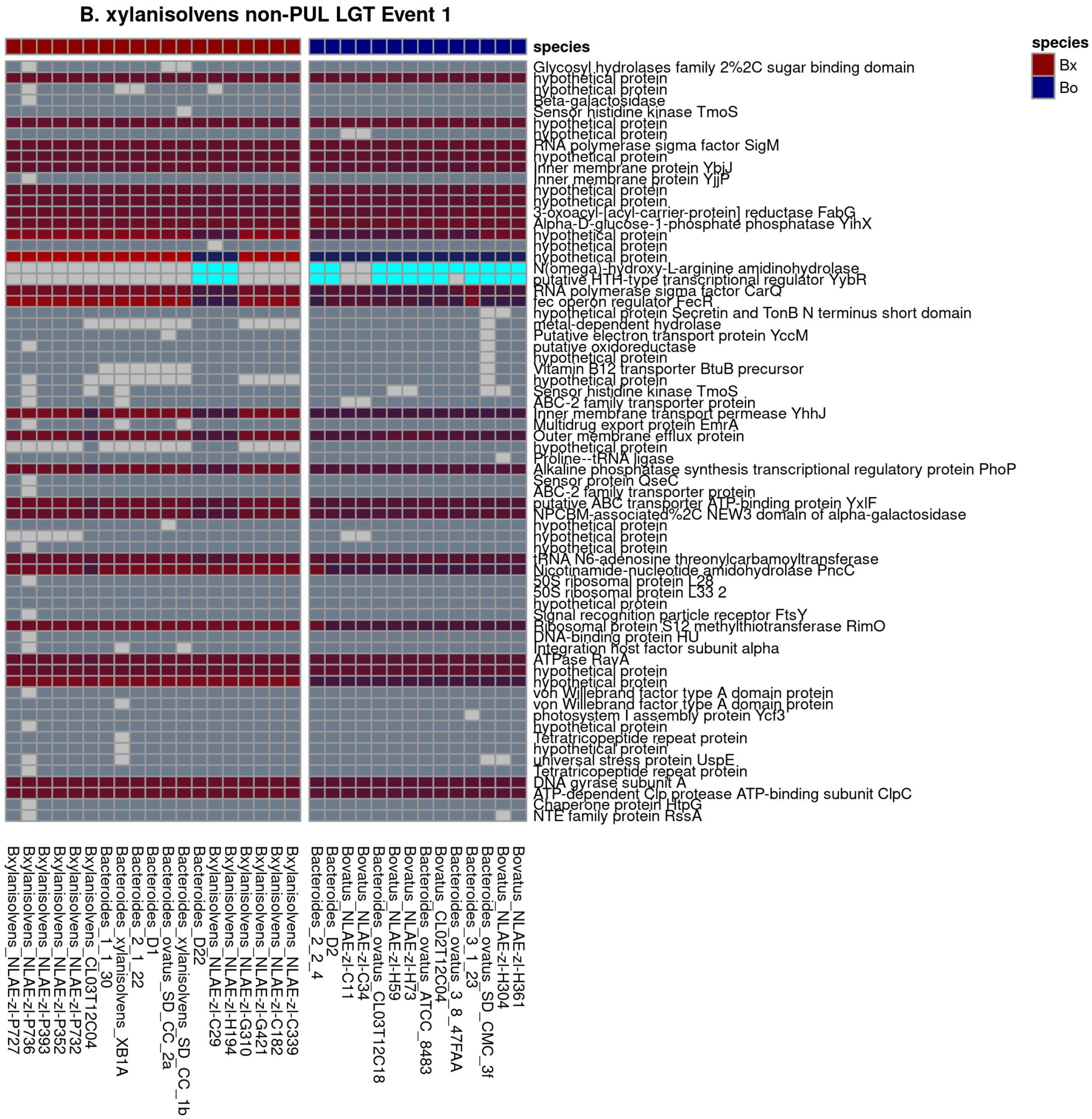
B. xylanisolvens non-PUL LGT Event 1
species
species
Bx
Bo
Glycosyl hydrolases family 2%2C sugar binding domain
hypothetical protein
hypothetical protein
Beta-galactosidase
Sensor histidine kinase TmoS
hypothetical protein
hypothetical protein
RNA polymerase sigma factor SigM
hypothetical protein
Inner membrane protein YbjJ
Inner membrane protein YjjP
hypothetical protein
hypothetical protein
3-oxoacyl-[acyl-carrier-protein] reductase FabG
Alpha-D-glucose-1-phosphate phosphatase YihX
hypothetical protein
hypothetical protein
hypothetical protein
N(omega)-hydroxy-L-arginine amidinohydrolase
putative HTH-type transcriptional regulator YybR
RNA polymerase sigma factor CarQ
fec operon regulator FecR
hypothetical protein Secretin and TonB N terminus short domain
metal-dependent hydrolase
Putative electron transport protein YccM
putative oxidoreductase
hypothetical protein
Vitamin B12 transporter BtuB precursor
hypothetical protein
Sensor histidine kinase TmoS
ABC-2 family transporter protein
Inner membrane transport permease YhhJ
Multidrug export protein EmrA
Outer membrane efflux protein
hypothetical protein
Proline--tRNA ligase
Alkaline phosphatase synthesis transcriptional regulatory protein PhoP
Sensor protein QseC
ABC-2 family transporter protein
putative ABC transporter ATP-binding protein YxlF
NPCBM-associated%2C NEW3 domain of alpha-galactosidase
hypothetical protein
hypothetical protein
hypothetical protein
tRNA N6-adenosine threonylcarbamoyltransferase
Nicotinamide-nucleotide amidohydrolase PncC
50S ribosomal protein L28
50S ribosomal protein L33 2
hypothetical protein
Signal recognition particle receptor FtsY
Ribosomal protein S12 methylthiotransferase RimO
DNA-binding protein HU
Integration host factor subunit alpha
ATPase RavA
hypothetical protein
hypothetical protein
von Willebrand factor type A domain protein
von Willebrand factor type A domain protein
photosystem I assembly protein Ycf3
hypothetical protein
Tetratricopeptide repeat protein
hypothetical protein
universal stress protein UspE
Tetratricopeptide repeat protein
DNA gyrase subunit A
ATP-dependent Clp protease ATP-binding subunit ClpC
Chaperone protein HtpG
NTE family protein RssA
Bxylanisolvens_NLAE-zl-P727
Bxylanisolvens_NLAE-zl-P736
Bxylanisolvens_NLAE-zl-P393
Bxylanisolvens_NLAE-zl-P352
Bxylanisolvens_NLAE-zl-P732
Bxylanisolvens_CL03T12C04
Bacteroides_1_1_30
Bacteroides_xylanisolvens_XB1A
Bacteroides_2_1_22
Bacteroides_D1
Bacteroides_ovatus_SD_CC_2a
Bacteroides_xylanisolvens_SD_CC_1b
Bacteroides_D22
Bxylanisolvens_NLAE-zl-C29
Bxylanisolvens_NLAE-zl-H194
Bxylanisolvens_NLAE-zl-G310
Bxylanisolvens_NLAE-zl-G421
Bxylanisolvens_NLAE-zl-C182
Bxylanisolvens_NLAE-zl-C339
Bacteroides_2_2_4
Bacteroides_D2
Bovatus_NLAE-zl-C11
Bovatus_NLAE-zl-C34
Bacteroides_ovatus_CL03T12C18
Bovatus_NLAE-zl-H59
Bovatus_NLAE-zl-H73
Bovatus_CL02T12C04
Bacteroides_ovatus_ATCC_8483
Bacteroides_ovatus_3_8_47FAA
Bacteroides_3_1_23
Bacteroides_ovatus_SD_CMC_3f
Bovatus_NLAE-zl-H304
Bovatus_NLAE-zl-H361

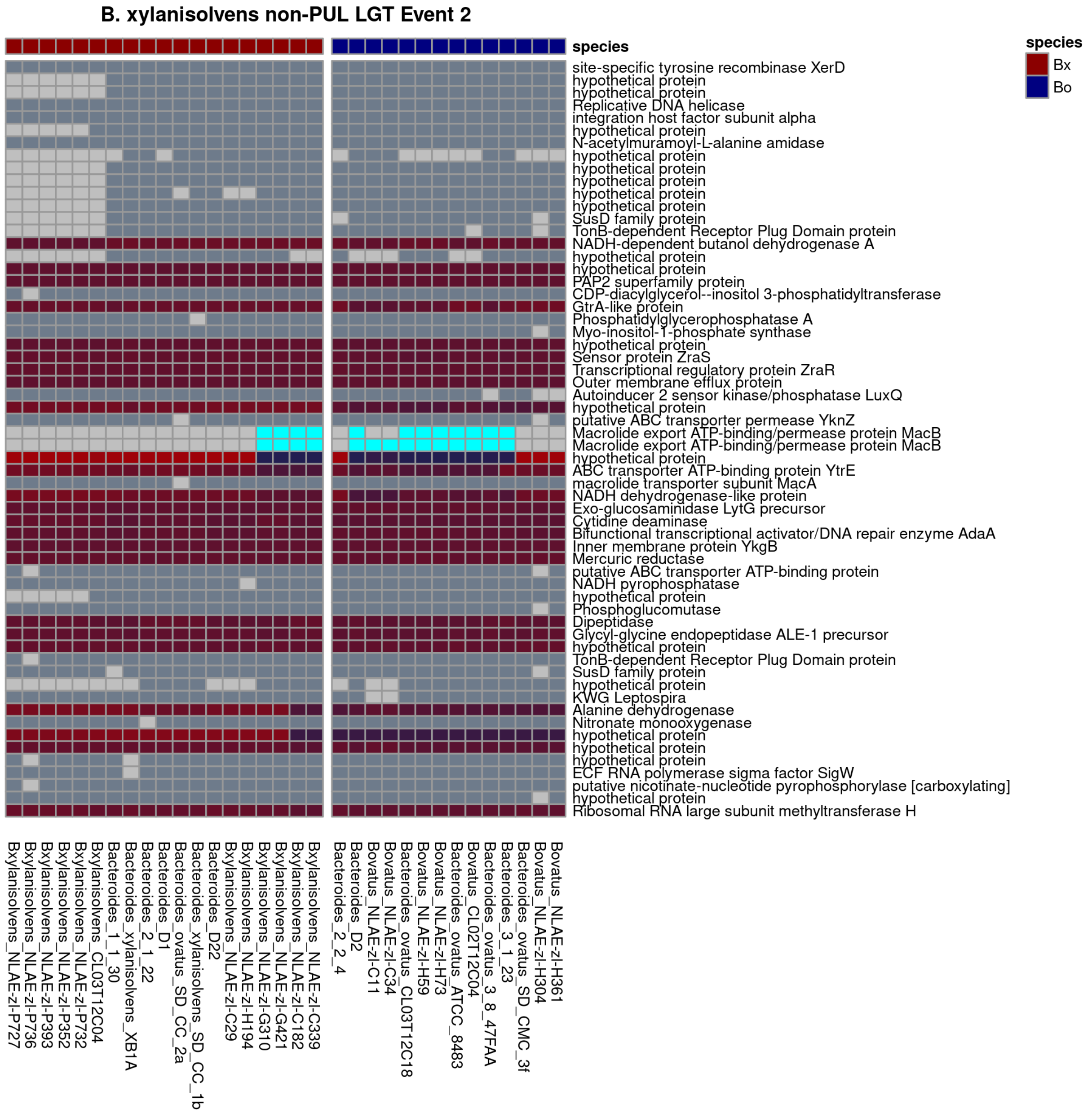
B. xylanisolvens non-PUL LGT Event 2
species
species
Bx
Bo
site-specific tyrosine recombinase XerD
hypothetical protein
hypothetical protein
Replicative DNA helicase
integration host factor subunit alpha
hypothetical protein
N-acetylmuramoyl-L-alanine amidase
hypothetical protein
hypothetical protein
hypothetical protein
hypothetical protein
hypothetical protein
SusD family protein
TonB-dependent Receptor Plug Domain protein
NADH-dependent butanol dehydrogenase A
hypothetical protein
hypothetical protein
PAP2 superfamily protein
CDP-diacylglycerol--inositol 3-phosphatidyltransferase
GtrA-like protein
Phosphatidylglycerophosphatase A
Myo-inositol-1-phosphate synthase
hypothetical protein
Sensor protein ZraS
Transcriptional regulatory protein ZraR
Outer membrane efflux protein
Autoinducer 2 sensor kinase/phosphatase LuxQ
hypothetical protein
putative ABC transporter permease YknZ
Macrolide export ATP-binding/permease protein MacB
Macrolide export ATP-binding/permease protein MacB
hypothetical protein
ABC transporter ATP-binding protein YtrE
macrolide transporter subunit MacA
NADH dehydrogenase-like protein
Exo-glucosaminidase LytG precursor
Cytidine deaminase
Bifunctional transcriptional activator/DNA repair enzyme AdaA
Inner membrane protein YkgB
Mercuric reductase
putative ABC transporter ATP-binding protein
NADH pyrophosphatase
hypothetical protein
Phosphoglucomutase
Dipeptidase
Glycyl-glycine endopeptidase ALE-1 precursor
hypothetical protein
TonB-dependent Receptor Plug Domain protein
SusD family protein
hypothetical protein
KWG Leptospira
Alanine dehydrogenase
Nitronate monooxygenase
hypothetical protein
hypothetical protein
hypothetical protein
ECF RNA polymerase sigma factor SigW
putative nicotinate-nucleotide pyrophosphorylase [carboxylating]
hypothetical protein
Ribosomal RNA large subunit methyltransferase H
Bxylanisolvens_NLAE-zl-P727
Bxylanisolvens_NLAE-zl-P736
Bxylanisolvens_NLAE-zl-P393
Bxylanisolvens_NLAE-zl-P352
Bxylanisolvens_NLAE-zl-P732
Bxylanisolvens_CL03T12C04
Bacteroides_1_1_30
Bacteroides_xylanisolvens_XB1A
Bacteroides_2_1_22
Bacteroides_D1
Bacteroides_ovatus_SD_CC_2a
Bacteroides_xylanisolvens_SD_CC_1b
Bacteroides_D22
Bxylanisolvens_NLAE-zl-C29
Bxylanisolvens_NLAE-zl-H194
Bxylanisolvens_NLAE-zl-G310
Bxylanisolvens_NLAE-zl-G421
Bxylanisolvens_NLAE-zl-C182
Bxylanisolvens_NLAE-zl-C339
Bacteroides_2_2_4
Bacteroides_D2
Bovatus_NLAE-zl-C11
Bovatus_NLAE-zl-C34
Bacteroides_ovatus_CL03T12C18
Bovatus_NLAE-zl-H59
Bovatus_NLAE-zl-H73
Bacteroides_ovatus_ATCC_8483
Bovatus_CL02T12C04
Bacteroides_ovatus_3_8_47FAA
Bacteroides_3_1_23
Bacteroides_ovatus_SD_CMC_3f
Bovatus_NLAE-zl-H304
Bovatus_NLAE-zl-H361

B. xylanisolvens non-PUL LGT Event 3

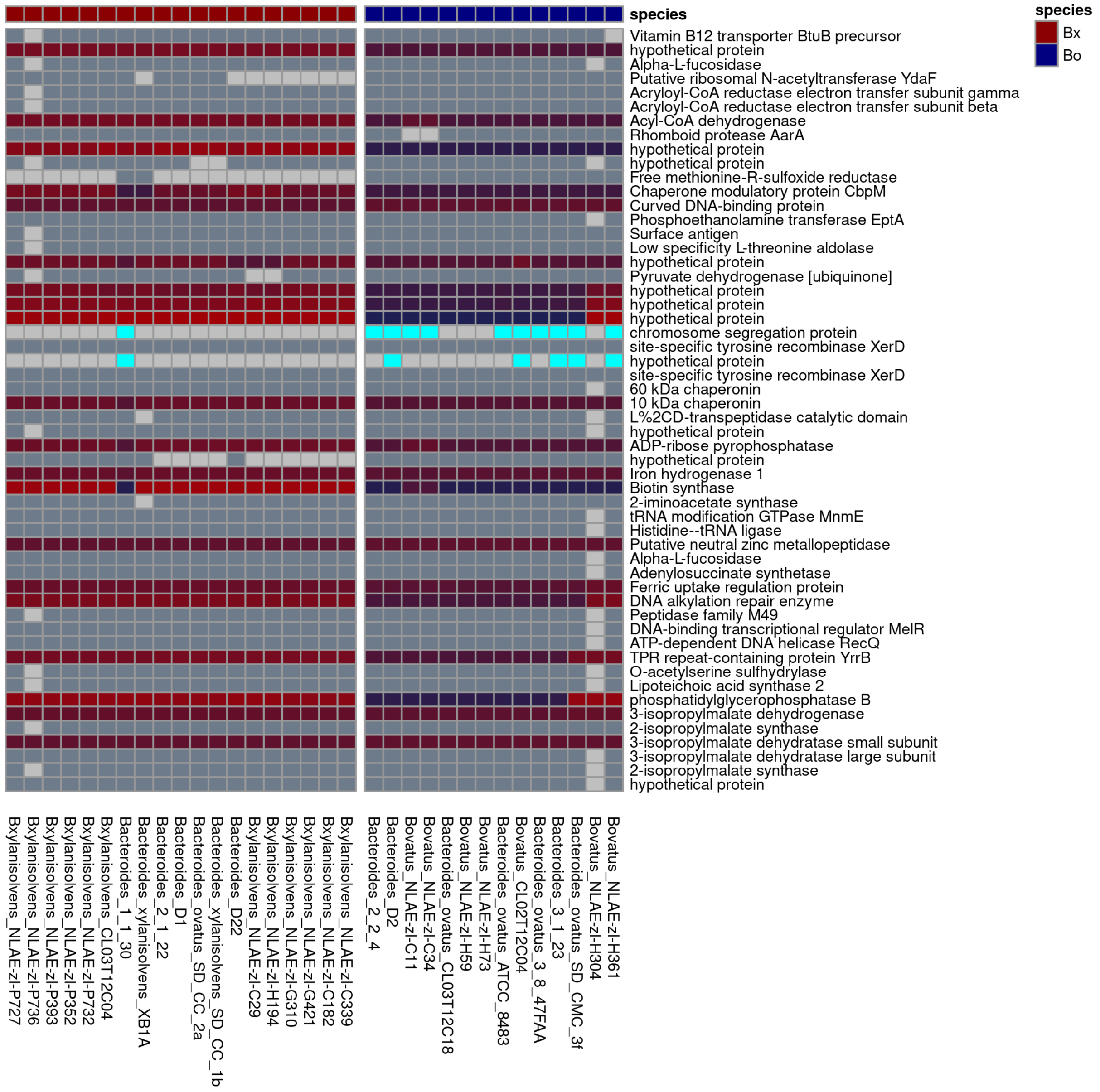

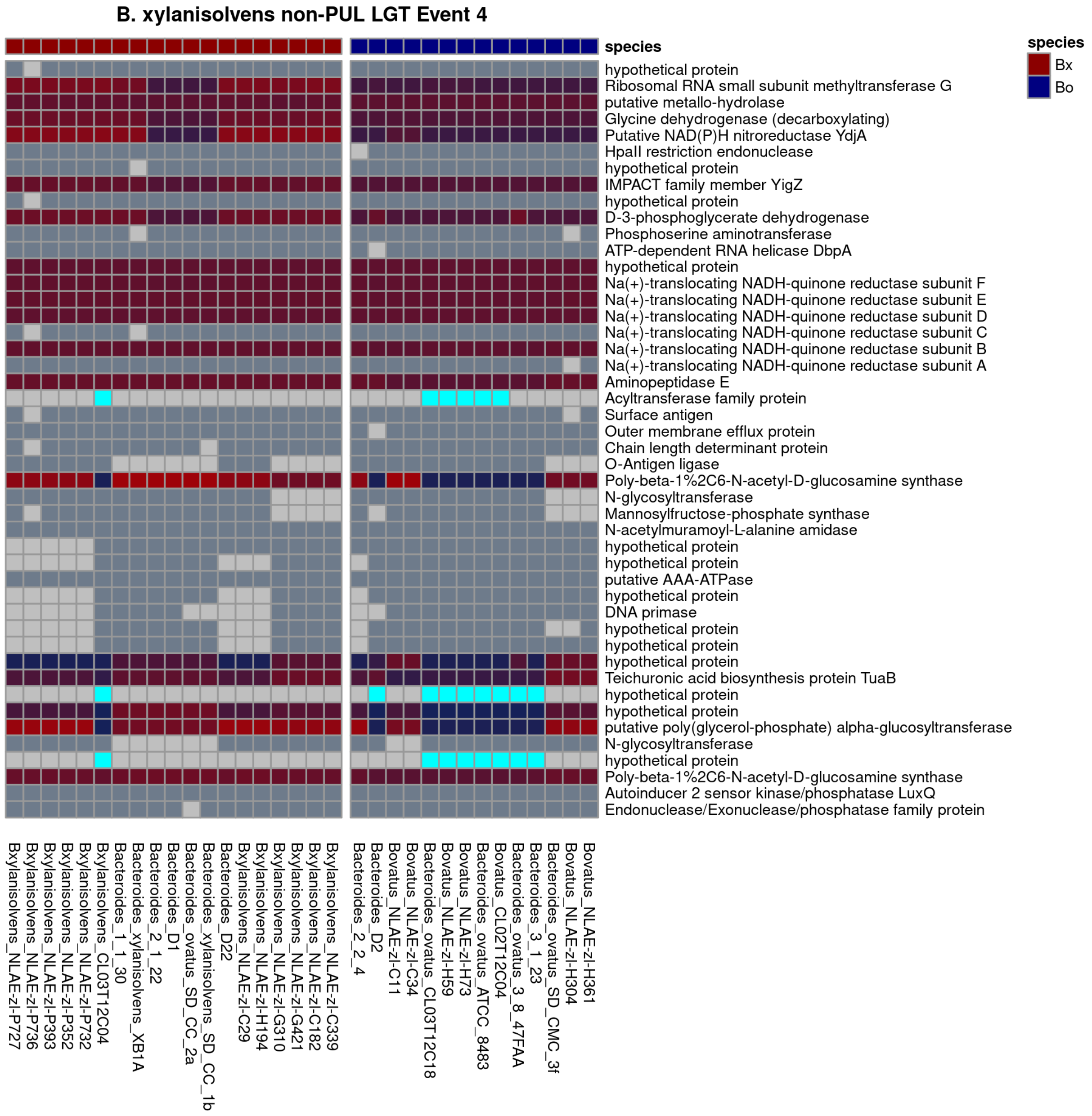
B. xylanisolvens non-PUL LGT Event 4
species
species
Bx
Bo
hypothetical protein
Ribosomal RNA small subunit methyltransferase G
putative metallo-hydrolase
Glycine dehydrogenase (decarboxylating)
Putative NAD(P)H nitroreductase YdjA
HpaII restriction endonuclease
hypothetical protein
IMPACT family member YigZ
hypothetical protein
D-3-phosphoglycerate dehydrogenase
Phosphoserine aminotransferase
ATP-dependent RNA helicase DbpA
hypothetical protein
Na(+)-translocating NADH-quinone reductase subunit F
Na(+)-translocating NADH-quinone reductase subunit E
Na(+)-translocating NADH-quinone reductase subunit D
Na(+)-translocating NADH-quinone reductase subunit C
Na(+)-translocating NADH-quinone reductase subunit B
Na(+)-translocating NADH-quinone reductase subunit A
Aminopeptidase E
Acyltransferase family protein
Surface antigen
Outer membrane efflux protein
Chain length determinant protein
O-Antigen ligase
Poly-beta-1%2C6-N-acetyl-D-glucosamine synthase
N-glycosyltransferase
Mannosylfructose-phosphate synthase
N-acetylmuramoyl-L-alanine amidase
hypothetical protein
hypothetical protein
putative AAA-ATPase
hypothetical protein
DNA primase
hypothetical protein
hypothetical protein
hypothetical protein
Teichuronic acid biosynthesis protein TuaB
hypothetical protein
hypothetical protein
putative poly(glycerol-phosphate) alpha-glucosyltransferase
N-glycosyltransferase
hypothetical protein
Poly-beta-1%2C6-N-acetyl-D-glucosamine synthase
Autoinducer 2 sensor kinase/phosphatase LuxQ
Endonuclease/Exonuclease/phosphatase family protein
Bxylanisolvens_NLAE-zl-P727
Bxylanisolvens_NLAE-zl-P736
Bxylanisolvens_NLAE-zl-P393
Bxylanisolvens_NLAE-zl-P352
Bxylanisolvens_NLAE-zl-P732
Bxylanisolvens_CL03T12C04
Bacteroides_1_1_30
Bacteroides_xylanisolvens_XB1A
Bacteroides_2_1_22
Bacteroides_D1
Bacteroides_ovatus_SD_CC_2a
Bacteroides_xylanisolvens_SD_CC_1b
Bacteroides_D22
Bxylanisolvens_NLAE-zl-C29
Bxylanisolvens_NLAE-zl-H194
Bxylanisolvens_NLAE-zl-G310
Bxylanisolvens_NLAE-zl-G421
Bxylanisolvens_NLAE-zl-C182
Bxylanisolvens_NLAE-zl-C339
Bacteroides_2_2_4
Bacteroides_D2
Bovatus_NLAE-zl-C11
Bovatus_NLAE-zl-C34
Bacteroides_ovatus_CL03T12C18
Bovatus_NLAE-zl-H59
Bovatus_NLAE-zl-H73
Bacteroides_ovatus_ATCC_8483
Bovatus_CL02T12C04
Bacteroides_ovatus_3_8_47FAA
Bacteroides_3_1_23
Bacteroides_ovatus_SD_CMC_3f
Bovatus_NLAE-zl-H304
Bovatus_NLAE-zl-H361

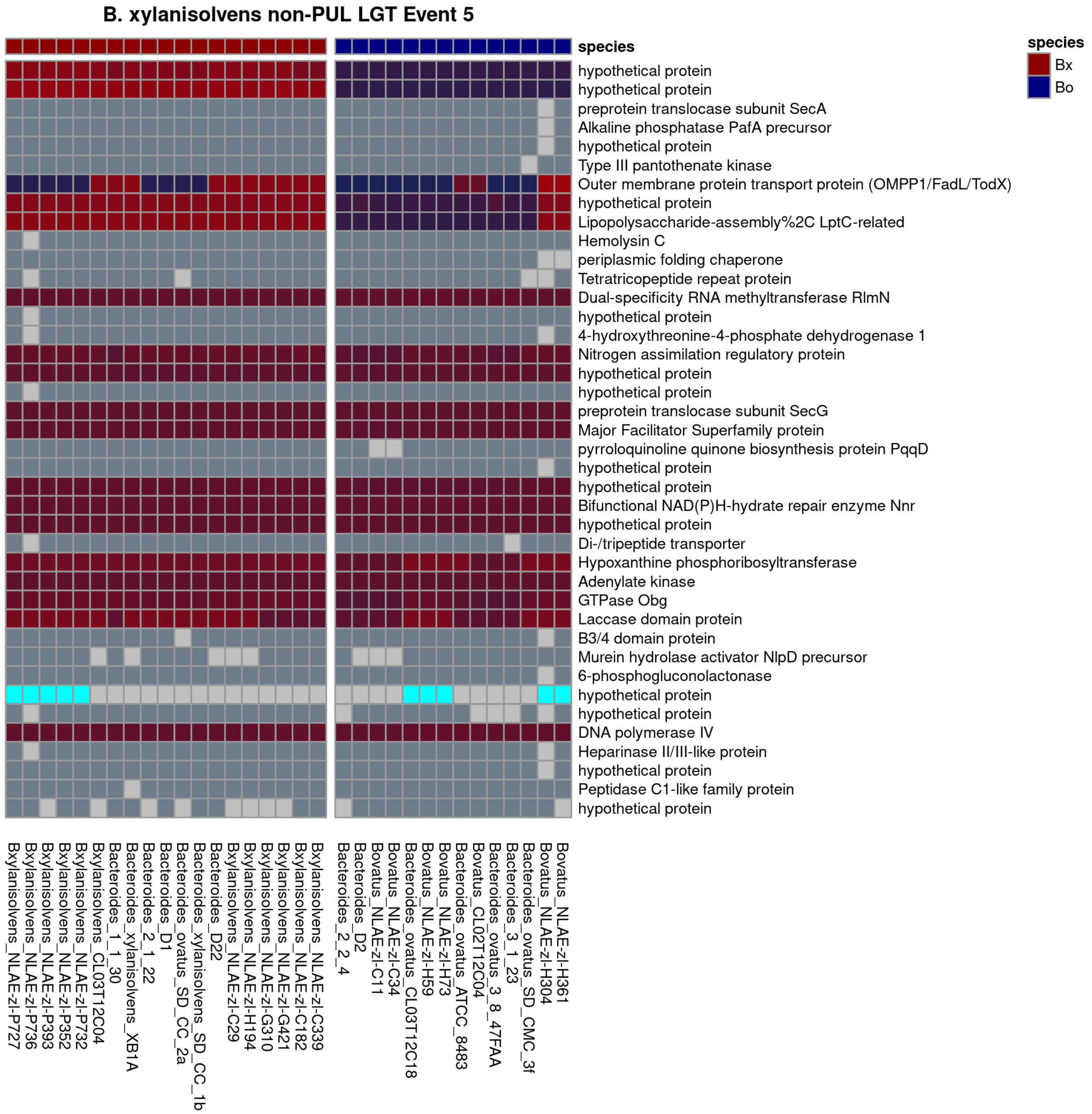
B. xylanisolvens non-PUL LGT Event 5
species
hypothetical protein
hypothetical protein
preprotein translocase subunit SecA
Alkaline phosphatase PafA precursor
hypothetical protein
Type III pantothenate kinase
Outer membrane protein transport protein (OMPP1/FadL/TodX)
hypothetical protein
Lipopolysaccharide-assembly%2C LptC-related
Hemolysin C
periplasmic folding chaperone
Tetratricopeptide repeat protein
Dual-specificity RNA methyltransferase RlmN
hypothetical protein
4-hydroxythreonine-4-phosphate dehydrogenase 1
Nitrogen assimilation regulatory protein
hypothetical protein
hypothetical protein
preprotein translocase subunit SecG
Major Facilitator Superfamily protein
pyrroloquinoline quinone biosynthesis protein PqqD
hypothetical protein
hypothetical protein
Bifunctional NAD(P)H-hydrate repair enzyme Nnr
hypothetical protein
Di-/tripeptide transporter
Hypoxanthine phosphoribosyltransferase
Adenylate kinase
GTPase Obg
Laccase domain protein
B3/4 domain protein
Murein hydrolase activator NlpD precursor
6-phosphogluconolactonase
hypothetical protein
hypothetical protein
DNA polymerase IV
Heparinase II/III-like protein
hypothetical protein
Peptidase C1-like family protein
hypothetical protein
species
Bx
Bo
Bxylanisolvens_NLAE-zl-P727
Bxylanisolvens_NLAE-zl-P736
Bxylanisolvens_NLAE-zl-P393
Bxylanisolvens_NLAE-zl-P352
Bxylanisolvens_NLAE-zl-P732
Bxylanisolvens_CL03T12C04
Bacteroides_1_1_30
Bacteroides_xylanisolvens_XB1A
Bacteroides_2_1_22
Bacteroides_D1
Bacteroides_ovatus_SD_CC_2a
Bacteroides_xylanisolvens_SD_CC_1b
Bacteroides_D22
Bxylanisolvens_NLAE-zl-C29
Bxylanisolvens_NLAE-zl-H194
Bxylanisolvens_NLAE-zl-G310
Bxylanisolvens_NLAE-zl-G421
Bxylanisolvens_NLAE-zl-C182
Bxylanisolvens_NLAE-zl-C339
Bacteroides_2_2_4
Bacteroides_D2
Bovatus_NLAE-zl-C11
Bovatus_NLAE-zl-C34
Bacteroides_ovatus_CL03T12C18
Bovatus_NLAE-zl-H59
Bovatus_NLAE-zl-H73
Bacteroides_ovatus_ATCC_8483
Bovatus_CL02T12C04
Bacteroides_ovatus_3_8_47FAA
Bacteroides_3_1_23
Bacteroides_ovatus_SD_CMC_3f
Bovatus_NLAE-zl-H304
Bovatus_NLAE-zl-H361

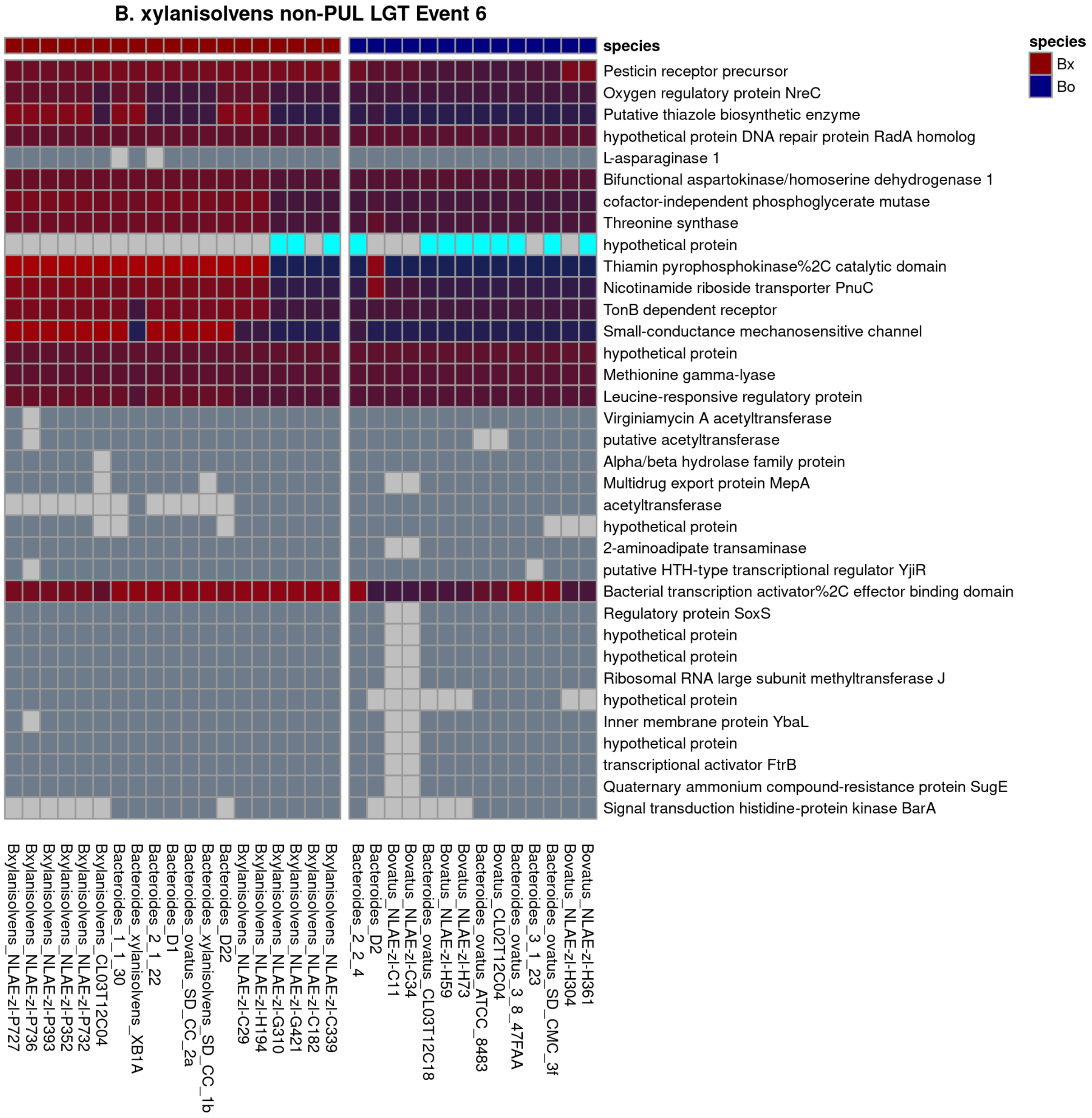
B. xylanisolvens non-PUL LGT Event 6
species
species
Bx
Bo
Pesticin receptor precursor
Oxygen regulatory protein NreC
Putative thiazole biosynthetic enzyme
hypothetical protein DNA repair protein RadA homolog
L-asparaginase 1
Bifunctional aspartokinase/homoserine dehydrogenase 1
cofactor-independent phosphoglycerate mutase
Threonine synthase
hypothetical protein
Thiamin pyrophosphokinase%2C catalytic domain
Nicotinamide riboside transporter PnuC
TonB dependent receptor
Small-conductance mechanosensitive channel
hypothetical protein
Methionine gamma-lyase
Leucine-responsive regulatory protein
Virginiamycin A acetyltransferase
putative acetyltransferase
Alpha/beta hydrolase family protein
Multidrug export protein MepA
acetyltransferase
hypothetical protein
2-aminoadipate transaminase
putative HTH-type transcriptional regulator YjiR
Bacterial transcription activator%2C effector binding domain
Regulatory protein SoxS
hypothetical protein
hypothetical protein
Ribosomal RNA large subunit methyltransferase J
hypothetical protein
Inner membrane protein YbaL
hypothetical protein
transcriptional activator FtrB
Quaternary ammonium compound-resistance protein SugE
Signal transduction histidine-protein kinase BarA
Bxylanisolvens_NLAE-zl-P727
Bxylanisolvens_NLAE-zl-P736
Bxylanisolvens_NLAE-zl-P393
Bxylanisolvens_NLAE-zl-P352
Bxylanisolvens_NLAE-zl-P732
Bxylanisolvens_CL03T12C04
Bacteroides_1_1_30
Bacteroides_xylanisolvens_XB1A
Bacteroides_2_1_22
Bacteroides_D1
Bacteroides_ovatus_SD_CC_2a
Bacteroides_xylanisolvens_SD_CC_1b
Bacteroides_D22
Bxylanisolvens_NLAE-zl-C29
Bxylanisolvens_NLAE-zl-H194
Bxylanisolvens_NLAE-zl-G310
Bxylanisolvens_NLAE-zl-G421
Bxylanisolvens_NLAE-zl-C182
Bxylanisolvens_NLAE-zl-C339
Bacteroides_2_2_4
Bacteroides_D2
Bovatus_NLAE-zl-C11
Bovatus_NLAE-zl-C34
Bacteroides_ovatus_CL03T12C18
Bovatus_NLAE-zl-H59
Bovatus_NLAE-zl-H73
Bacteroides_ovatus_ATCC_8483
Bovatus_CL02T12C04
Bacteroides_ovatus_3_8_47FAA
Bacteroides_3_1_23
Bacteroides_ovatus_SD_CMC_3f
Bovatus_NLAE-zl-H304
Bovatus_NLAE-zl-H361

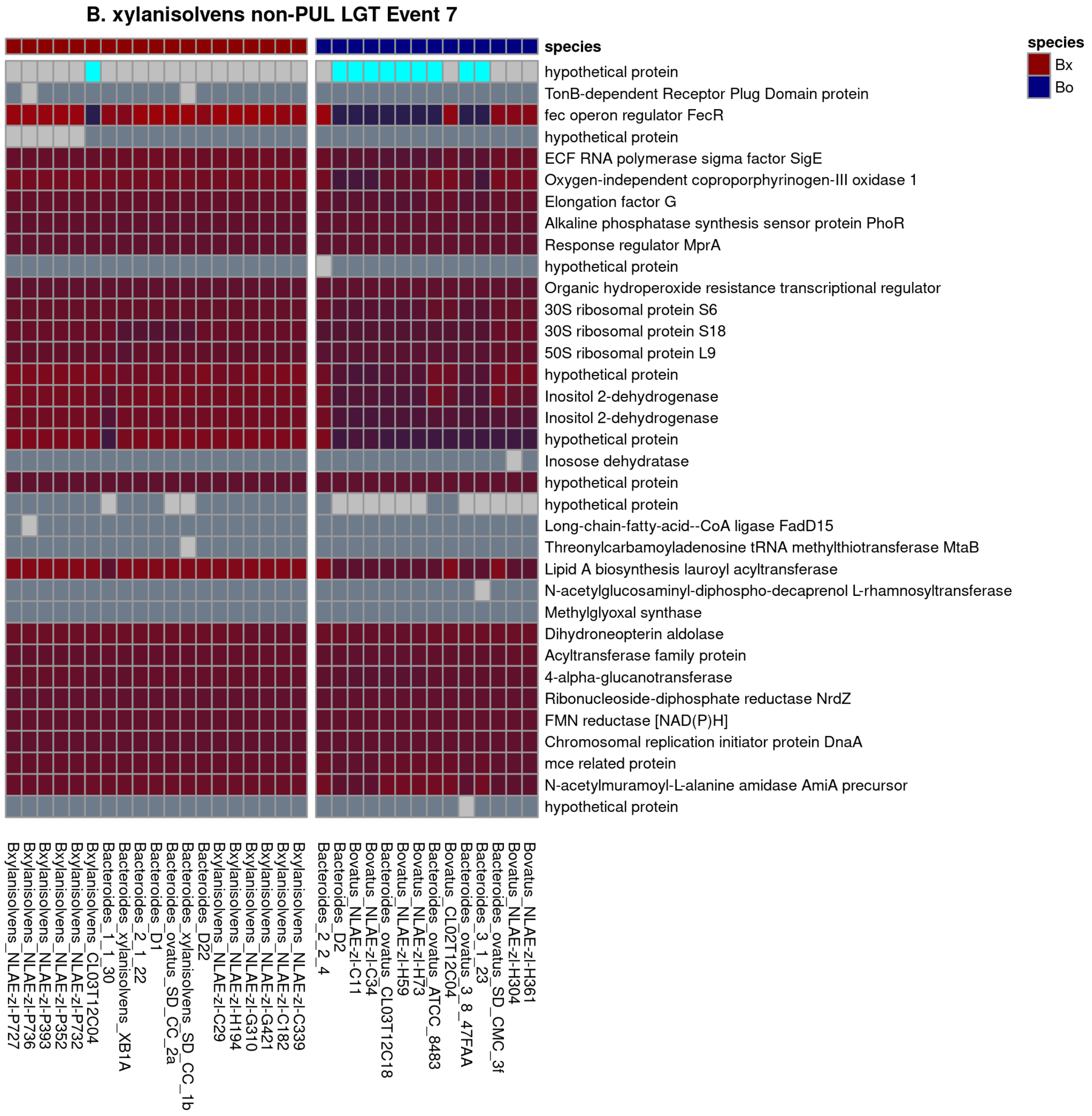
B. xylanisolvens non-PUL LGT Event 7
species
hypothetical protein
TonB-dependent Receptor Plug Domain protein
fec operon regulator FecR
hypothetical protein
ECF RNA polymerase sigma factor SigE
Oxygen-independent coproporphyrinogen-III oxidase 1
Elongation factor G
Alkaline phosphatase synthesis sensor protein PhoR
Response regulator MprA
hypothetical protein
Organic hydroperoxide resistance transcriptional regulator
30S ribosomal protein S6
30S ribosomal protein S18
50S ribosomal protein L9
hypothetical protein
Inositol 2-dehydrogenase
Inositol 2-dehydrogenase
hypothetical protein
Inosose dehydratase
hypothetical protein
hypothetical protein
Long-chain-fatty-acid--CoA ligase FadD15
Threonylcarbamoyladenosine tRNA methylthiotransferase MtaB
Lipid A biosynthesis lauroyl acyltransferase
N-acetylglucosaminyl-diphospho-decaprenol L-rhamnosyltransferase
Methylglyoxal synthase
Dihydroneopterin aldolase
Acyltransferase family protein
4-alpha-glucanotransferase
Ribonucleoside-diphosphate reductase NrdZ
FMN reductase [NAD(P)H]
Chromosomal replication initiator protein DnaA
mce related protein
N-acetylmuramoyl-L-alanine amidase AmiA precursor
hypothetical protein
species
Bx
Bo
Bxylanisolvens_NLAE-zl-P727
Bxylanisolvens_NLAE-zl-P736
Bxylanisolvens_NLAE-zl-P393
Bxylanisolvens_NLAE-zl-P352
Bxylanisolvens_NLAE-zl-P732
Bxylanisolvens_CL03T12C04
Bacteroides_1_1_30
Bacteroides_xylanisolvens_XB1A
Bacteroides_2_1_22
Bacteroides_D1
Bacteroides_ovatus_SD_CC_2a
Bacteroides_xylanisolvens_SD_CC_1b
Bacteroides_D22
Bxylanisolvens_NLAE-zl-C29
Bxylanisolvens_NLAE-zl-H194
Bxylanisolvens_NLAE-zl-G310
Bxylanisolvens_NLAE-zl-G421
Bxylanisolvens_NLAE-zl-C182
Bxylanisolvens_NLAE-zl-C339
Bacteroides_2_2_4
Bacteroides_D2
Bovatus_NLAE-zl-C11
Bovatus_NLAE-zl-C34
Bacteroides_ovatus_CL03T12C18
Bovatus_NLAE-zl-H59
Bovatus_NLAE-zl-H73
Bacteroides_ovatus_ATCC_8483
Bovatus_CL02T12C04
Bacteroides_ovatus_3_8_47FAA
Bacteroides_3_1_23
Bacteroides_ovatus_SD_CMC_3f
Bovatus_NLAE-zl-H304
Bovatus_NLAE-zl-H361

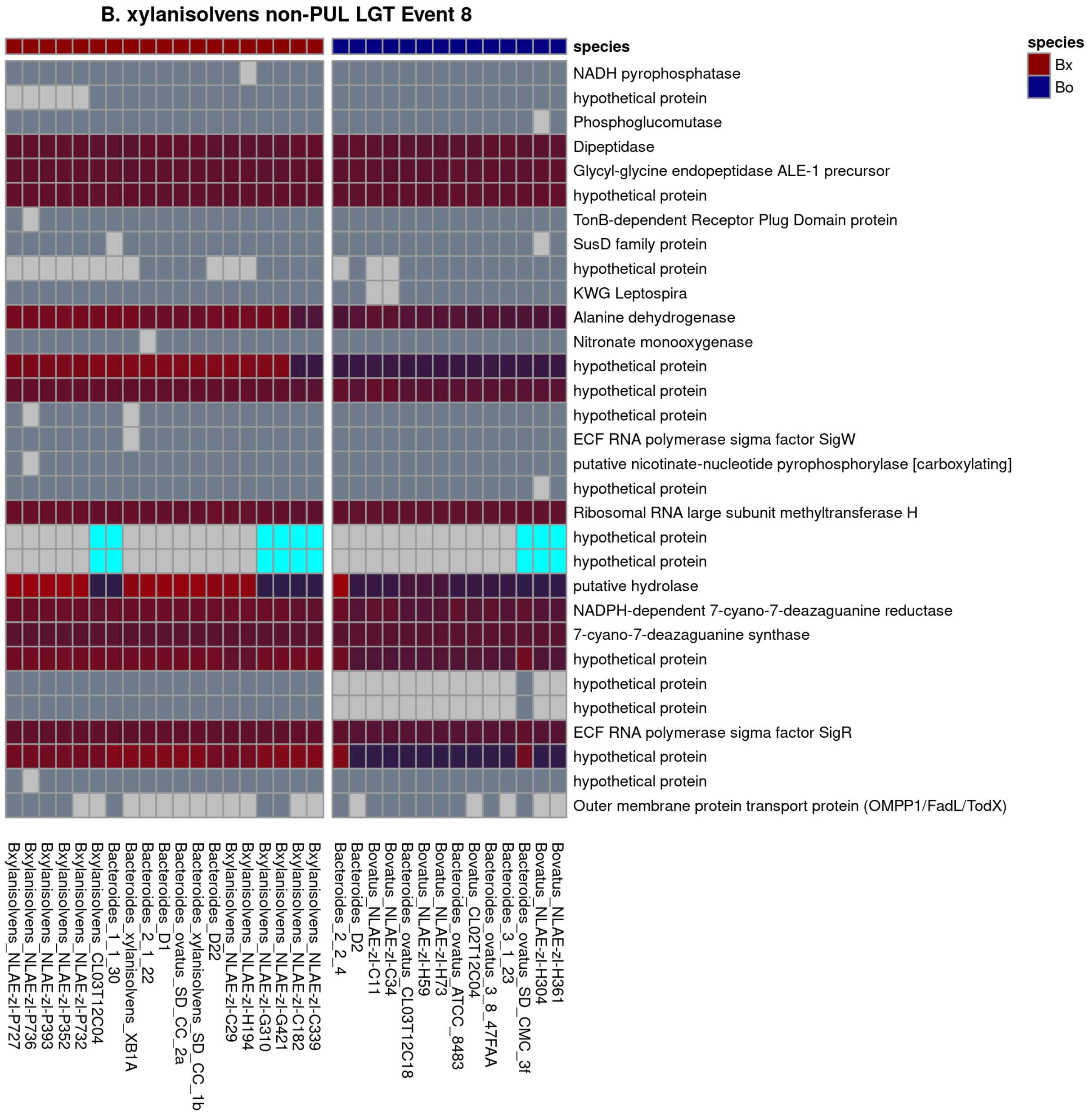
B. xylanisolvens non-PUL LGT Event 8
species
species
Bx
Bo
NADH pyrophosphatase
hypothetical protein
Phosphoglucomutase
Dipeptidase
Glycyl-glycine endopeptidase ALE-1 precursor
hypothetical protein
TonB-dependent Receptor Plug Domain protein
SusD family protein
hypothetical protein
KWG Leptospira
Alanine dehydrogenase
Nitronate monooxygenase
hypothetical protein
hypothetical protein
hypothetical protein
ECF RNA polymerase sigma factor SigW
putative nicotinate-nucleotide pyrophosphorylase [carboxylating]
hypothetical protein
Ribosomal RNA large subunit methyltransferase H
hypothetical protein
hypothetical protein
putative hydrolase
NADPH-dependent 7-cyano-7-deazaguanine reductase
7-cyano-7-deazaguanine synthase
hypothetical protein
hypothetical protein
hypothetical protein
ECF RNA polymerase sigma factor SigR
hypothetical protein
hypothetical protein
Outer membrane protein transport protein (OMPP1/FadL/TodX)
Bxylanisolvens_NLAE-zl-P727
Bxylanisolvens_NLAE-zl-P736
Bxylanisolvens_NLAE-zl-P393
Bxylanisolvens_NLAE-zl-P352
Bxylanisolvens_NLAE-zl-P732
Bxylanisolvens_CL03T12C04
Bacteroides_1_1_30
Bacteroides_xylanisolvens_XB1A
Bacteroides_2_1_22
Bacteroides_D1
Bacteroides_ovatus_SD_CC_2a
Bacteroides_xylanisolvens_SD_CC_1b
Bacteroides_D22
Bxylanisolvens_NLAE-zl-C29
Bxylanisolvens_NLAE-zl-H194
Bxylanisolvens_NLAE-zl-G310
Bxylanisolvens_NLAE-zl-G421
Bxylanisolvens_NLAE-zl-C182
Bxylanisolvens_NLAE-zl-C339
Bacteroides_2_2_4
Bacteroides_D2
Bovatus_NLAE-zl-C11
Bovatus_NLAE-zl-C34
Bacteroides_ovatus_CL03T12C18
Bovatus_NLAE-zl-H59
Bovatus_NLAE-zl-H73
Bacteroides_ovatus_ATCC_8483
Bovatus_CL02T12C04
Bacteroides_ovatus_3_8_47FAA
Bacteroides_3_1_23
Bacteroides_ovatus_SD_CMC_3f
Bovatus_NLAE-zl-H304
Bovatus_NLAE-zl-H361

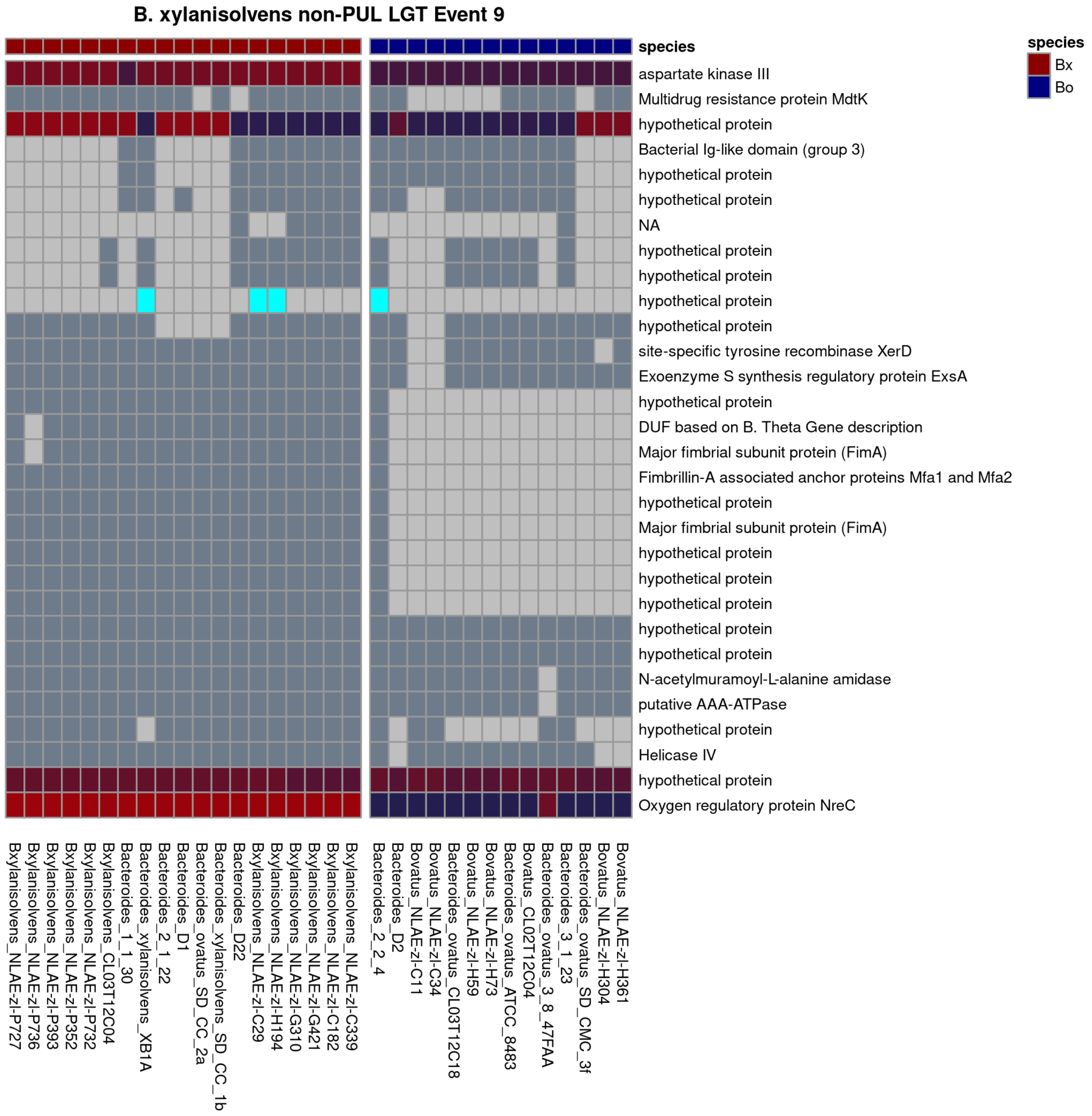
B. xylanisolvens non-PUL LGT Event 9
species
aspartate kinase III
Multidrug resistance protein MdtK
hypothetical protein
Bacterial Ig-like domain (group 3)
hypothetical protein
hypothetical protein
NA
hypothetical protein
hypothetical protein
hypothetical protein
hypothetical protein
site-specific tyrosine recombinase XerD
Exoenzyme S synthesis regulatory protein ExsA
hypothetical protein
DUF based on B. Theta Gene description
Major fimbrial subunit protein (FimA)
Fimbrillin-A associated anchor proteins Mfa1 and Mfa2
hypothetical protein
Major fimbrial subunit protein (FimA)
hypothetical protein
hypothetical protein
hypothetical protein
hypothetical protein
hypothetical protein
N-acetylmuramoyl-L-alanine amidase
putative AAA-ATPase
hypothetical protein
Helicase IV
hypothetical protein
Oxygen regulatory protein NreC
species
Bx
Bo
Bxylanisolvens_NLAE-zl-P727
Bxylanisolvens_NLAE-zl-P736
Bxylanisolvens_NLAE-zl-P393
Bxylanisolvens_NLAE-zl-P352
Bxylanisolvens_NLAE-zl-P732
Bxylanisolvens_CL03T12C04
Bacteroides_1_1_30
Bacteroides_xylanisolvens_XB1A
Bacteroides_2_1_22
Bacteroides_D1
Bacteroides_ovatus_SD_CC_2a
Bacteroides_xylanisolvens_SD_CC_1b
Bacteroides_D22
Bxylanisolvens_NLAE-zl-C29
Bxylanisolvens_NLAE-zl-H194
Bxylanisolvens_NLAE-zl-G310
Bxylanisolvens_NLAE-zl-G421
Bxylanisolvens_NLAE-zl-C182
Bxylanisolvens_NLAE-zl-C339
Bacteroides_2_2_4
Bacteroides_D2
Bovatus_NLAE-zl-C11
Bovatus_NLAE-zl-C34
Bacteroides_ovatus_CL03T12C18
Bovatus_NLAE-zl-H59
Bovatus_NLAE-zl-H73
Bacteroides_ovatus_ATCC_8483
Bovatus_CL02T12C04
Bacteroides_ovatus_3_8_47FAA
Bacteroides_3_1_23
Bacteroides_ovatus_SD_CMC_3f
Bovatus_NLAE-zl-H304
Bovatus_NLAE-zl-H361

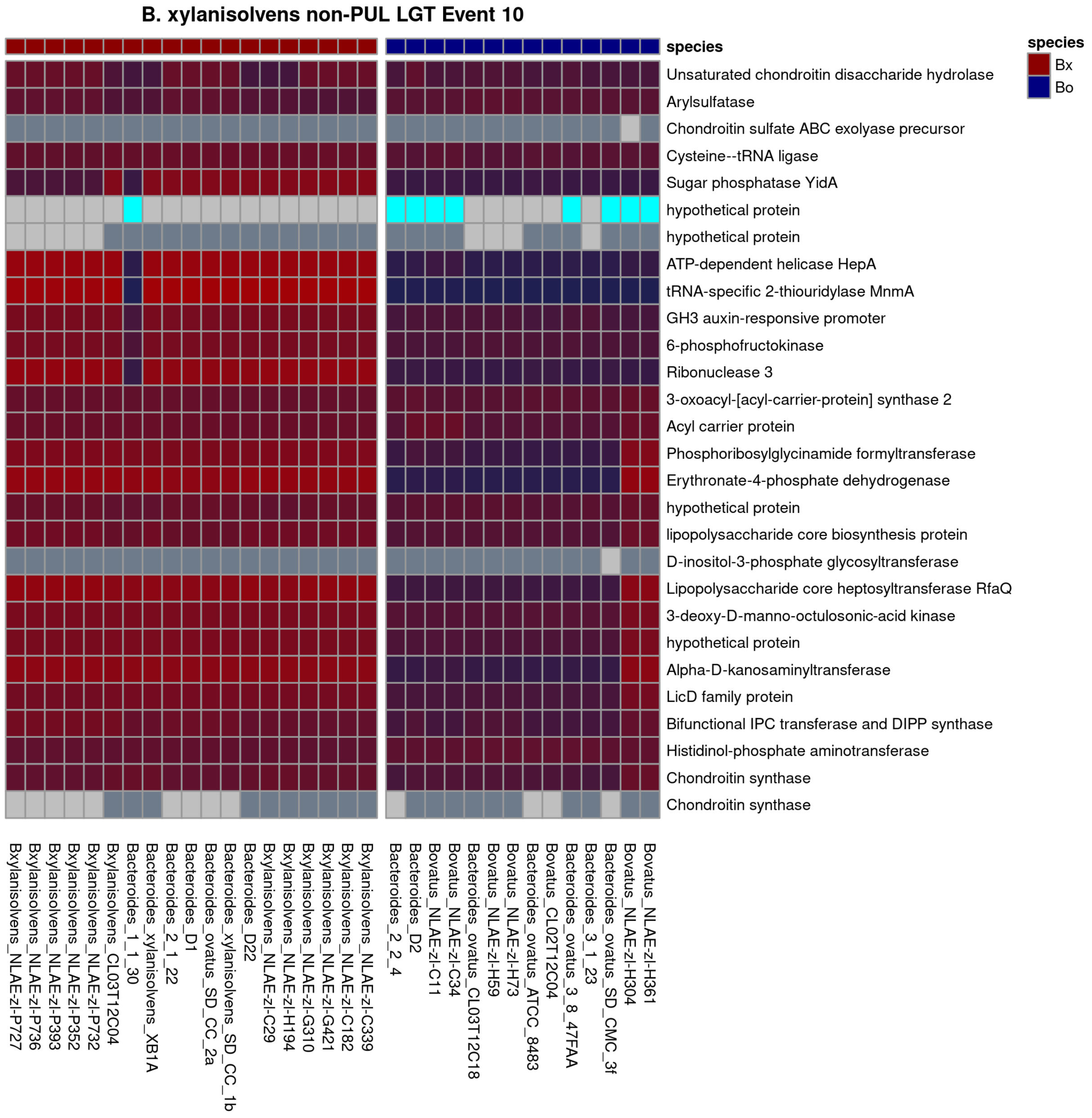
B. xylanisolvens non-PUL LGT Event 10
species
Unsaturated chondroitin disaccharide hydrolase
Arylsulfatase
Chondroitin sulfate ABC exolyase precursor
Cysteine--tRNA ligase
Sugar phosphatase YidA
hypothetical protein
hypothetical protein
ATP-dependent helicase HepA
tRNA-specific 2-thiouridylase MnmA
GH3 auxin-responsive promoter
6-phosphofructokinase
Ribonuclease 3
3-oxoacyl-[acyl-carrier-protein] synthase 2
Acyl carrier protein
Phosphoribosylglycinamide formyltransferase
Erythronate-4-phosphate dehydrogenase
hypothetical protein
lipopolysaccharide core biosynthesis protein
D-inositol-3-phosphate glycosyltransferase
Lipopolysaccharide core heptosyltransferase RfaQ
3-deoxy-D-manno-octulosonic-acid kinase
hypothetical protein
Alpha-D-kanosaminyltransferase
LicD family protein
Bifunctional IPC transferase and DIPP synthase
Histidinol-phosphate aminotransferase
Chondroitin synthase
Chondroitin synthase
species
Bx
Bo
Bxylanisolvens_NLAE-zl-P727
Bxylanisolvens_NLAE-zl-P736
Bxylanisolvens_NLAE-zl-P393
Bxylanisolvens_NLAE-zl-P352
Bxylanisolvens_NLAE-zl-P732
Bxylanisolvens_CL03T12C04
Bacteroides_1_1_30
Bacteroides_xylanisolvens_XB1A
Bacteroides_2_1_22
Bacteroides_D1
Bacteroides_ovatus_SD_CC_2a
Bacteroides_xylanisolvens_SD_CC_1b
Bacteroides_D22
Bxylanisolvens_NLAE-zl-C29
Bxylanisolvens_NLAE-zl-H194
Bxylanisolvens_NLAE-zl-G310
Bxylanisolvens_NLAE-zl-G421
Bxylanisolvens_NLAE-zl-C182
Bxylanisolvens_NLAE-zl-C339
Bacteroides_2_2_4
Bacteroides_D2
Bovatus_NLAE-zl-C11
Bovatus_NLAE-zl-C34
Bacteroides_ovatus_CL03T12C18
Bovatus_NLAE-zl-H59
Bovatus_NLAE-zl-H73
Bacteroides_ovatus_ATCC_8483
Bovatus_CL02T12C04
Bacteroides_ovatus_3_8_47FAA
Bacteroides_3_1_23
Bacteroides_ovatus_SD_CMC_3f
Bovatus_NLAE-zl-H304
Bovatus_NLAE-zl-H361

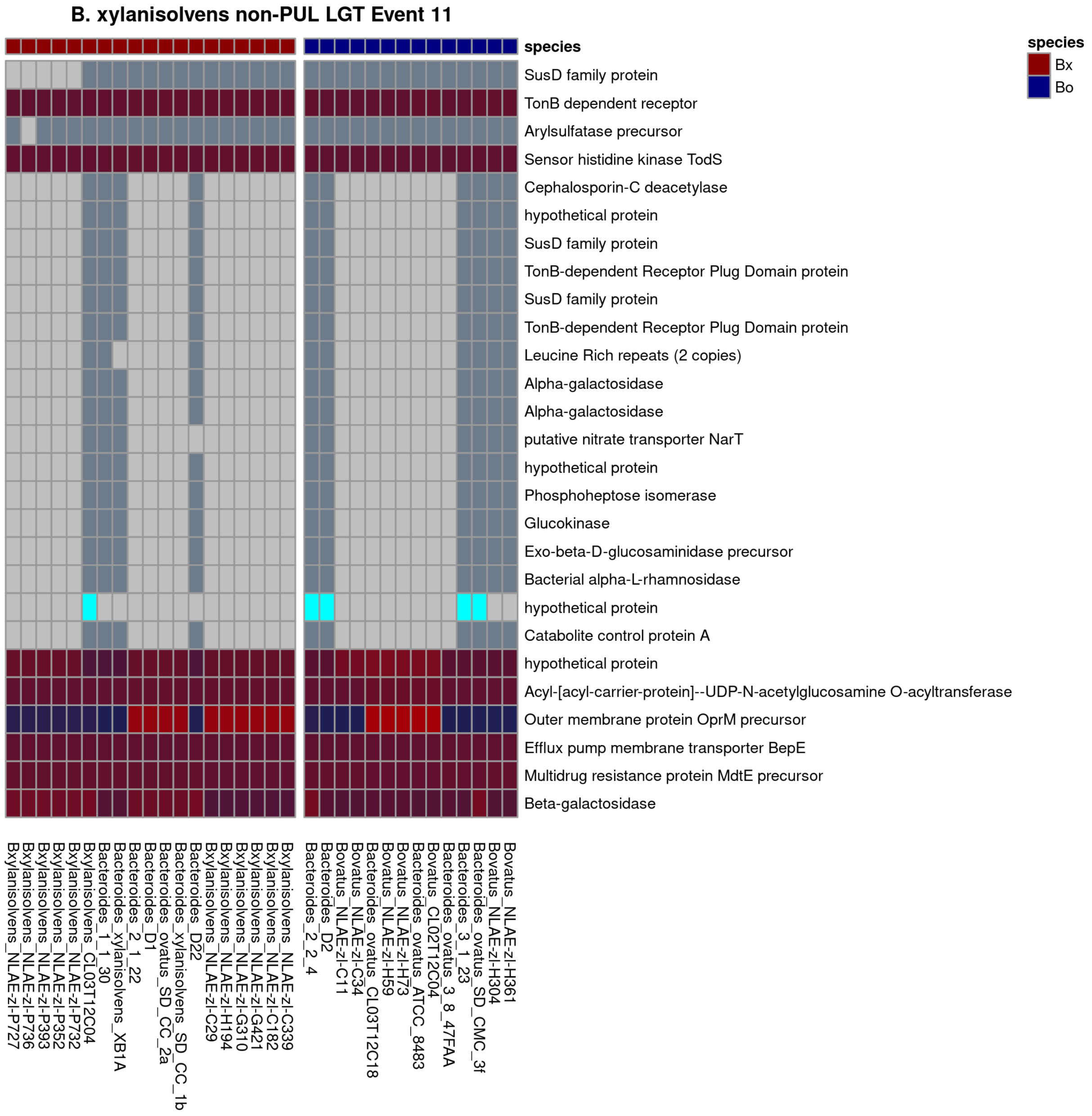
B. xylanisolvens non-PUL LGT Event 11
species
SusD family protein
TonB dependent receptor
Arylsulfatase precursor
Sensor histidine kinase TodS
Cephalosporin-C deacetylase
hypothetical protein
SusD family protein
TonB-dependent Receptor Plug Domain protein
SusD family protein
TonB-dependent Receptor Plug Domain protein
Leucine Rich repeats (2 copies)
Alpha-galactosidase
Alpha-galactosidase
putative nitrate transporter NarT
hypothetical protein
Phosphoheptose isomerase
Glucokinase
Exo-beta-D-glucosaminidase precursor
Bacterial alpha-L-rhamnosidase
hypothetical protein
Catabolite control protein A
hypothetical protein
Acyl-[acyl-carrier-protein]--UDP-N-acetylglucosamine O-acyltransferase
Outer membrane protein OprM precursor
Efflux pump membrane transporter BepE
Multidrug resistance protein MdtE precursor
Beta-galactosidase
species
Bx
Bo
Bxylanisolvens_NLAE-zl-P727
Bxylanisolvens_NLAE-zl-P736
Bxylanisolvens_NLAE-zl-P393
Bxylanisolvens_NLAE-zl-P352
Bxylanisolvens_NLAE-zl-P732
Bxylanisolvens_CL03T12C04
Bacteroides_1_1_30
Bacteroides_xylanisolvens_XB1A
Bacteroides_2_1_22
Bacteroides_D1
Bacteroides_ovatus_SD_CC_2a
Bacteroides_xylanisolvens_SD_CC_1b
Bacteroides_D22
Bxylanisolvens_NLAE-zl-C29
Bxylanisolvens_NLAE-zl-H194
Bxylanisolvens_NLAE-zl-G310
Bxylanisolvens_NLAE-zl-G421
Bxylanisolvens_NLAE-zl-C182
Bxylanisolvens_NLAE-zl-C339
Bacteroides_2_2_4
Bacteroides_D2
Bovatus_NLAE-zl-C11
Bovatus_NLAE-zl-C34
Bacteroides_ovatus_CL03T12C18
Bovatus_NLAE-zl-H59
Bovatus_NLAE-zl-H73
Bacteroides_ovatus_ATCC_8483
Bovatus_CL02T12C04
Bacteroides_ovatus_3_8_47FAA
Bacteroides_3_1_23
Bacteroides_ovatus_SD_CMC_3f
Bovatus_NLAE-zl-H304
Bovatus_NLAE-zl-H361

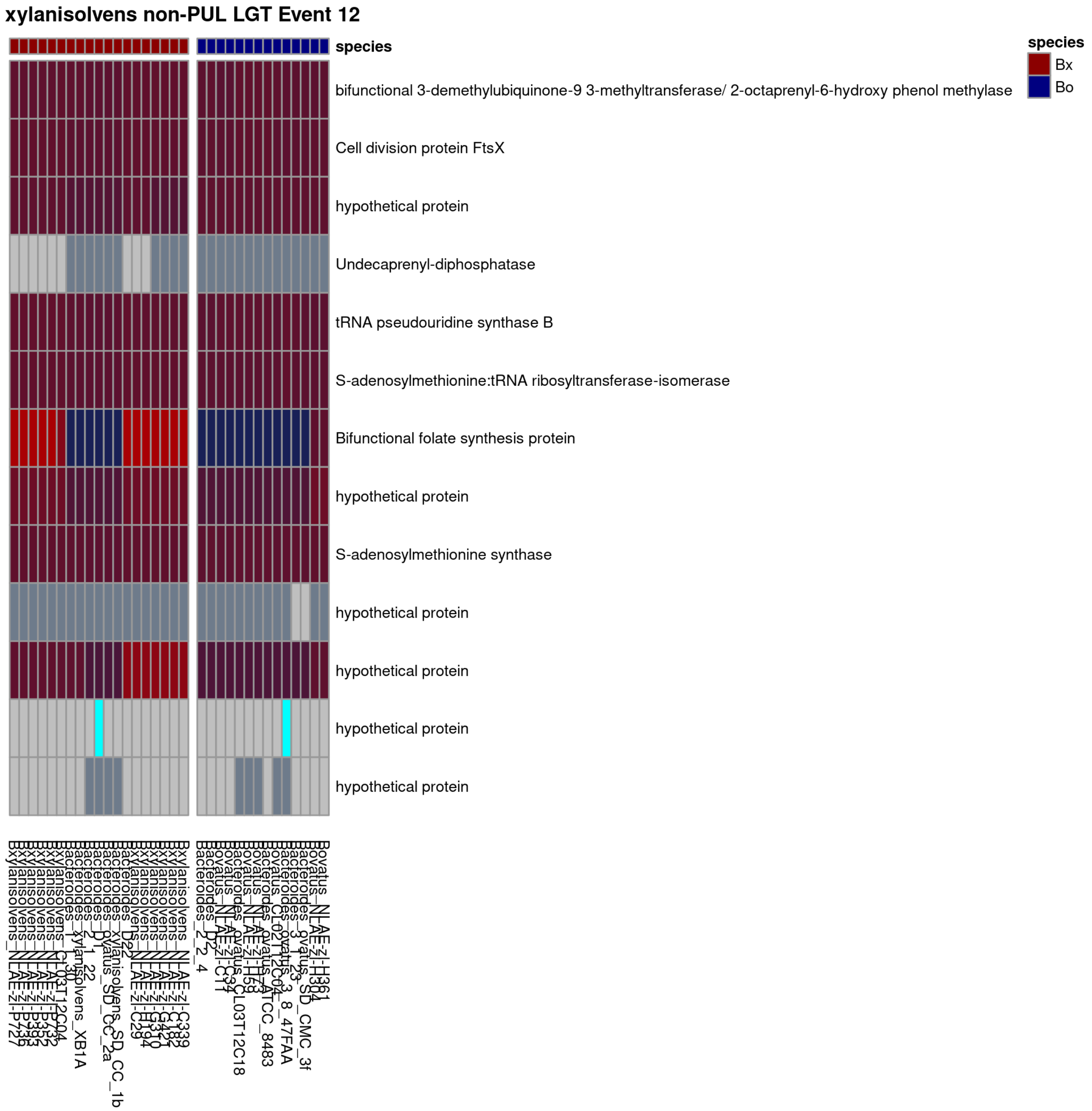
xylanisolvens non-PUL LGT Event 12
species
bifunctional 3-demethylubiquinone-9 3-methyltransferase/ 2-octaprenyl-6-hydroxy phenol methylase
Cell division protein FtsX
hypothetical protein
Undecaprenyl-diphosphatase
tRNA pseudouridine synthase B
S-adenosylmethionine:tRNA ribosyltransferase-isomerase
Bifunctional folate synthesis protein
hypothetical protein
S-adenosylmethionine synthase
hypothetical protein
hypothetical protein
hypothetical protein
hypothetical protein
species
Bx
Bo
Bxylanisolvens_NLAE-zl-P727
Bxylanisolvens_NLAE-zl-P736
Bxylanisolvens_NLAE-zl-P393
Bxylanisolvens_NLAE-zl-P352
Bxylanisolvens_NLAE-zl-P732
Bxylanisolvens_CL03T12C04
Bacteroides_1_1_30
Bacteroides_xylanisolvens_XB1A
Bacteroides_2_1_22
Bacteroides_D1
Bacteroides_ovatus_SD_CC_2a
Bacteroides_xylanisolvens_SD_CC_1b
Bacteroides_D22
Bxylanisolvens_NLAE-zl-C29
Bxylanisolvens_NLAE-zl-H194
Bxylanisolvens_NLAE-zl-G310
Bxylanisolvens_NLAE-zl-G421
Bxylanisolvens_NLAE-zl-C182
Bxylanisolvens_NLAE-zl-C339
Bacteroides_2_2_4
Bacteroides_D2
Bovatus_NLAE-zl-C11
Bovatus_NLAE-zl-C34
Bacteroides_ovatus_CL03T12C18
Bovatus_NLAE-zl-H59
Bovatus_NLAE-zl-H73
Bacteroides_ovatus_ATCC_8483
Bovatus_CL02T12C04
Bacteroides_ovatus_3_8_47FAA
Bacteroides_3_1_23
Bacteroides_ovatus_SD_CMC_3f
Bovatus_NLAE-zl-H304
Bovatus_NLAE-zl-H361

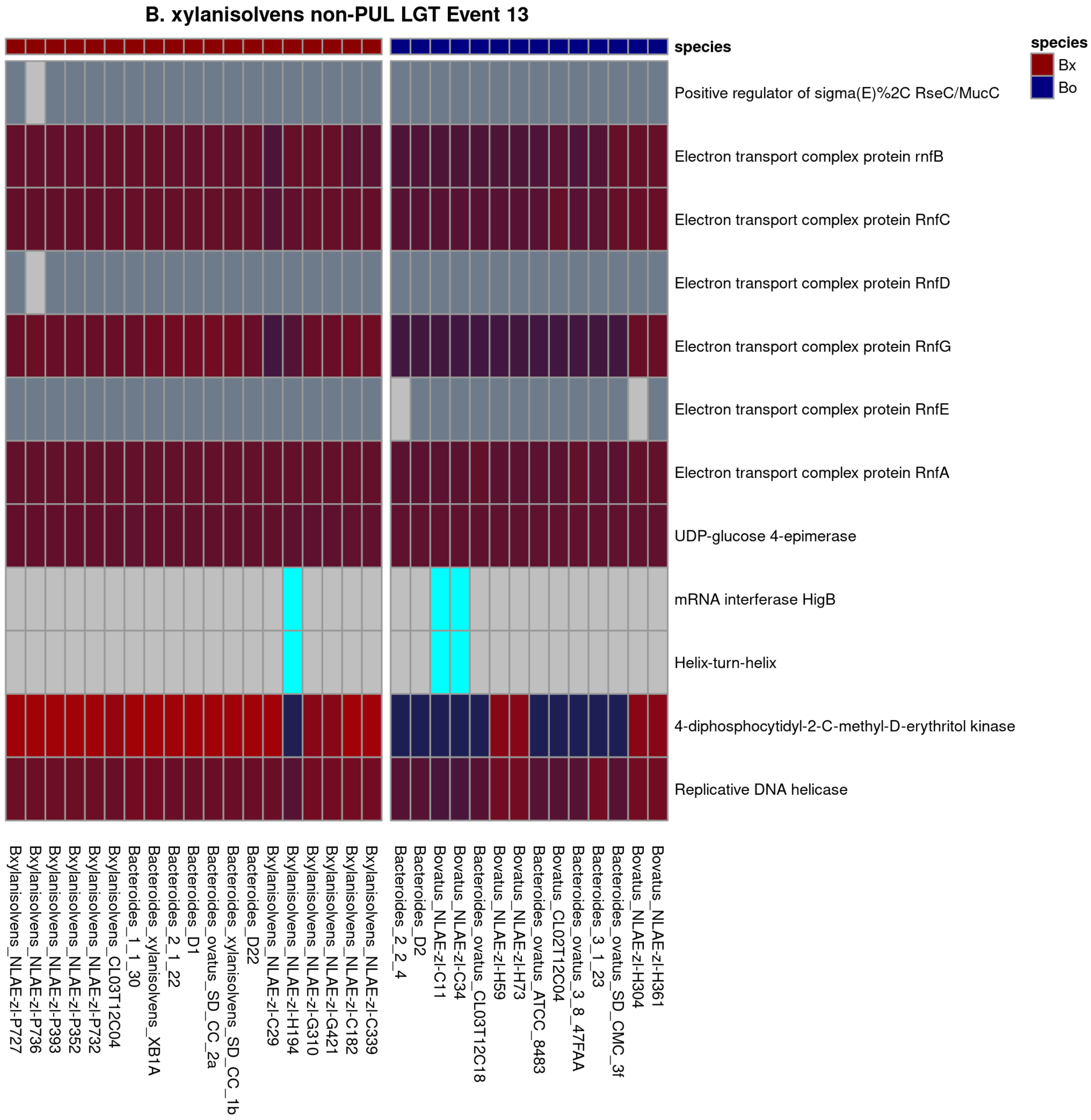
B. xylanisolvens non-PUL LGT Event 13
species
species
Bx
Bo
Positive regulator of sigma(E)%2C RseC/MucC
Electron transport complex protein rnfB
Electron transport complex protein RnfC
Electron transport complex protein RnfD
Electron transport complex protein RnfG
Electron transport complex protein RnfE
Electron transport complex protein RnfA
UDP-glucose 4-epimerase
mRNA interferase HigB
Helix-turn-helix
4-diphosphocytidyl-2-C-methyl-D-erythritol kinase
Replicative DNA helicase
Bxylanisolvens_NLAE-zl-P727
Bxylanisolvens_NLAE-zl-P736
Bxylanisolvens_NLAE-zl-P393
Bxylanisolvens_NLAE-zl-P352
Bxylanisolvens_NLAE-zl-P732
Bxylanisolvens_CL03T12C04
Bacteroides_1_1_30
Bacteroides_xylanisolvens_XB1A
Bacteroides_2_1_22
Bacteroides_D1
Bacteroides_ovatus_SD_CC_2a
Bacteroides_xylanisolvens_SD_CC_1b
Bacteroides_D22
Bxylanisolvens_NLAE-zl-C29
Bxylanisolvens_NLAE-zl-H194
Bxylanisolvens_NLAE-zl-G310
Bxylanisolvens_NLAE-zl-G421
Bxylanisolvens_NLAE-zl-C182
Bxylanisolvens_NLAE-zl-C339
Bacteroides_2_2_4
Bacteroides_D2
Bovatus_NLAE-zl-C11
Bovatus_NLAE-zl-C34
Bacteroides_ovatus_CL03T12C18
Bovatus_NLAE-zl-H59
Bovatus_NLAE-zl-H73
Bacteroides_ovatus_ATCC_8483
Bovatus_CL02T12C04
Bacteroides_ovatus_3_8_47FAA
Bacteroides_3_1_23
Bacteroides_ovatus_SD_CMC_3f
Bovatus_NLAE-zl-H304
Bovatus_NLAE-zl-H361

Figure S9

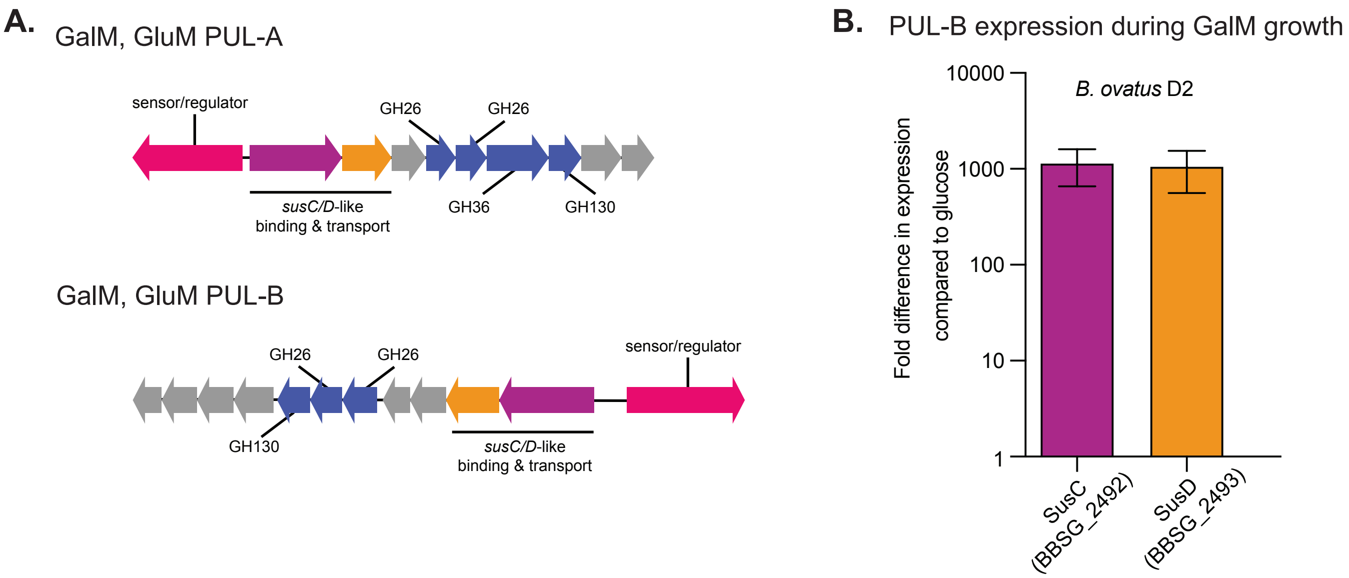
A.
GalM, GluM PUL-A
sensor/regulator
GH26
GH26
susC/D-like
binding & transport
GH36
GH130
GalM, GluM PUL-B
GH26
GH26
sensor/regulator
GH130
susC/D-like
binding & transport
B.
PUL-B expression during GalM growth
B. ovatus D2
Fold difference in expression compared to glucose
10000
1000
100
10
1
SusC (BBSG_2492)
SusD (BBSG_2493)